AD-A040 058 ARMY ENGINEER WATERWAYS EXPERIMENT STATION VICKSBURG MISS F/G 13/13
CHARTS FOR PRELIMINARY DESIGN OF DEEP UNDERGROUND STRUCTURES SU--ETC(U)
APR 77 J R BRITT

UNCLASSIFIED WES-MP-N-77-3 NL

| OF |
AD
A040058

END

DATE
FILMED
6-77

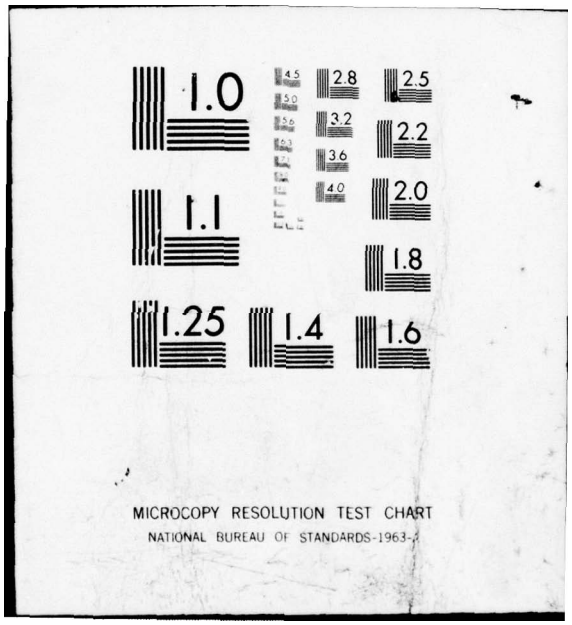
1.0
1.1
1.25
1.4
1.6
1.8
2.0
2.2
2.5
2.8
3.2
3.6
4.0
4.5
5.0
5.6
MICROCOPY RESOLUTION TEST CHART
NATIONAL BUREAU OF STANDARDS-1963-A

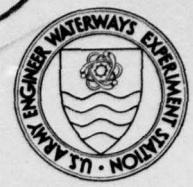

MISCELLANEOUS PAPER N-77-3

CHARTS FOR PRELIMINARY DESIGN OF DEEP UNDERGROUND STRUCTURES SUBJECTED TO DYNAMIC LOADS

by

J. R. Britt

Weapons Effects Laboratory
U. S. Army Engineer Waterways Experiment Station
P. O. Box 631, Vicksburg, Miss. 39180

April 1977
Final Report

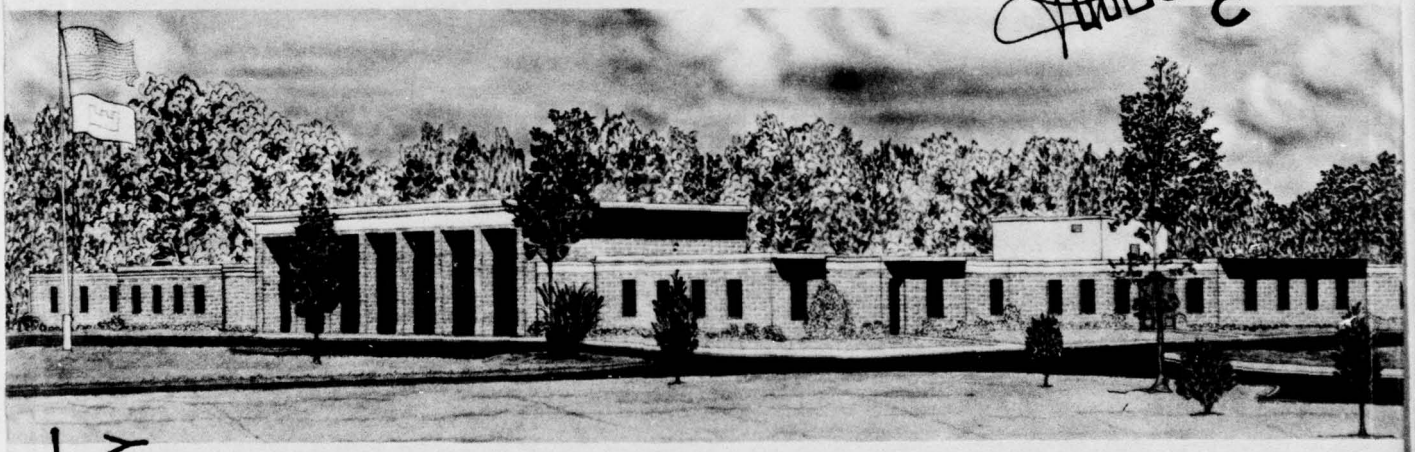

Prepared for Defense Nuclear Agency, Washington, D. C. 20305
and Office, Chief of Engineers, U. S. Army
Washington, D. C. 20314

Under DNA Subtask J34CAXSX311 and
OCE Subtask 4A762719AT40-A1-017

Destroy this report when no longer needed. Do not return it to the originator.

Unclassified

SECURITY CLASSIFICATION OF THIS PAGE (When Data Entered)

REPORT DOCUMENTATION PAGE

READ INSTRUCTIONS BEFORE COMPLETING FORM

1. REPORT NUMBER: Miscellaneous Paper N-77-3

2. GOVT ACCESSION NO.

3. RECIPIENT'S CATALOG NUMBER

4. TITLE (and Subtitle): CHARTS FOR PRELIMINARY DESIGN OF DEEP UNDERGROUND STRUCTURES SUBJECTED TO DYNAMIC LOADS

5. TYPE OF REPORT & PERIOD COVERED: Final report January 1975-June 1976

6. PERFORMING ORG. REPORT NUMBER

7. AUTHOR(s): J. R. Britt

8. CONTRACT OR GRANT NUMBER(s)

9. PERFORMING ORGANIZATION NAME AND ADDRESS: U. S. Army Engineer Waterways Experiment Station, Weapons Effects Laboratory, P. O. Box 631, Vicksburg, Miss. 39180

10. PROGRAM ELEMENT, PROJECT, TASK AREA & WORK UNIT NUMBERS: See Block 18

11. CONTROLLING OFFICE NAME AND ADDRESS: Defense Nuclear Agency, Washington, D. C. 20305; and Office, Chief of Engineers, U. S. Army, Washington, D. C. 20314

12. REPORT DATE: April 1977

13. NUMBER OF PAGES: 71

14. MONITORING AGENCY NAME & ADDRESS (if different from Controlling Office): WES-MP-N-77-3

15. SECURITY CLASS. (of this report): Unclassified

15a. DECLASSIFICATION/DOWNGRADING SCHEDULE

16. DISTRIBUTION STATEMENT (of this Report)

Approved for public release; distribution unlimited.

17. DISTRIBUTION STATEMENT (of the abstract entered in Block 20, if different from Report)

18. SUPPLEMENTARY NOTES

This research was sponsored by the Defense Nuclear Agency under Subtask J34CAXSX311, "Underground Structures Studies"; and by the Office, Chief of Engineers, under Subtask 4A762719AT40, A1, 017, "Stability of Deep Underground Structures in Rock."

19. KEY WORDS (Continue on reverse side if necessary and identify by block number)

Charts
Dynamic loads
Ground shock
Nuclear explosion effects
Underground structures

038 100

20. ABSTRACT (Continue on reverse side if necessary and identify by block number)

This report presents charts suitable for preliminary dynamic design of deep underground protective structures in rock subjected to long-duration ground shock loadings produced by nuclear weapons. The charts were calculated using a theoretical model which consists of multilayered concentric cylinders of elastoplastic materials with a time-dependent, axially symmetric applied load representing the free-field stress. Each element in the cross section is assumed to be incompressible and its yield is governed by a Mohr-Coulomb failure criterion. A first-order correction factor is given to account for compressibility of the materials.

DD FORM 1 JAN 73 1473 EDITION OF 1 NOV 65 IS OBSOLETE

Unclassified

SECURITY CLASSIFICATION OF THIS PAGE (When Data Entered)

PREFACE

This report presents results of a theoretical study which evaluates the response of hardened underground facilities in rock to dynamically applied loads produced by explosions. The salient features of the theoretical model are summarized in charts suitable for preliminary design of deep underground structures. This research was conducted by personnel of the Phenomenology and Effects Division (PED) of the Weapons Effects Laboratory (WEL), U. S. Army Engineer Waterways Experiment Station (WES), during the period January 1975-June 1976.

The primary analytical development was sponsored by the Defense Nuclear Agency under Subtask J34CAXSX311, "Underground Structures Studies," under the guidance of Dr. Kent Goering. Computer parameter studies and the preparation of this report were sponsored by the Office, Chief of Engineers (OCE), under Subtask 4A762719AT40/A1/017, "Stability of Deep Underground Structures in Rock," which was monitored by Mr. D. S. Reynolds.

This report was written by Mr. J. R. Britt, PED, under the general supervision of Messrs. L. F. Ingram, Chief, PED, and W. J. Flathau, Chief, WEL.

COL G. H. Hilt, CE, and COL John L. Cannon, CE, were Directors of WES during the study and preparation and publication of this report. Mr. F. R. Brown was Technical Director.

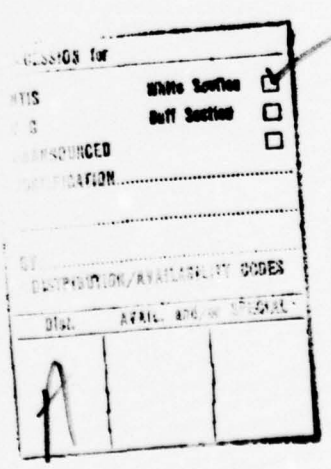

CONTENTS

CONVERSION FACTORS, U. S. CUSTOMARY TO METRIC (SI) UNITS OF MEASUREMENT

U. S. customary units of measurement used in this report can be converted to metric (SI) units as follows:

Multiply	By	To Obtain
inches	2.54	centimetres
pounds (force) per square inch	6.894757	kilopascals
kilobars	100.0	megapascals
pounds (force) per square inch-second^2	6.894757	kilopascals-second^2
pounds (force) per square inch-second^2 per square inch	1.06869×10^7	kilograms per cubic metre
degrees (angle)	0.01745329	radians

CHARTS FOR PRELIMINARY DESIGN OF DEEP UNDERGROUND STRUCTURES SUBJECTED TO DYNAMIC LOADS

CHAPTER 1

INTRODUCTION

1.1 BACKGROUND

Design of deep underground structures to resist the shock levels induced by nuclear weapons must take into account the strength of the surrounding rock. Hence, conventional, dynamic structural design procedures[1] are not adequate for designing these facilities, and design engineers have resorted to static methods such as outlined by Newmark[2] and Hendron and Aiyer.[3] Drake and Britt[4] have extended these static procedures to accommodate dynamic loads. The present report summarizes the salient features of this dynamic design method in charts suitable for preliminary design of deep underground structures in rock.

1.2 APPLICATIONS AND LIMITATIONS OF THE DESIGN CHARTS

The charts of this report are applicable to the preliminary design of cylindrical, lined tunnels in rock subjected to the long-duration ground shock loadings produced by nuclear weapons. (It is suggested that the final design be confirmed by more sophisticated techniques such as nonlinear finite element computer codes.) The theoretical model

---

1 Headquarters, Department of the Army; "Engineering and Design: Design of Structures to Resist the Effects of Atomic Weapons"; Technical Manual TM 5-856-3, 15 March 1957; Washington, D. C.

2 N. M. Newmark; "Design of Rock Silo and Rock Cavity Linings"; Technical Report TR 70-114, August 1969; Space and Missiles Systems Organization, Air Force Systems Command, Norton Air Force Base, Calif.

3 A. J. Hendron and A. K. Aiyer; "Stresses and Strains Around a Cylindrical Tunnel in an Elasto-Plastic Material with Dilatancy"; Technical Report 10, September 1972; U. S. Army Engineer District, Omaha, CE, Omaha, Nebr.

4 J. L. Drake and J. R. Britt; "A Method for Designing Deep Underground Structures Subjected to Dynamic Loads"; Technical Report N-76-9; September 1976; U. S. Army Engineer Waterways Experiment Station, CE, Vicksburg, Miss.

consists of multilayered concentric cylinders of elastoplastic materials with a time-dependent, axially symmetric load representing the free-field stress applied to the exterior boundary. Each element in the cross section is assumed incompressible and its yield governed by a Mohr-Coulomb failure criterion. A first-order correction factor is given to account for compressibility of the materials.

Experience has shown that the present model can be a useful design tool if the assumptions of the theory are met. In particular, the following conditions should be approximated before using the design charts:

1. The structure is composed of concentric cylinders of circular cross section as shown in Figure 1.1.

2. The yield of the structure and surrounding rock is governed by the Mohr-Coulomb failure criterion.

3. The expected deformation (especially compaction) of liner and rock is small.

4. The ultimate loading of the structure is nearly axisymmetric.

5. The duration of the loading is at least 5 to 10 times the response and engulfment times of the structure.

For example, use of the charts appears to be appropriate for design of cylindrical tunnels with concrete and steel liners sited in hard rock such as granite. But the charts will provide only a conservative lower bound estimate of the response of structures located in weak, highly compactible rocks such as tuff.

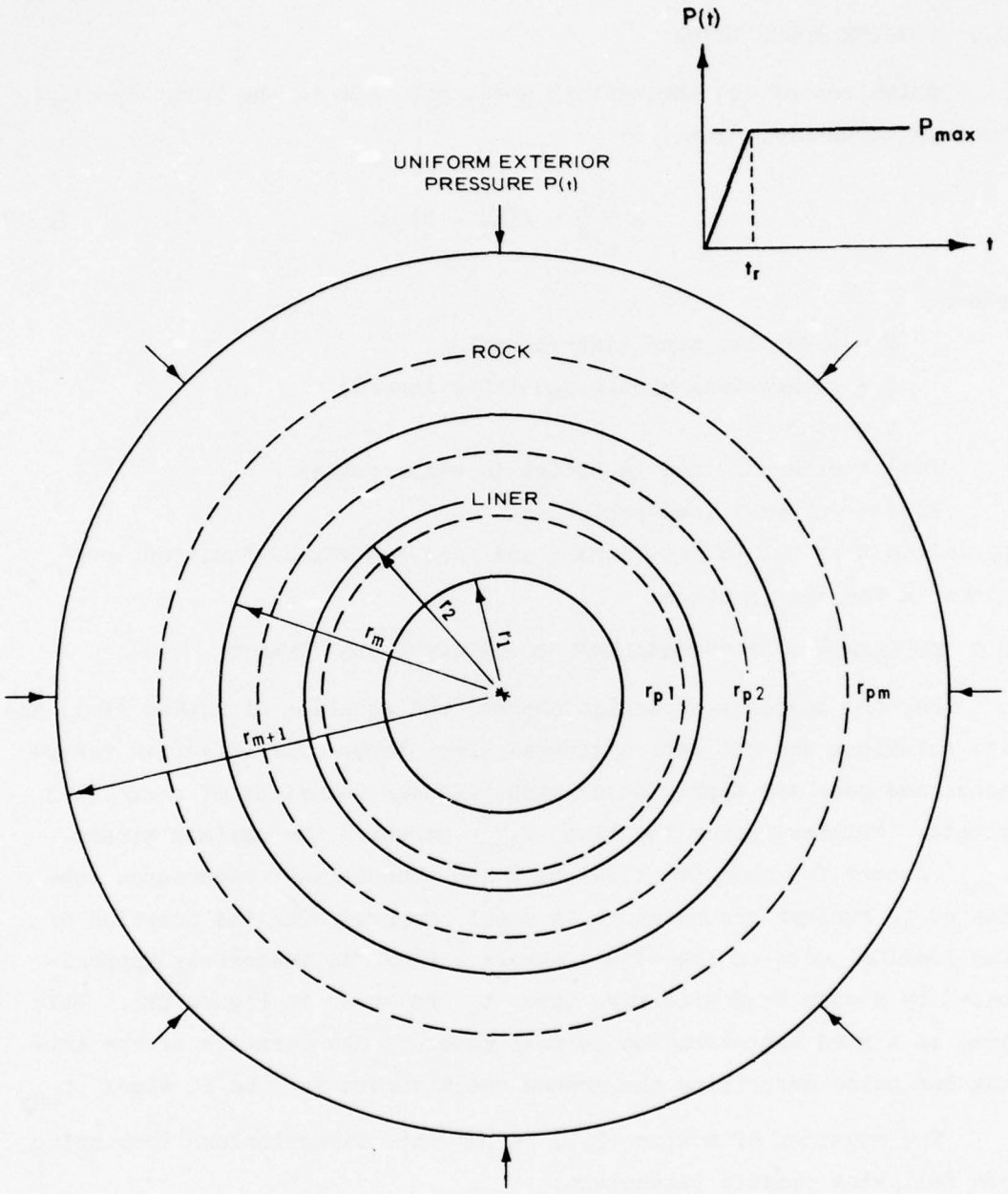

Figure 1.1. Geometry of rock/liner system.

CHAPTER 2

THEORY

2.1 PROBLEM FORMULATION

Solutions of the theoretical model are cast in the form normally used in structural dynamics:

$$M \frac{d^2\varepsilon}{dt^2} = P(t) - R(\varepsilon) \qquad (2.1)$$

where:[1]

M = effective mass (mass/length)

ε = diametrical strain (positive inward)

t = time

$P(t)$ = external load (positive in compression)

$R(\varepsilon)$ = internal load-resistance

Definitions of the effective mass and load-resistance functions are given in the next section.

2.2 APPLICATION OF THE ANALYSIS TO OBTAIN DESIGN CHARTS

For the purposes of design charts, the equation of motion (2.1) and its solutions are put into a dimensionless form. The effective resistance and mass are approximated with bilinear functions of normalized strain. Further, since the time t_{max} at which the maximum strain ε_{max} occurs for most practical hardened tunnel-liner structures subjected to nuclear ground shock is small compared with the duration of the loading pulse or free-field stress, $P(t)$ is adequately approximated by a step load with rise time t_r as shown in Figure 1.1. This load is a good approximation in most cases if the duration of the triangular pulse describing the ground shock stress is 5 to 10 times t_{max}.

The equation of motion (2.1) is put into dimensionless form using the following elastic parameters:

---

[1] For convenience, symbols and unusual abbreviations used in this report are listed and defined in the Notation (Appendix B).

ε_e = elastic limit or maximum elastic strain

K_e = effective elastic stiffness

$R_e = K_e \varepsilon_e$ = maximum elastic resistance

M_e = effective mass (mass/length) in elastic deformation

$T_e = 2\pi \sqrt{\frac{M_e}{K_e}}$ = effective elastic period

The dimensionless variables are then

$$\bar{\varepsilon} = \frac{\varepsilon}{\varepsilon_e} \tag{2.2}$$

$$\bar{t} = \frac{t}{T_e} \tag{2.3}$$

$$\bar{t}_r = \frac{t_r}{T_e} \tag{2.4}$$

$$A = \frac{P_{max}}{R_e} \tag{2.5}$$

$$\bar{R}(\bar{\varepsilon}) = \frac{R(\varepsilon)}{R_e} \tag{2.6}$$

$$\bar{M}(\bar{\varepsilon}) = \frac{M}{M_e} \tag{2.7}$$

where P_{max} is the peak value of $P(t)$. Equation 2.1 becomes

$$\frac{\bar{M}(\bar{\varepsilon})}{(2\pi)^2} \frac{d^2\bar{\varepsilon}}{d\bar{t}^2} = \begin{cases} A\bar{t} \Big/ \bar{t}_r - \bar{R}(\bar{\varepsilon}) & \text{for } 0 \leq \bar{t} < \bar{t}_r \\ A - \bar{R}(\bar{\varepsilon}) & \text{for } \bar{t} \geq \bar{t}_r \end{cases} \tag{2.8}$$

where $\bar{R}(\bar{\varepsilon}) = \bar{M}(\bar{\varepsilon})$ are expressed as the bilinear functions

$$\bar{R}(\bar{\varepsilon}) = \begin{cases} \bar{\varepsilon} & \text{for } \bar{\varepsilon} \leq 1 \\ 1 + B(\bar{\varepsilon} - 1) & \text{for } \bar{\varepsilon} > 1 \end{cases} \tag{2.9}$$

$$\bar{M}(\varepsilon) = \begin{cases} 1 & \text{for } \bar{\varepsilon} \leq 1 \\ 1 + C(\bar{\varepsilon} - 1) & \text{for } \bar{\varepsilon} > 1 \end{cases} \tag{2.10}$$

and

$$B = \frac{K_p}{K_e} \tag{2.11}$$

$$K_p = \frac{\Delta R}{\Delta \varepsilon} \quad \text{for} \quad \varepsilon > \varepsilon_e (\bar{\varepsilon} > 1) \tag{2.12}$$

$$C = \frac{\varepsilon_e}{M_e} \frac{\Delta M}{\Delta \varepsilon} \quad \text{for} \quad \varepsilon > \varepsilon_e (\bar{\varepsilon} > 1) \tag{2.13}$$

Examples of bilinear fits to $R(\varepsilon)$ and $M(\varepsilon)$ curves are shown in Figure 2.1. The lines 1 are better approximations for $\varepsilon < 2$ percent, but lines 2 would be used if strains up to 4 or 5 percent were of interest.

The charts, Figures A.1-A.48, summarize the maximum values of the normalized strain $\bar{\varepsilon}_{max} = \varepsilon_{max}/\varepsilon_e$, and dimensionless time $\bar{t}_{max} = t_{max}/T_e$, at which $\bar{\varepsilon}_{max}$ occurs for the parameters A, B, and C. Note that A is a measure of the magnitude of the applied load or free-field stress, B is a measure of the stiffness of the rock-liner structure in plastic deformation, and C is a measure of the change in effective mass or density as the structure yields. The determination of B and C and the elastic normalizing parameters from material properties is discussed in the next section.

2.3 DETERMINING CHART PARAMETERS FROM MATERIAL PROPERTIES

The geometry of the rock-liner system is shown in Figure 1.1. The number of concentric material layers of the system is denoted by m. Generally, the liner is represented by $m-1$ layers and the rock by the single m^{th} layer. Each material denoted by the subscript i is

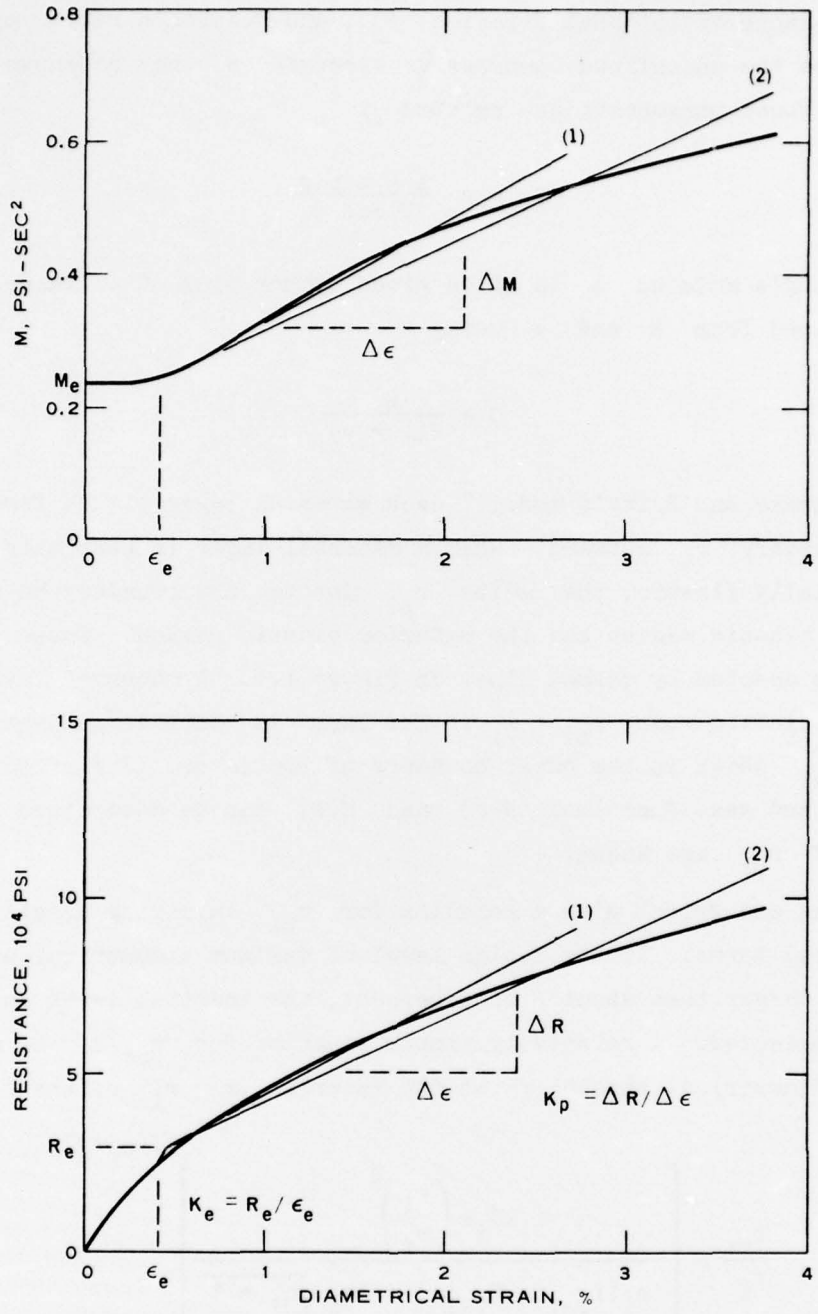

Figure 2.1. Examples of bilinear fits to effective resistance and mass functions.

described by the properties density ρ_i, shear modulus G_i, cohesion q_i, the angle of internal friction ϕ_i, and Poisson's ratio ν_i. In some cases the unconfined compressive strength σ_u may be known instead of q. These parameters are related by

$$q = \sigma_u \frac{1 - \sin \phi}{2 \cos \phi} \tag{2.14}$$

Also, Young's modulus E is often given rather than G. Values of G are obtained from E and ν using

$$G = \frac{E}{2(1 + \nu)} \tag{2.15}$$

In Drake and Britt's model,[2] each material layer yields from its inner boundary r_i outward. When a material layer is partially plastic and partially elastic, the radius r_{pi} denotes the boundary between the interior plastic region and the exterior elastic region. These boundaries are denoted by dashed lines in Figure 1.1. A material layer is entirely elastic when $r_{pi} = r_i$. The layer is completely plastic when $r_{pi} = r_{i+1}$ which is the outer boundary of the layer. The effective resistance and mass functions $R(\varepsilon)$ and $M(\varepsilon)$ can be determined when the values of r_{pi} are known.

Drake and Britt[2] give a relation for r_{pi} involving acceleration or inertial terms. If the design level of maximum diametrical strain is not much larger than about 2 to 5 percent, the inertial terms in r_{pi} can be neglected. A relatively simple equation for r_{pi}/r_i as a function of diametrical strain ε at the interior $r = r_i$ of the liner is

$$\frac{r_{pi}}{r_i} = \left[\frac{4G_i \varepsilon \left(\frac{r_1}{r_i} \right)^2}{n_i (Y_{i-1} + K_{i-1} \varepsilon) + 2q_i \sqrt{n_i + 1}} \right]^{1/(n_i+2)} \tag{2.16}$$

---

[2] Drake and Britt, op. cit.

where

$$n_i = \frac{2 \sin \phi_i}{1 - \sin \phi_i} \tag{2.17}$$

the effective plastic resistance of layer i is

$$Y_i = Y_{i-1}\left(\frac{r_{pi}}{r_i}\right)^{n_i} + \frac{2q_i\sqrt{n_i + 1}}{n_i}\left[\left(\frac{r_{pi}}{r_i}\right)^{n_i} - 1\right] \tag{2.18}$$

and the effective elastic stiffness is

$$K_i = K_{i-1}\left(\frac{r_{pi}}{r_i}\right)^{n_i} + 2G_i\left(\frac{r_1}{r_i}\right)^2\left[1 - \left(\frac{r_i}{r_{pi}}\right)^2\right] \tag{2.19}$$

where $Y_0 = 0$ and $K_0 = 0$. In the case $n_i = 0$, $(\phi_i = 0)$,

$$\lim_{n_i \to 0} \frac{1}{n_i}\left[\left(\frac{r_{pi}}{r_i}\right)^{n_i} - 1\right] = \ln\left(\frac{r_{pi}}{r_i}\right) \tag{2.20}$$

Whenever Equation 2.16 gives a value of r_{pi}/r_i greater than r_{i+1}/r_i, the layer is completely plastic and $r_{pi}/r_i = r_{i+1}/r_i$ must be used. To calculate r_{pi}/r_i, begin at $i = 1$, the inside boundary of the liner. In this case Y_{i-1} and K_{i-1} are zero. Then with r_{p1}/r_1 known, Y_1 and K_1 can be calculated and hence also r_{p2}/r_2. Continuing this process out to the rock $(i = m)$ surrounding the liner, all the Y_i and K_i can be determined. In the equations for Y_i and K_i, the outside rock boundary Y_{m+1} should be taken as ∞ in the case of nuclear ground shock loading. The total resistance function $R(\varepsilon)$ is given by

$$R(\varepsilon) = K_m\varepsilon + Y_m \tag{2.21}$$

where Y_m is zero if the liner and rock are elastic, and the effective mass is obtained from

$$M = r_1^2 \sum_{j=1}^{m} \left\{ \frac{\rho_j}{n_j} \left[\left(\frac{r_{pj}}{r_j} \right)^{n_j} - 1 \right] \prod_{k=j+1}^{m} \left(\frac{r_{pk}}{r_k} \right)^{n_k} + \rho_j \ln \left(\frac{r_{j+1}}{r_{pj}} \right) \right\} \quad (2.22)$$

Here we cannot let $r_{m+1} \to \infty$ since M would be ∞ also. Parametric studies have shown that an appropriate value of r_{m+1} to use in calculating M is $r_{m+1} \approx 3r_m$. Equations 2.21 and 2.22 supply the effective resistance and mass functions needed in determining the parameters B and C of the charts.

To obtain B and C from $R(\varepsilon)$ and $M(\varepsilon)$, the elastic normalizing constant must first be computed from the relations

$$K_e = \sum_{j=1}^{m} 2G_j \left[\left(\frac{r_1}{r_j} \right)^2 - \left(\frac{r_1}{r_{j+1}} \right)^2 \right] \quad (2.23)$$

where $r_{m+1} \to \infty$ and $r_1/r_{m+1} \to 0$.

$$M_e = r_1^2 \sum_{j=1}^{m} \rho_j \ln \left(\frac{r_{j+1}}{r_j} \right) \quad (2.24)$$

where $r_{m+1} \approx 3r_m$. If the inner layer of the liner fails first, then the elastic limit is

$$\varepsilon_e = \frac{q_1 \sqrt{n_1 + 1}}{2G_1} \quad (2.25)$$

Using Equations 2.11, 2.13, and 2.16 through 2.25, values of B and C can be calculated.

In practice one may not use ε_e as given in Equation 2.25 but rather fit $R(\varepsilon)$ and $M(\varepsilon)$ to the "best" bilinear curves. In this way effective values of K_e, M_e, ε_e, and R_e are obtained. Usually, plotting a few points of the $R(\varepsilon)$ and $M(\varepsilon)$ curves is adequate to allow one to draw accurate visual fits to the curves. Static resistance-strain curves, $R(\varepsilon)$, can also be obtained using the charts of Newmark,[3] and Hendron and Aiyer.[4]

2.4 A FIRST-ORDER COMPRESSIBILITY CORRECTION

The equations described above and the charts of $\bar{t}_{max}$ and $\bar{\varepsilon}_{max}$ (Figures A.1 through A.48) are for incompressible media. The first-order correction factor given in Drake and Britt[5] may be used to approximately account for the compressibility of the liner and surrounding rock. The corrected normalized maximum strain, $\bar{\varepsilon}^c_{max}$, is related to the incompressible value $\bar{\varepsilon}_{max}$ through

$$\bar{\varepsilon}^c_{max} = 2(1 - \nu)\bar{\varepsilon}_{max} \tag{2.26}$$

where ν is an average of the Poisson's ratios of the liner and rock. For common rock and liner materials, ν ranges from about 0.2 to 0.3 and $2(1 - \nu) = 1.5$ is adequate for most preliminary design calculations.

---

[3] Newmark, op. cit.
[4] Hendron and Aiyer, op. cit.
[5] Drake and Britt, op. cit.

CHAPTER 3

EXAMPLE APPLICATIONS OF THE CHARTS

To illustrate the use of the design charts, consider the following steel and concrete liner sited in a relatively weak granite. The inner liner is steel which has an inside diameter of 48 inches[1] (radius = 24 inches) and is 1.5 inches thick. Between the steel and the granite there is 11 inches of concrete. The radii r_i are then

$$r_1 = 24 \text{ inches}$$

$$r_2 = 25.5 \text{ inches}$$

$$r_3 = 36.5 \text{ inches}$$

For the resistance calculation, take the outside rock radius to be $r_4 = \infty$ so that $1/r_4 = 0$. For the effective mass calculation use $r_4 = 3r_3$.

The material properties[2] are

Steel: $\rho_1 = 7.5 \times 10^{-4}$ psi-sec^2/in^2

$G_1 = 12 \times 10^6$ psi

$q_1 = 27{,}500$ psi

$\phi_1 = 0$ deg

$\nu_1 = 0.27$

---

[1] A table of factors for converting U. S. customary units of measurement to metric (SI) units is presented on page 3.

[2] The units of density were chosen to be consistent with P_{max} in psi and r_i in inches. To convert unit weight in lb/ft^3 to density in psi-sec^2/in^2 divide by 667,000. To convert density in kg/m^3 to density in psi-sec^2/in^2 multiply by 9.36×10^{-8}.

Concrete: $\rho_2 = 2.25 \times 10^{-4}$ psi-sec^2/in^2

$G_2 = 2.13 \times 10^6$ psi

$q_2 = 2{,}000$ psi

$\phi_2 = 37$ deg

$\nu_2 = 0.25$

Granite: $\rho_3 = 2.5 \times 10^{-4}$ psi-sec^2/in^2

$G_3 = 4 \times 10^6$ psi

$q_3 = 2{,}900$ psi

$\phi_3 = 30$ deg

$\nu_3 = 0.25$

First determine the effective elastic stiffness K_e, effective mass M_e, and elastic limit ε_e using Equations 2.23, 2.24, and 2.25. Expanding the summation in Equation 2.23 for three material layers, obtain

$$K_e = 2\left\{G_1\left[\left(\frac{r_1}{r_1}\right)^2 - \left(\frac{r_1}{r_2}\right)^2\right] + G_2\left[\left(\frac{r_1}{r_2}\right)^2 - \left(\frac{r_1}{r_3}\right)^2\right] + G_3\left(\frac{r_1}{r_3}\right)^2\right\}$$

where $r_1/r_4 \approx r_1/\infty = 0$. Substituting the numerical values of the parameters yields

$$K_e = 2\left\{12 \times 10^6\left[1 - \left(\frac{24}{25.5}\right)^2\right] + 2.13 \times 10^6\left[\left(\frac{24}{25.5}\right)^2 - \left(\frac{24}{36.5}\right)^2\right] + 4 \times 10^6\left(\frac{24}{36.5}\right)^2\right\} = 8.13 \times 10^6 \text{psi}$$

Similarly, $M_e = 0.231$ psi-sec^2 is obtained from Equation 2.24. Using Equation 2.17, the value $n_1 = 0$ is obtained, and from Equation 2.25 $\varepsilon_e = 0.00115$.

To determine resistance points in the region of plastic deformation ($\varepsilon > \varepsilon_e$), use Equations 2.16 through 2.22. From Equation 2.17 calculate $n_1 = 0$, $n_2 = 3.02$, and $n_3 = 2.00$. Next, using Equation 2.16 determine the ratios of the plastic boundaries r_{pi} to the inside radii r_i starting at $i = 1$ and working up to $i = 3$. Calculate for $\varepsilon = 0.01$. When $i = 1$, $Y_{i-1} = Y_o = 0$, $K_{i-1} = K_o = 0$; hence,

$$\frac{r_{p1}}{r_1} = \left(\frac{4G_1\varepsilon}{2q_1\sqrt{n_1 + 1}}\right)^{1/n_1+2} = \left[\frac{4(12 \times 10^6)0.01}{2(27,500)\sqrt{0 + 1}}\right]^{1/0+2} = 2.95$$

But $r_2/r_1 = 1.0625$. This means that the steel layer is completely plastic, and hence, $r_{p1}/r_1 = r_2/r_1 = 1.0625$ must be used for $\varepsilon = 0.01$ and larger strains.

Y_1 and K_1 can now be evaluated using Equations 2.18, 2.19, and 2.20. Equation 2.20 applies because $n_1 = 0$. Since $Y_o = 0$ and $K_o = 0$, the equations reduce to

$$Y_1 = 2q_1\sqrt{n_1 + 1}\ \ln\frac{r_{p1}}{r_1} = 2q_1\ \ln\frac{r_2}{r_1} = 3334 \text{ psi}$$

and

$$K_1 = 2G_1\left(\frac{r_1}{r_2}\right)^2\left[1 - \left(\frac{r_2}{r_{p1}}\right)^2\right] = 2G_1\left(\frac{r_1}{r_2}\right)^2\left[1 - \left(\frac{r_2}{r_2}\right)^2\right] = 0 \text{ psi}$$

These values of Y_1 and K_1 do not change for increasing strain ε since the plastic boundary r_{p1} has reached its maximum value.

All information needed to calculate r_{p2}/r_2 from Equation 2.16 is now available, and the result is $r_{p2}/r_2 = 1.33$ and $r_{p2} = 33.9$ inches. Thus, at the strain $\varepsilon = 0.01$ the concrete layer is about half plastic

and half elastic. For $i = 2$, Equations 2.18 and 2.19 become

$$Y_2 = Y_1\left(\frac{r_{p2}}{r_2}\right)^{n_2} + \frac{2q_2\sqrt{n_2 + 1}}{n_2}\left[\left(\frac{r_{p2}}{r_2}\right)^{n_2} - 1\right] = 11{,}520 \text{ psi}$$

and

$$K_2 = K_1\left(\frac{r_{p2}}{r_2}\right)^{n_2} + 2G_2\left[\left(\frac{r_1}{r_{p2}}\right)^2 - \left(\frac{r_1}{r_3}\right)^2\right] = 2.93 \times 10^5 \text{ psi}$$

These values of Y_2 and K_2 can be substituted into Equation 2.16 to obtain $r_{p3}/r_3 = 1.15$ and $r_{p3} = 42.0$ inches. For $i = 3$, Equations 2.18 and 2.19 become, with $r_4 = \infty$ and $r_1/r_4 = 0$,

$$Y_3 = Y_2\left(\frac{r_{p3}}{r_3}\right)^{n_3} + \frac{2q_3\sqrt{n_3 + 1}}{n_3}\left[\left(\frac{r_{p3}}{r_3}\right)^{n_3} - 1\right] = 16{,}900 \text{ psi}$$

and

$$K_3 = K_2\left(\frac{r_{p3}}{r_3}\right)^{n_3} + 2G_3\left(\frac{r_1}{r_{p3}}\right)^2 = 3.00 \times 10^6 \text{ psi}$$

For the present example the number m of material layers is 3. Thus Equation 2.21 for the total resistance of the liner-rock system becomes

$$R(\varepsilon) = K_3\varepsilon + Y_3$$

Substituting the values of K_3 and Y_3 above and $\varepsilon = 0.01$ yields $R(0.01) = 47{,}000$ psi, which is plotted on the lower graph of Figure 2.1.

From Equations 2.22 and 2.20 the effective mass M is calculated:

$$M = r_1^2\left(\left\{\left[\rho_1 \ln\left(\frac{r_{p1}}{r_1}\right)\right]\left(\frac{r_{p2}}{r_2}\right)^{n_2} + \frac{\rho_2}{n_2}\left[\left(\frac{r_{p2}}{r_2}\right)^{n_2} - 1\right]\right\}\left(\frac{r_{p3}}{r_3}\right)^{n_3}\right.$$

$$\left. + \frac{\rho_3}{n_3}\left[\left(\frac{r_{p3}}{r_3}\right)^{n_3} - 1\right] + \rho_1 \ln\left(\frac{r_2}{r_{p1}}\right) + \rho_2 \ln\left(\frac{r_3}{r_{p2}}\right) + \rho_3 \ln\left(\frac{r_4}{r_{p3}}\right)\right)$$

$$M(0.01) = 0.33 \text{ psi-sec}^2$$

where the value $r_4 = 3r_3$ has been used as suggested previously.

Using the same procedure as for $\varepsilon = 0.01$, additional points at $\varepsilon = 0.005$, 0.02, and 0.03 were calculated and plotted, along with the elastic values, in Figure 2.1. Smooth curves were then drawn through these points and the bilinear fits denoted (1) and (2) were visually produced.

From previous experience with similar structures it was determined that the liner in the example could safely take about 2 percent strain without buckling. This figure was then taken as the design criterion for the structure. To apply the dynamic design charts, the bilinear fits (1) in Figure 2.1, which are good up to 2 to 2.5 percent, should be used. From these curves the effective elastic limit is $\varepsilon_e = 0.004$, the effective elastic stiffness is $K_e = 7.5 \times 10^6$ psi, and the effective elastic period is $T_e = 2\pi\sqrt{M_e/K_e} = 1.1$ msec. These values of ε_e and K_e should be used instead of the results obtained earlier from Equations 2.23 and 2.25. The effective maximum elastic resistance from the fit (1) is then $R_e = 30{,}000$ psi, the effective plastic stiffness is $K_p = \Delta R/\Delta\varepsilon \approx 2.5 \times 10^6$ psi, and the slope of the M curve in plastic deformation is $\Delta M/\Delta\varepsilon \approx 15$. The chart parameters B and C are then obtained from Equations 2.11 and 2.13:

$$B = \frac{K_p}{K_e} \approx \frac{2.5 \times 10^6}{7.5 \times 10^6} \approx 0.33$$

$$C = \frac{\varepsilon_e}{M_e} \frac{\Delta M}{\Delta \varepsilon} = \frac{0.004}{0.213} 15 \approx 0.26$$

The $B = 0.3$ curve of Figures A.17 and A.18 should be used to obtain $\bar{\varepsilon}_{max} = \varepsilon_{max}/\varepsilon_e$ and $\bar{t}_{max} = t_{max}/T_e$.

For a peak free-field stress $P_{max} = 43{,}500$ psi (3 kilobars), $A = P_{max}/R_e = 43{,}500/30{,}000 = 1.45$. For $\bar{t}_r = 0$ Figure A.17 gives $\bar{\varepsilon}_{max} \approx 7$ and Figure A.18 gives $\bar{t}_{max} \approx 1.1$. Hence, $\varepsilon_{max} = \varepsilon_e \bar{\varepsilon}_{max}$ $\approx 0.004 \times 7 = 0.028$ or 2.8 percent and $t_{max} = T_e \bar{t}_{max} \approx 1.1$ msec $\times 1.1$ ≈ 1.2 msec. Using the average value of Poisson's ratio $\nu = 0.25$, Equation 2.26 gives a compressibility correction factor of 1.5 and a corrected maximum strain of $\varepsilon^c_{max} = 4.2$ percent. Thus for a suddenly applied load ($\bar{t}_r = 0$) and $P_{max} = 43{,}500$ psi, the dynamic strain is more than double the 2 percent design level of maximum strain that has been assumed for the structure.

Figures A.19 through A.24 would be used to determine the structural response if $P(t)$ had a nonzero rise time. In Figures A.23 and A.24 for $\bar{t}_r = 5$ the response is essentially quasi-static. These charts show that for the present example the maximum static strain is less than half the dynamic strain produced by a suddenly applied load.

At the lower stress level $P_{max} = 29{,}000$ psi (2 kilobars), $A = 0.97$. With $\bar{t}_r = 0$ the charts give values of $\bar{\varepsilon}_{max} \approx 3$ and $\bar{t}_{max}$ ≈ 0.8 which yield $\varepsilon_{max} \approx 1.2$ percent and $t_{max} \approx 0.9$ msec. Using $\nu = 0.25$, the corrected maximum strain is $\varepsilon^c_{max} \approx 1.8$ percent, which is within the design level.

APPENDIX A

DESIGN CHARTS

The maximum dynamic response of cylindrical underground structures subjected to the long-duration ground shock loading of nuclear explosions is summarized in Figures A.1 through A.48. The maximum normalized diametrical strain $\bar{\varepsilon}_{max} = \varepsilon_{max}/\varepsilon_e$ and the dimensionless time of maximum strain $\bar{t}_{max} = t_{max}/T_e$ are given in the charts for the characteristic parameters A , B , C , and $\bar{t}_r$ where:

$T_e = 2\pi\sqrt{M_e/K_e}$ = effective elastic period

$A = P_{max}/R_e$ = dimensionless maximum applied load

$B = K_p/K_e$ = dimensionless plastic stiffness

$C = (\varepsilon_e/M_e)(\Delta M/\Delta\varepsilon)$ = dimensionless rate of change of effective mass in plastic deformation

$\bar{t}_r = t_r/T_e$ = normalized rise time of applied load

The material properties needed to determine the chart parameters are illustrated in Figure 2.1; an example using the charts is given in Chapter 3. Charts are included in this appendix for normalized rise times ranging from $\bar{t}_r = 0$ for a suddenly applied load to $\bar{t}_r = 2$ or 5 where the structural response is essentially quasi-static. On the figures for $\bar{t}_r = 2$ or 5 some of the $\bar{t}_{max}$ curves for the larger values of B have been smoothed to produce readable "average" curves which deviate from the original ones by less than about one fourth.

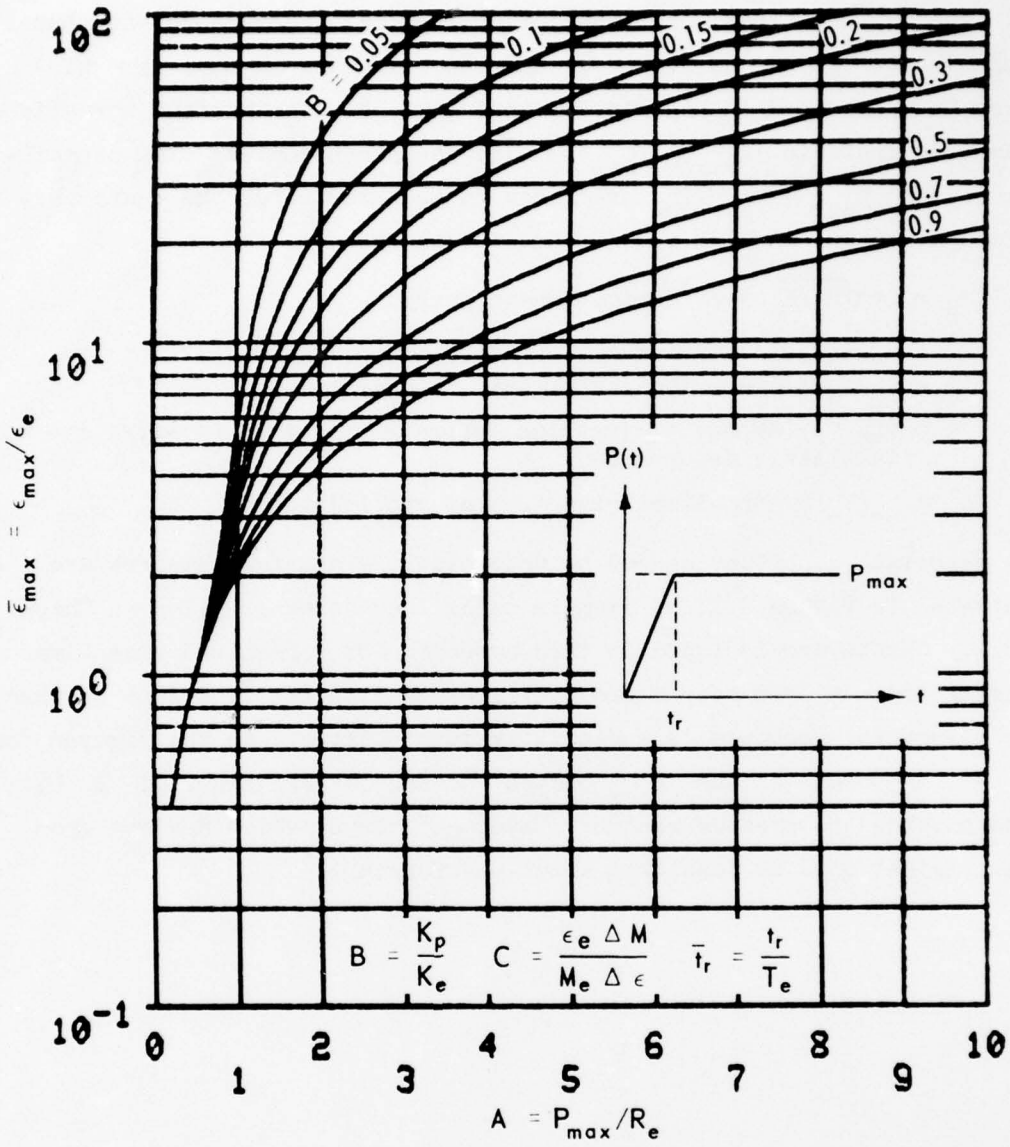

Figure A.1. $\bar{\epsilon}_{max}$ curves for tunnel-liner systems with $C = 0$ and $\bar{t}_r = 0$.

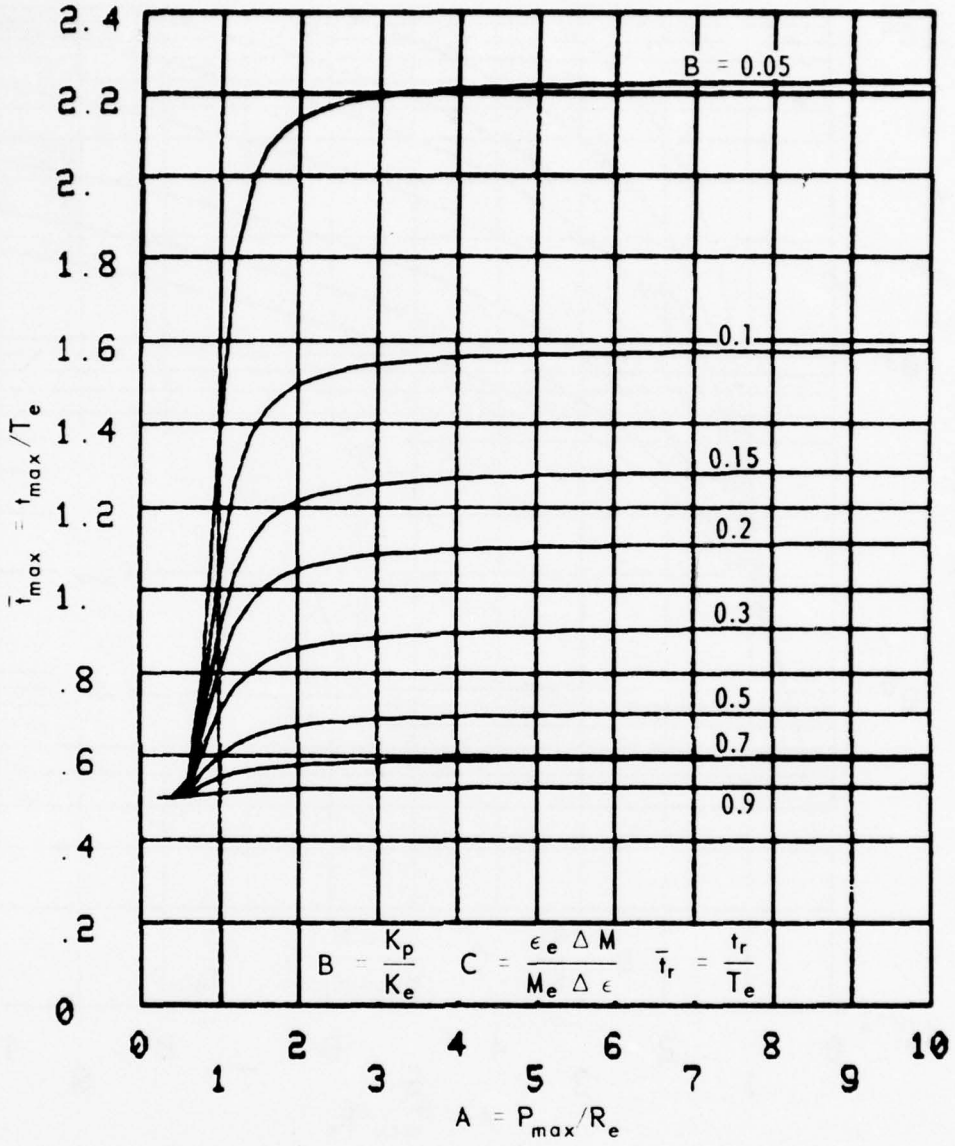

Figure A.2. $\bar{t}_{max}$ curves for tunnel-liner systems with $C = 0$ and $\bar{t}_r = 0$.

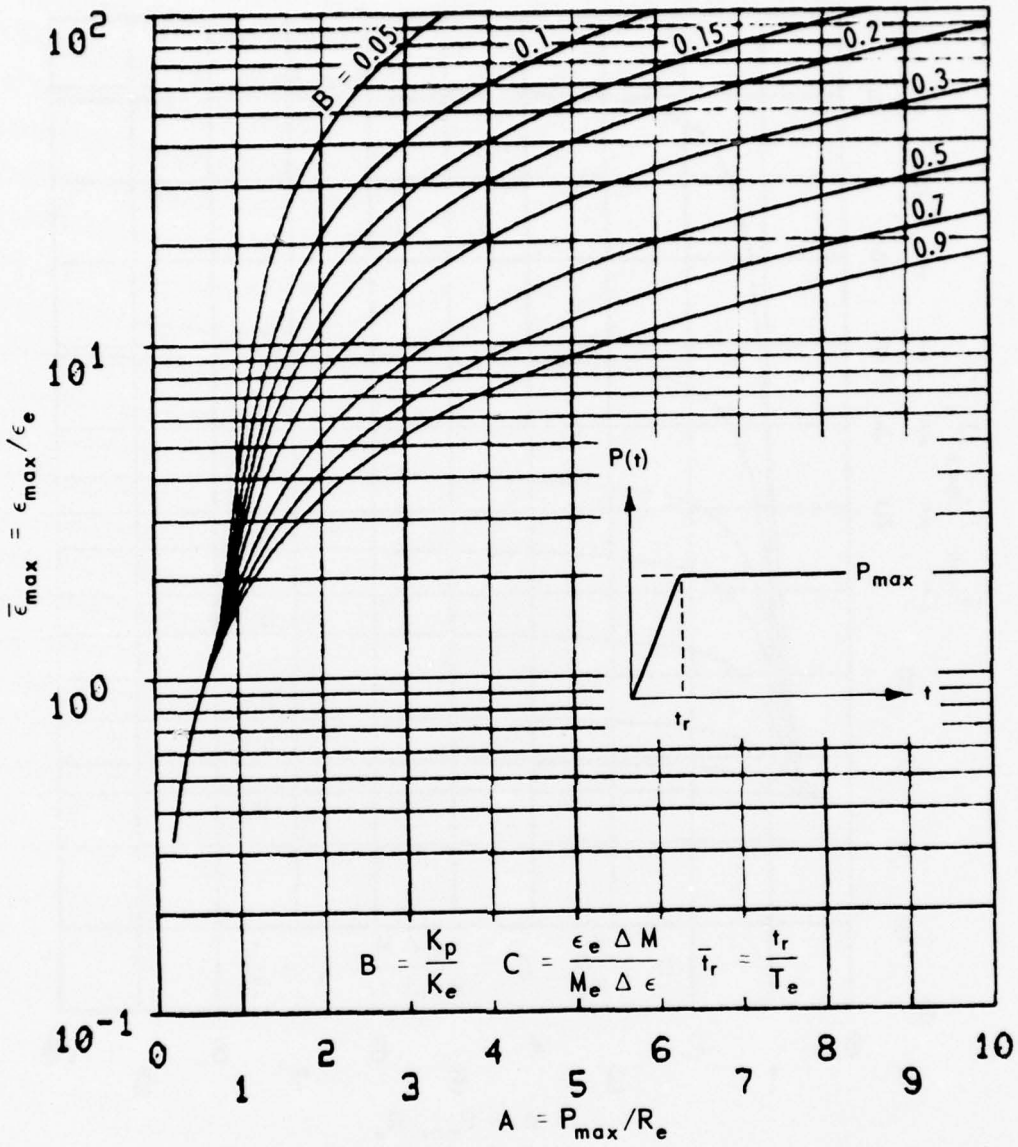

Figure A.3. $\bar{\epsilon}_{max}$ curves for tunnel-liner systems with $C = 0$ and $\bar{t}_r = 0.5$.

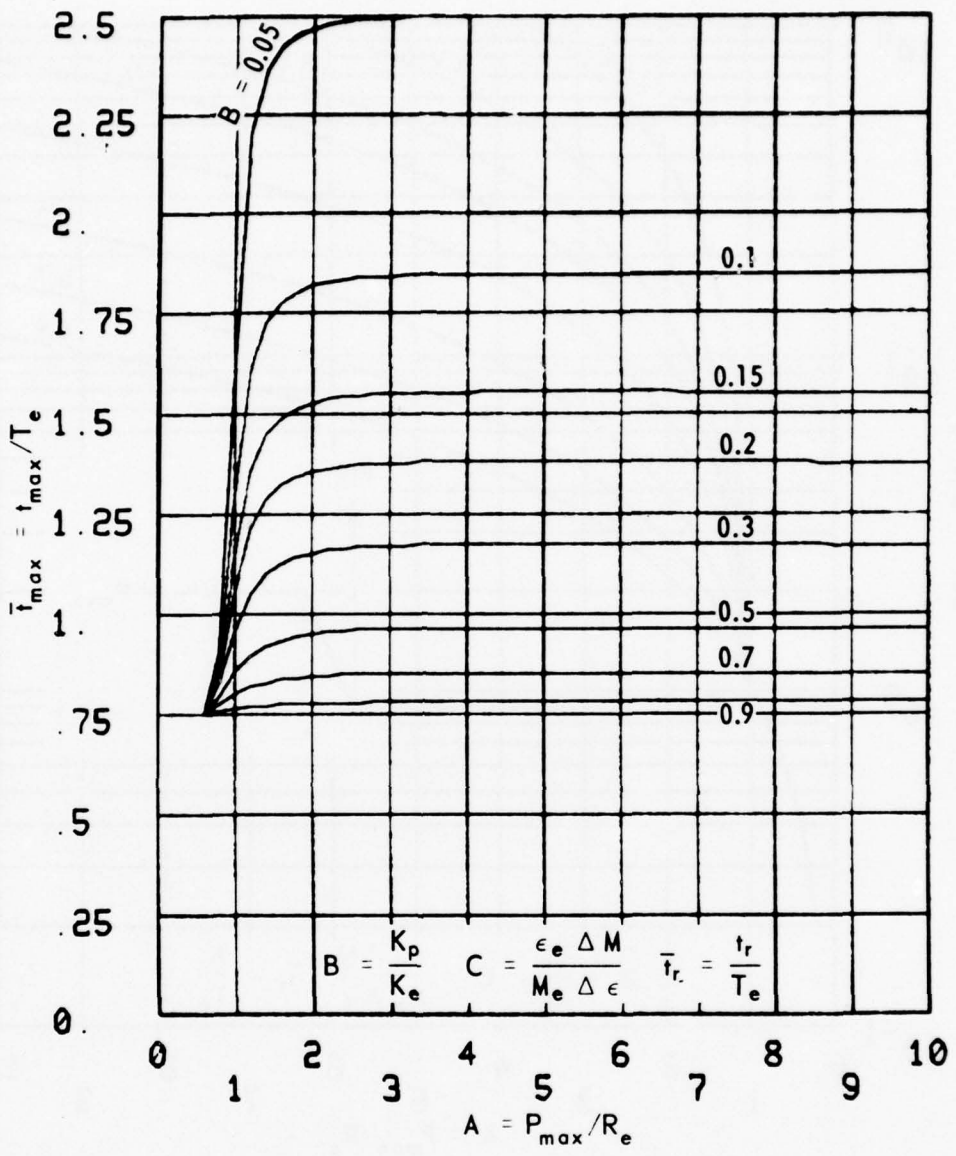

Figure A.4. $\bar{t}_{max}$ curves for tunnel-liner systems with C = 0 and $\bar{t}_r = 0.5$.

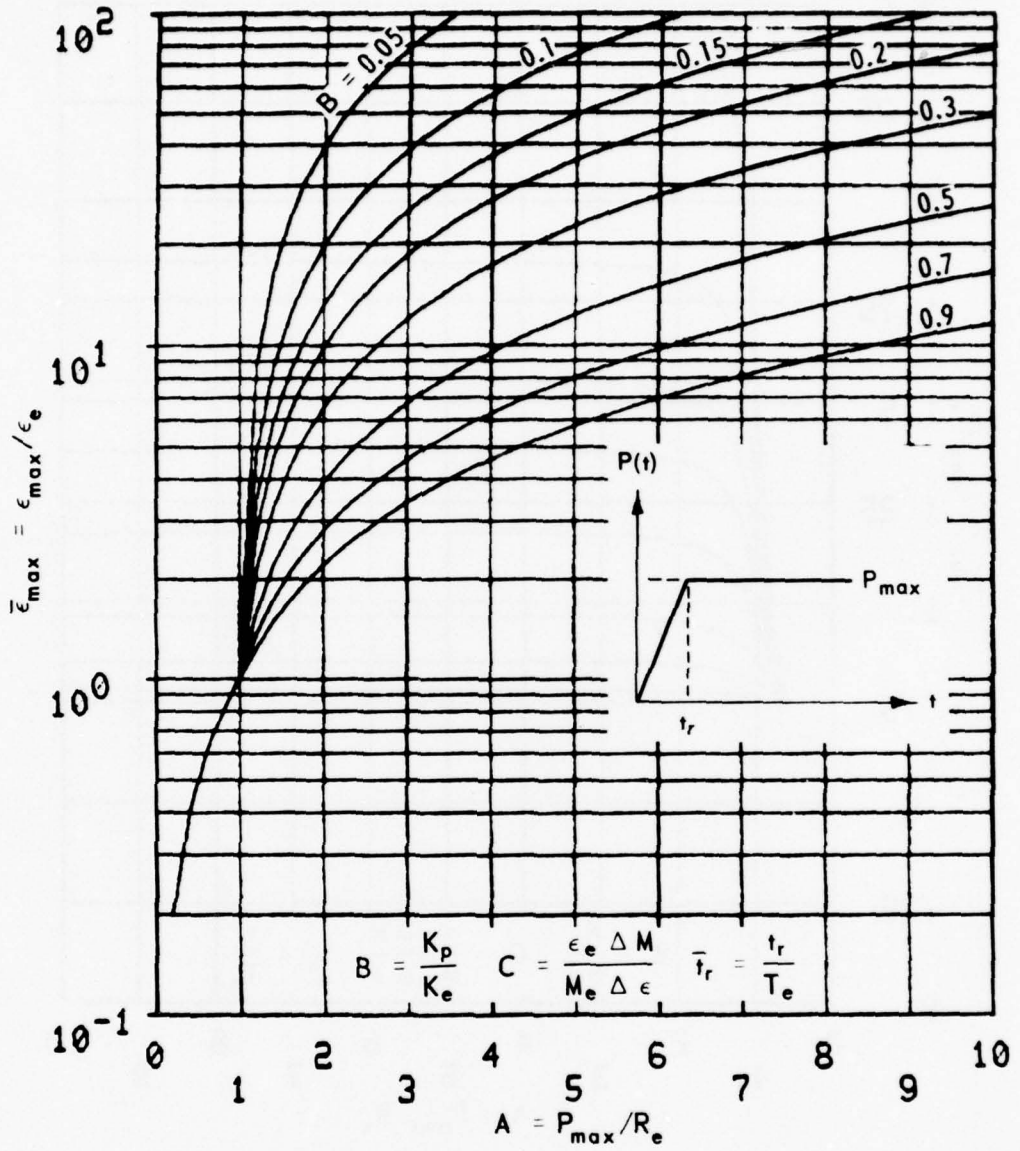

Figure A.5. $\bar{\varepsilon}_{max}$ curves for tunnel-liner systems with C = 0 and $\bar{t}_r = 1$.

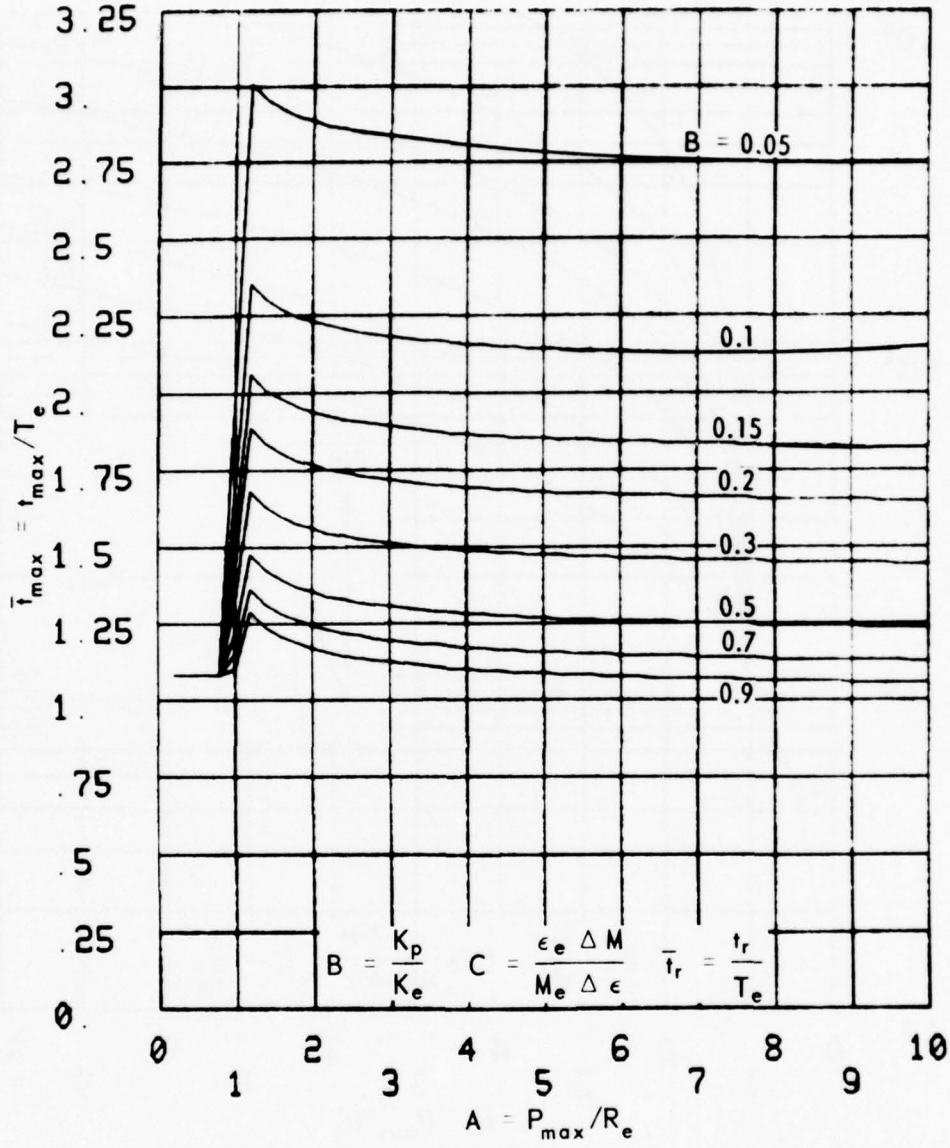

Figure A.6. $\bar{t}_{max}$ curves for tunnel-liner systems with $C = 0$ and $\bar{t}_r = 1$.

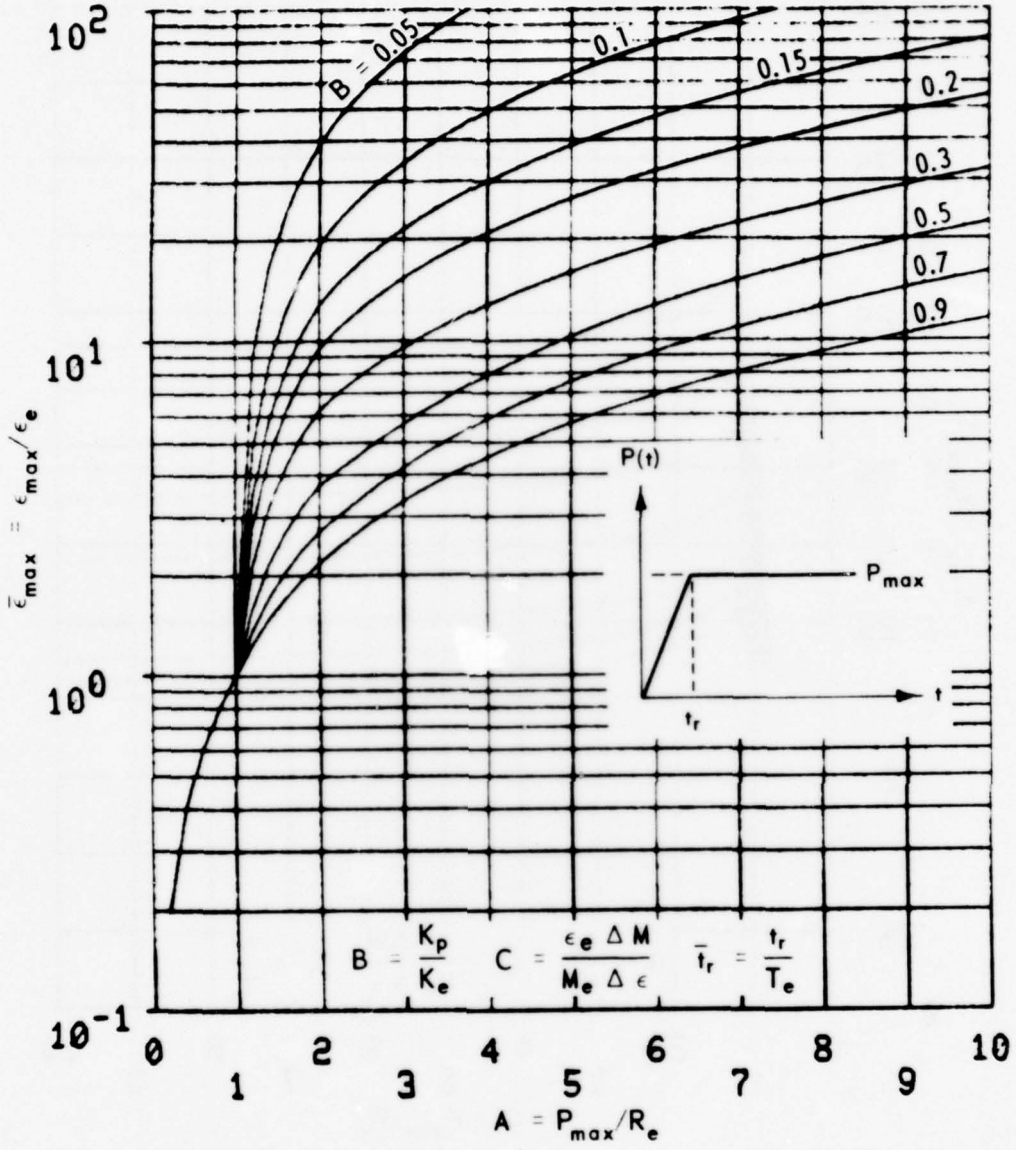

Figure A.7. $\bar{\epsilon}_{max}$ curves for tunnel-liner systems with $C = 0$ and $\bar{t}_r = 2$.

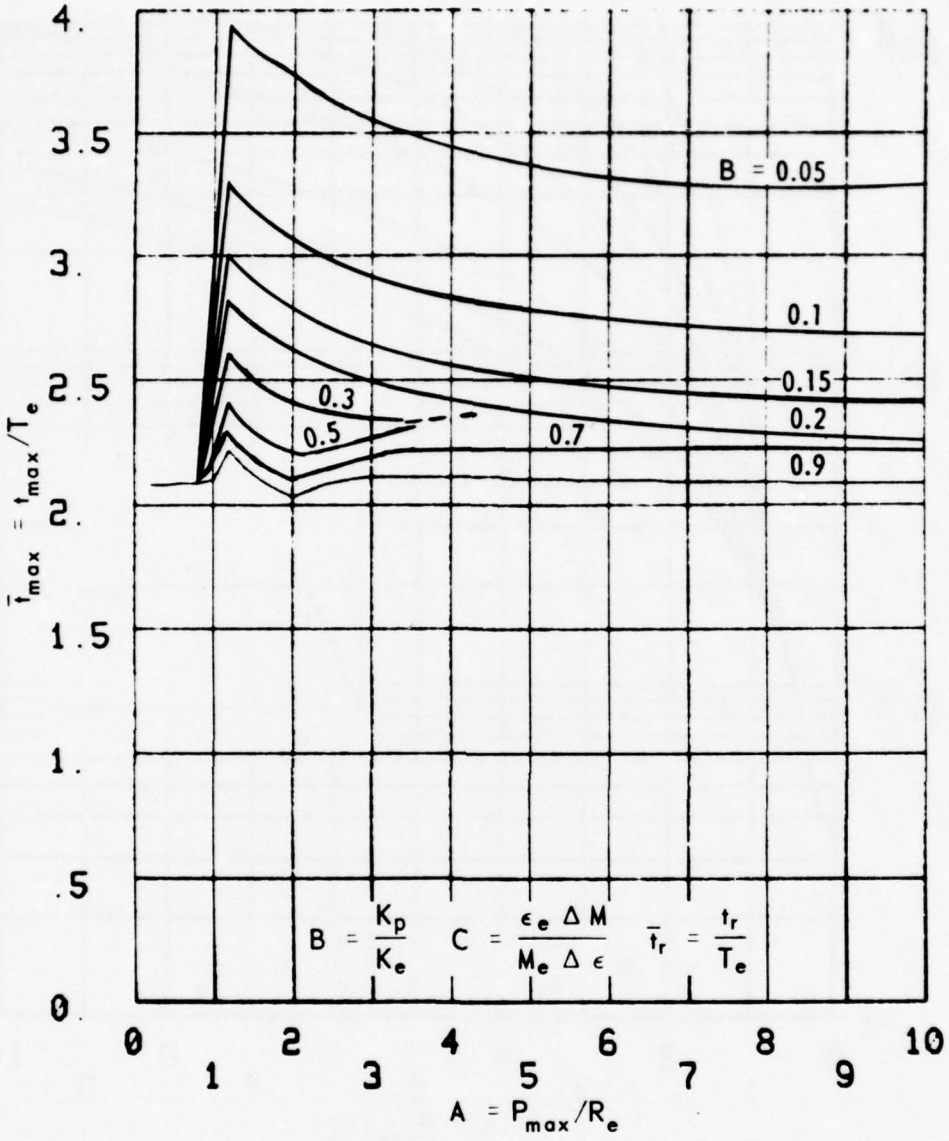

Figure A.8. $\bar{t}_{max}$ curves for tunnel-liner systems with $C = 0$ and $\bar{t}_r = 2$.

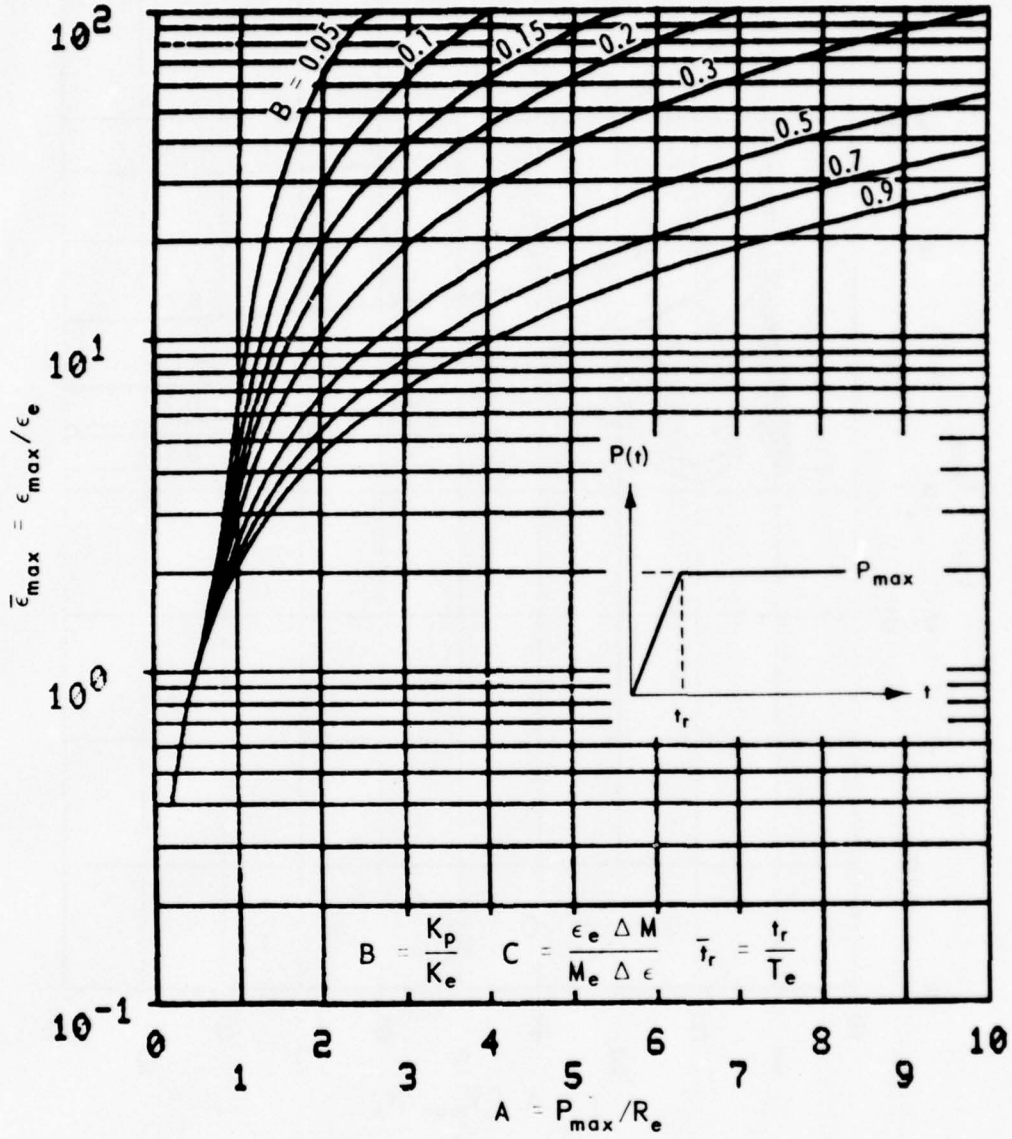

Figure A.9. $\bar{\epsilon}_{max}$ curves for tunnel-liner systems with C = 0.1 and $\bar{t}_r = 0$.

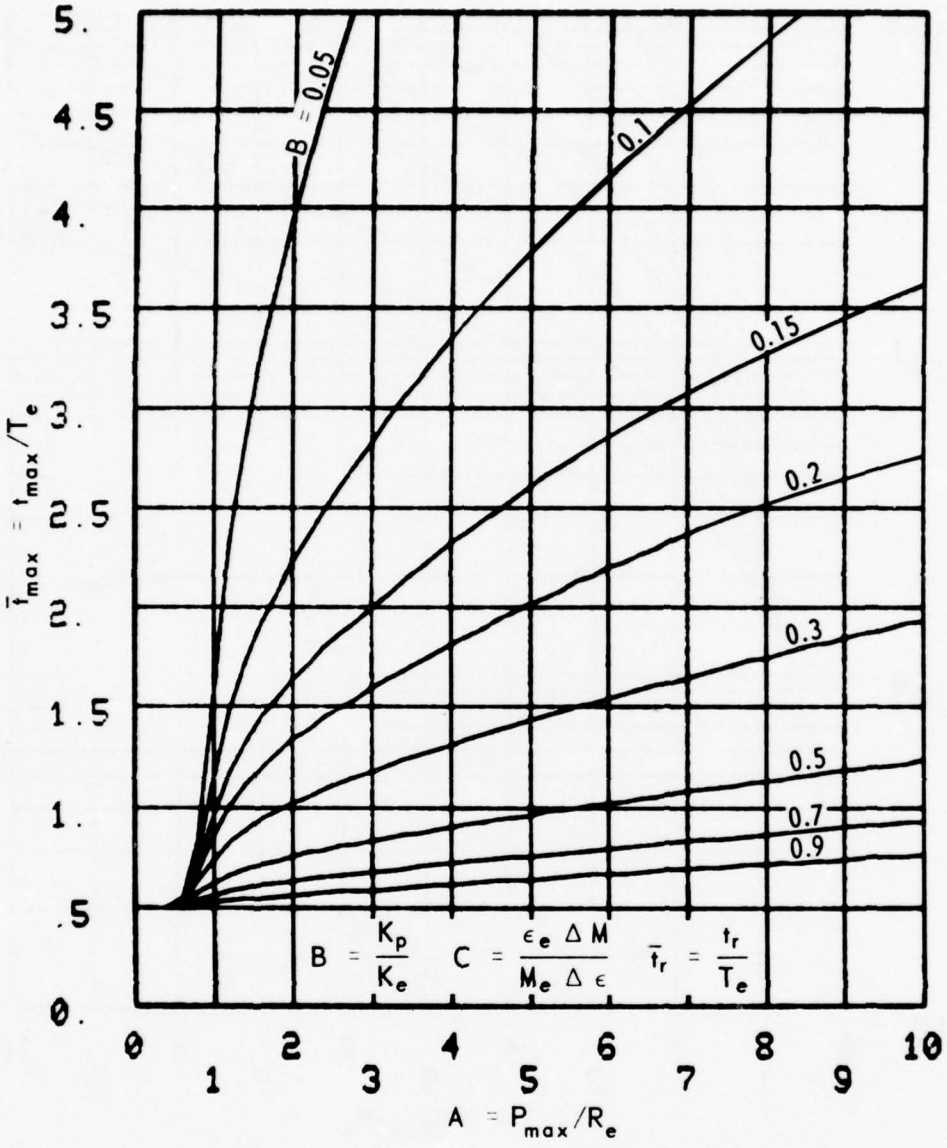

Figure A.10. $\bar{t}_{max}$ curves for tunnel-liner systems with $C = 0.1$ and $\bar{t}_r = 0$.

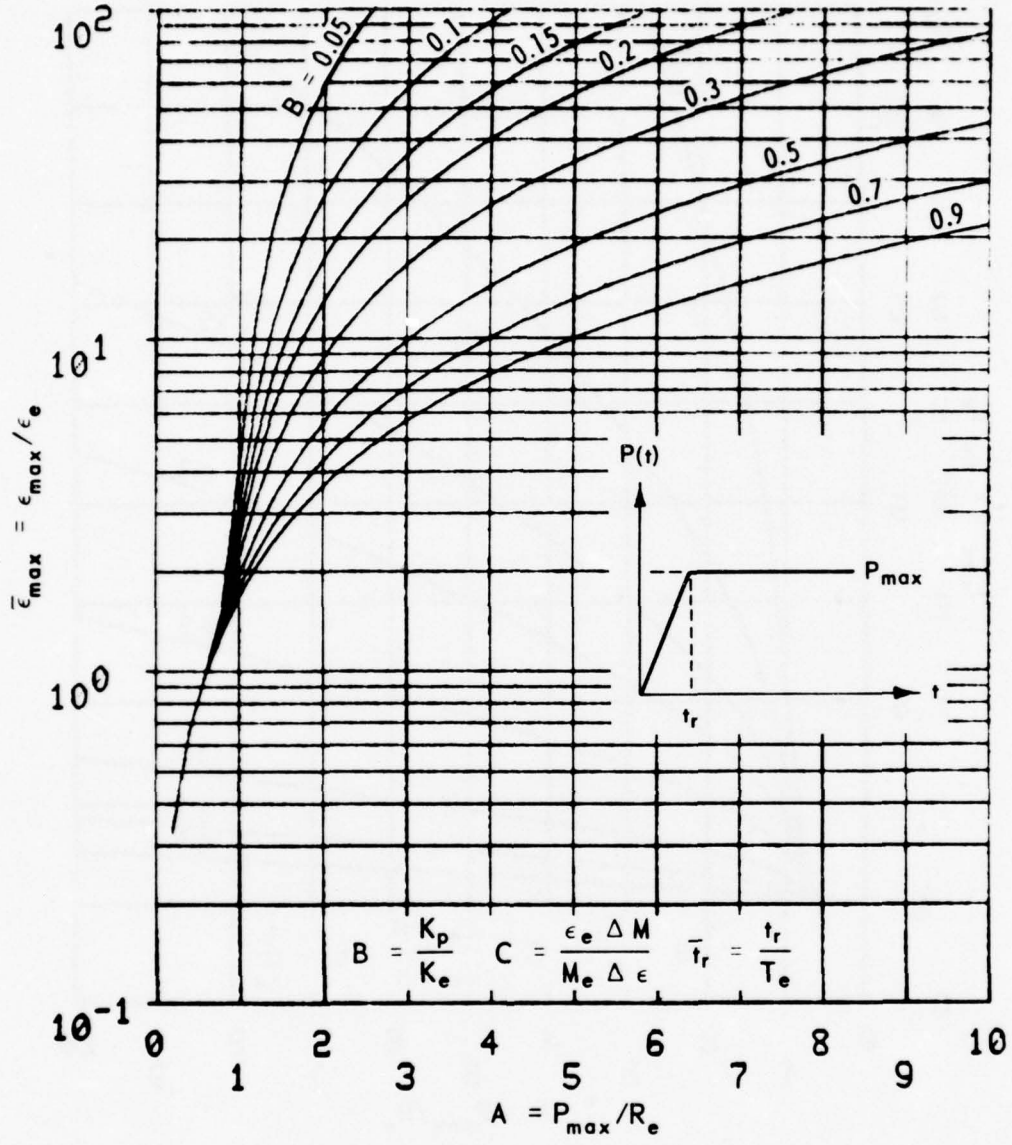

Figure A.11. $\bar{\epsilon}_{max}$ curves for tunnel-liner systems with C = 0.1 and $\bar{t}_r = 0.5$.

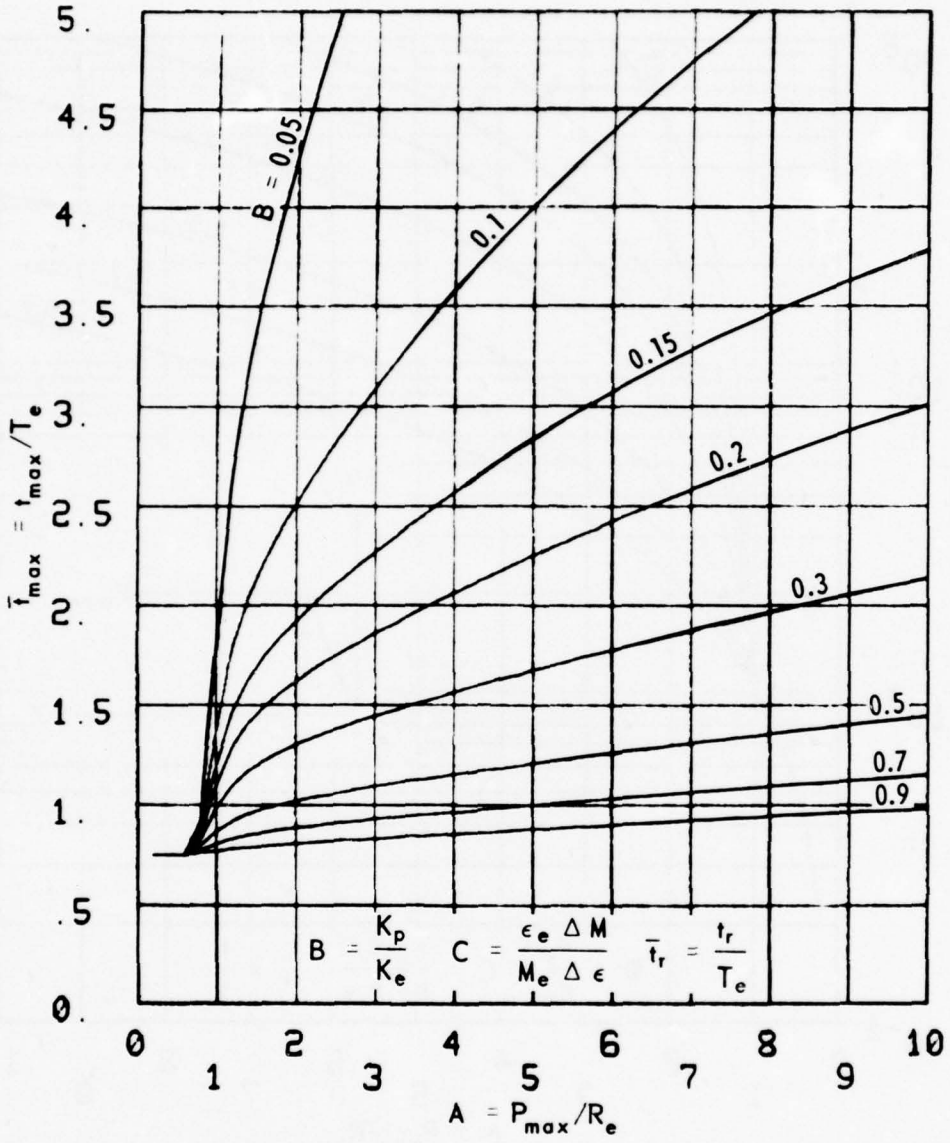

Figure A.12. $\bar{t}_{max}$ curves for tunnel-liner systems with $C = 0.1$ and $\bar{t}_r = 0.5$.

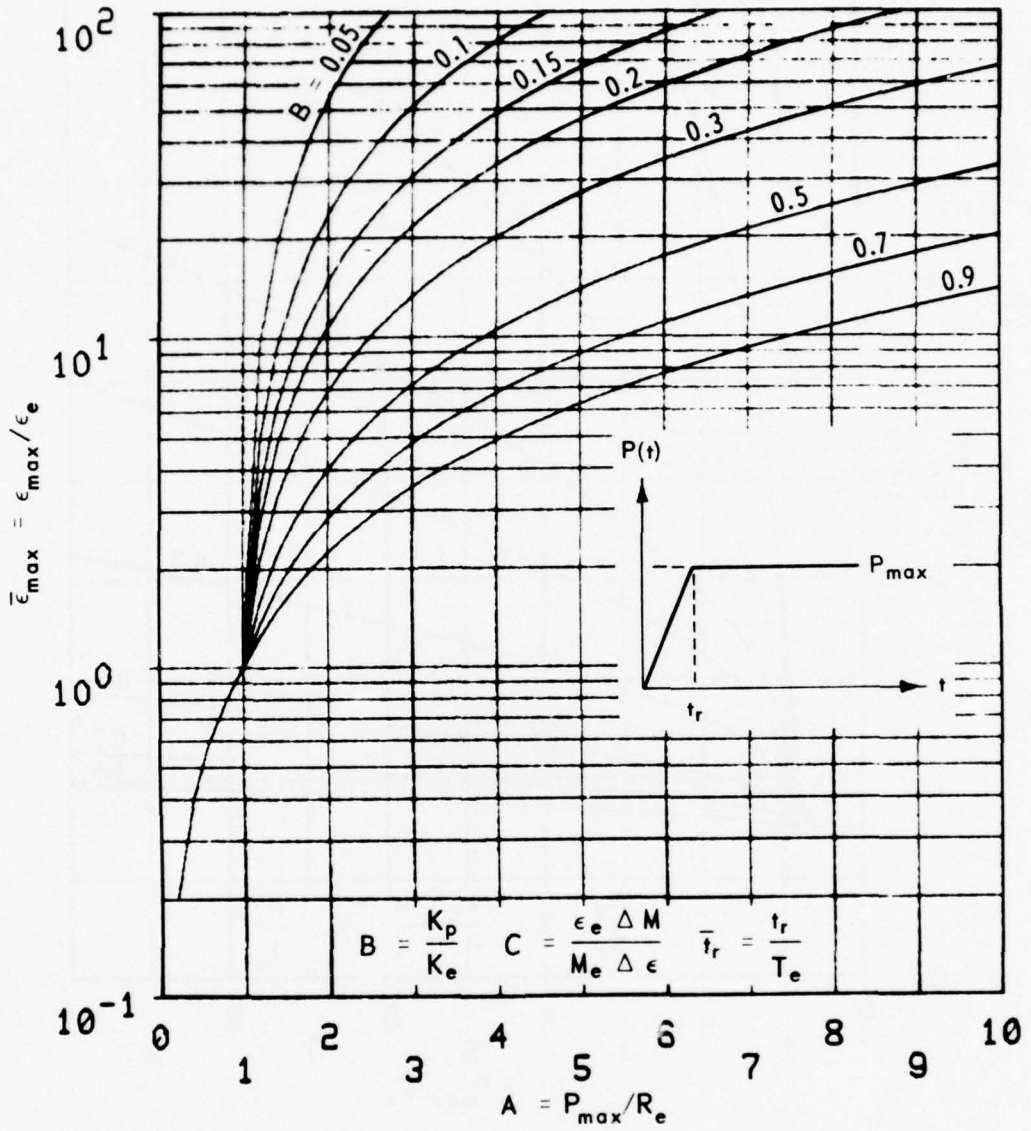

Figure A.13. $\bar{\epsilon}_{max}$ curves for tunnel-liner systems with $C = 0.1$ and $\bar{t}_r = 1$.

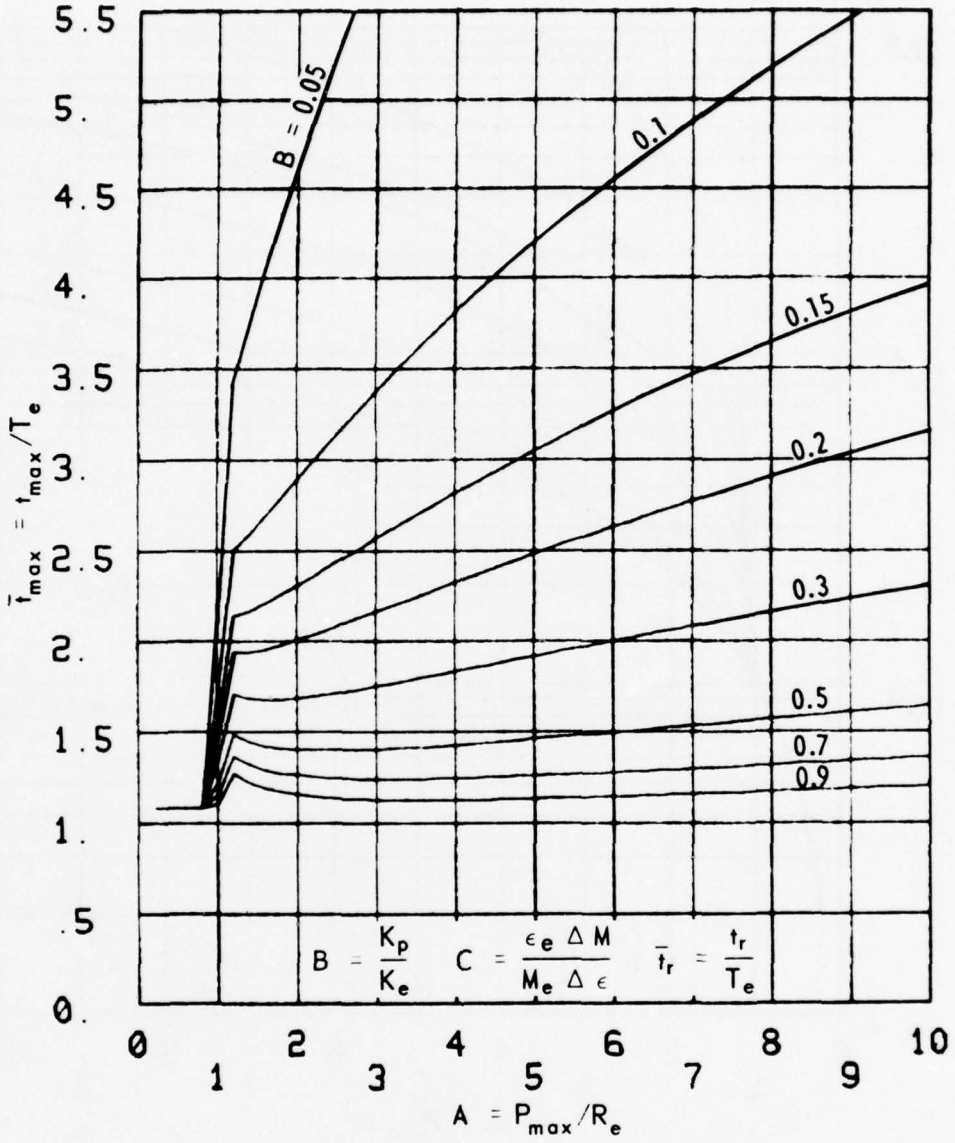

Figure A.14. $\bar{t}_{max}$ curves for tunnel-liner systems with C = 0.1 and $\bar{t}_r = 1$.

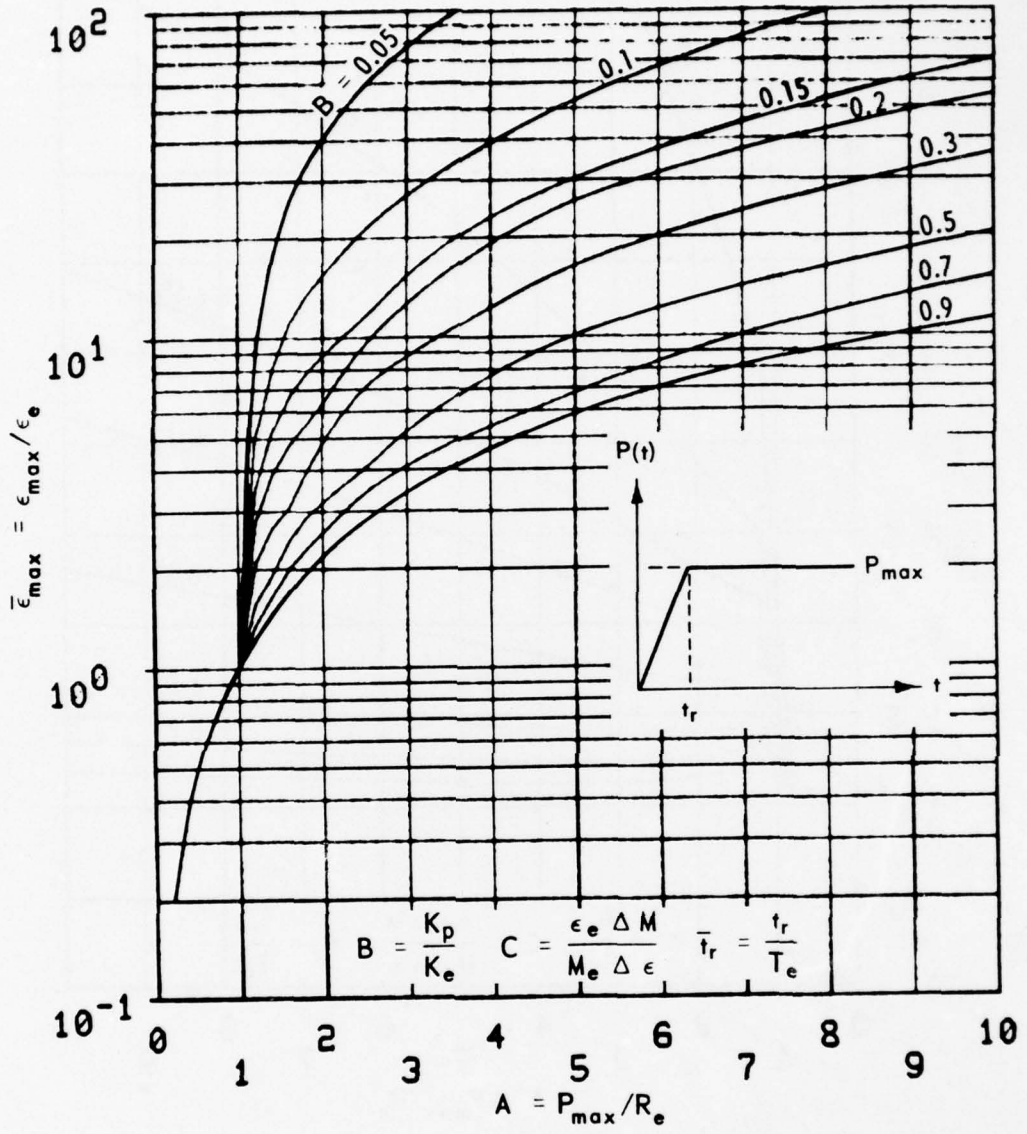

Figure A.15. $\bar{\epsilon}_{max}$ curves for tunnel-liner systems with C = 0.1 and $\bar{t}_r = 5$.

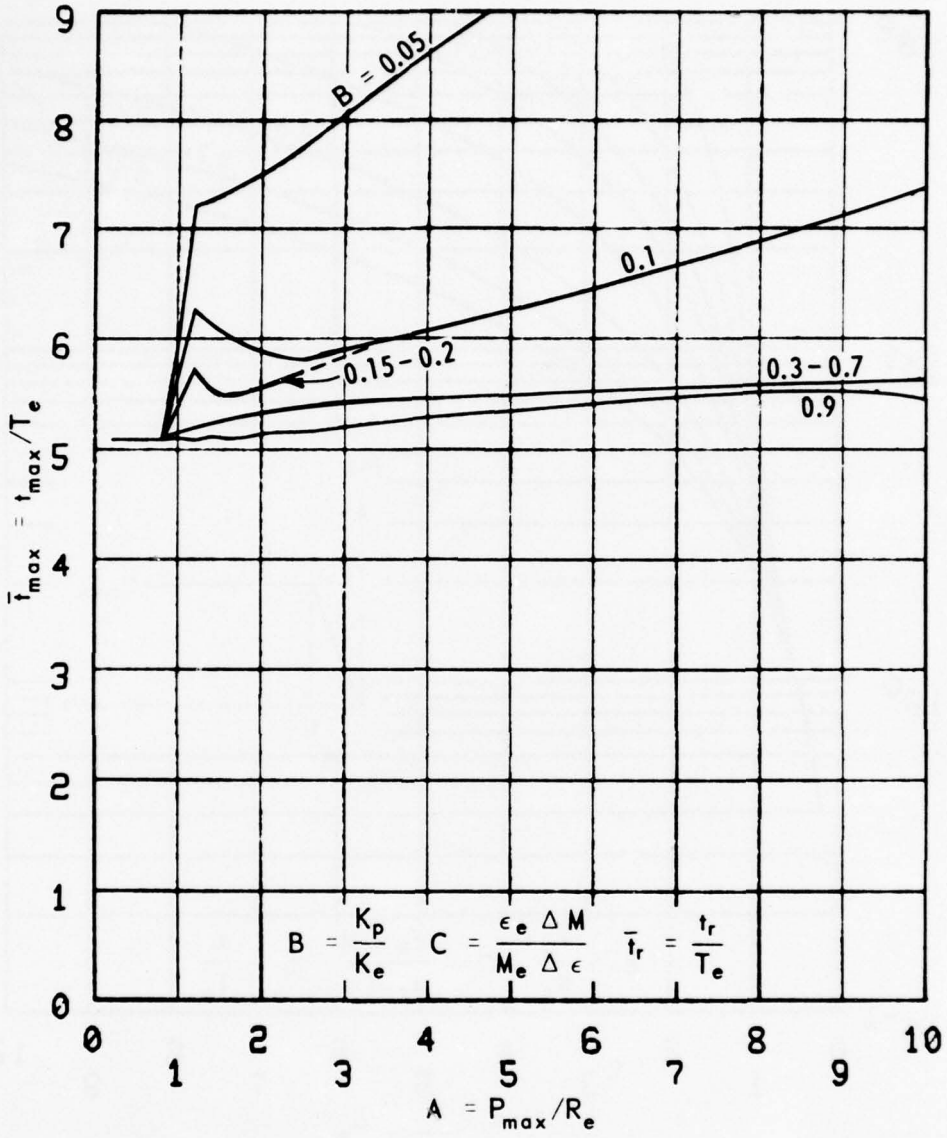

Figure A.16. $\bar{t}_{max}$ curves for tunnel-liner systems with $C = 0.1$ and $\bar{t}_r = 5$.

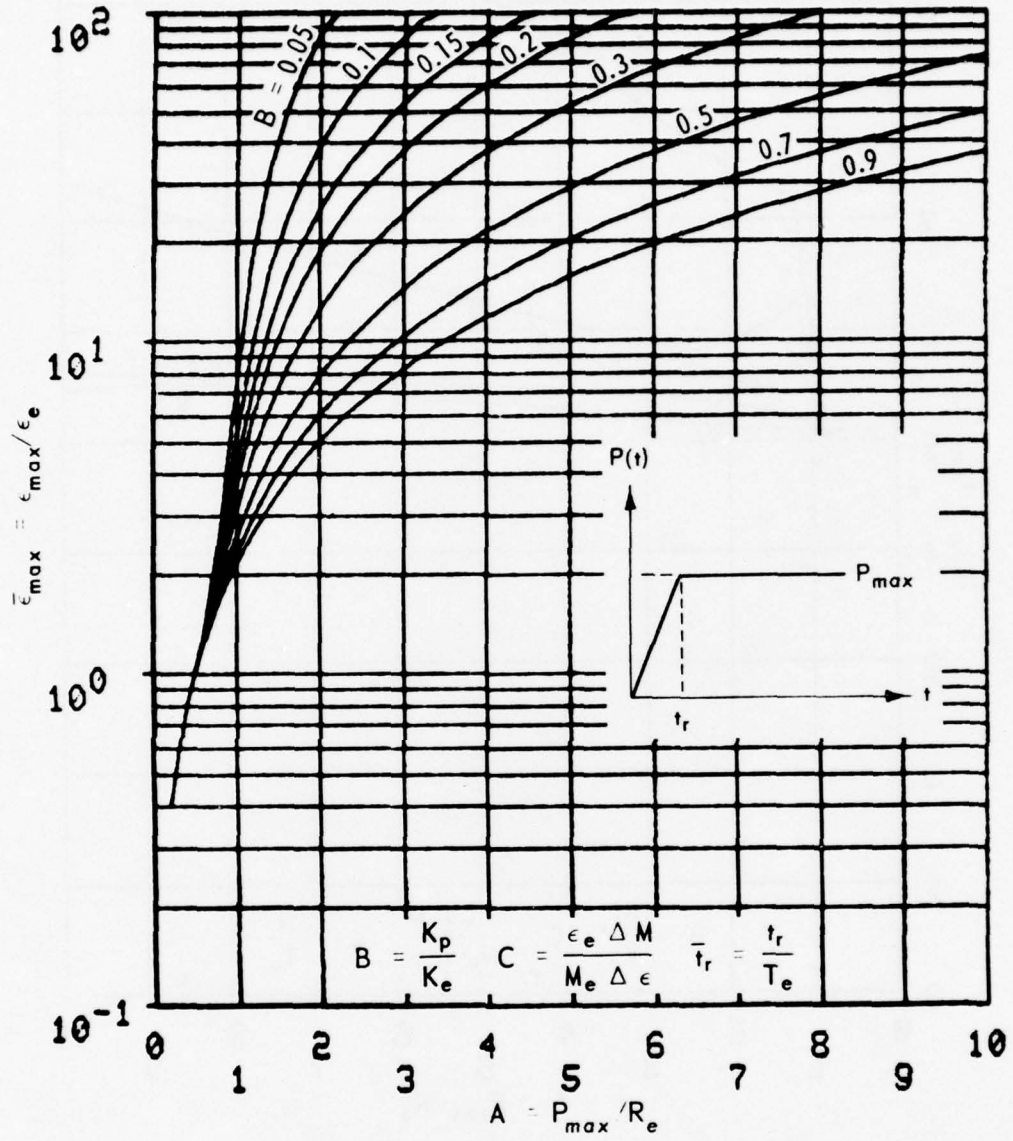

Figure A.17. $\bar{\epsilon}_{max}$ curves for tunnel-liner systems with C = 0.3 and $\bar{t}_r = 0$.

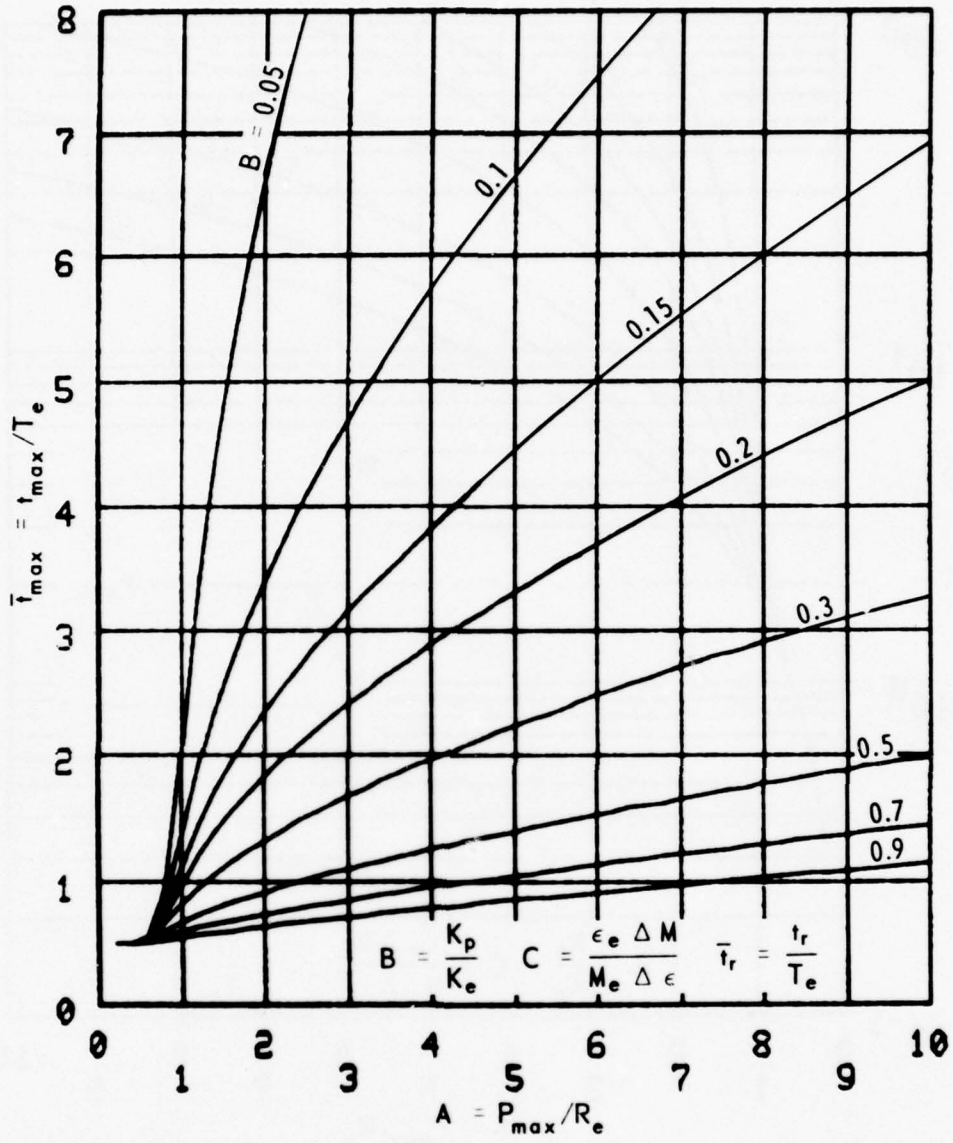

Figure A.18. $\bar{t}_{max}$ curves for tunnel-liner systems with $C = 0.3$ and $\bar{t}_r = 0$.

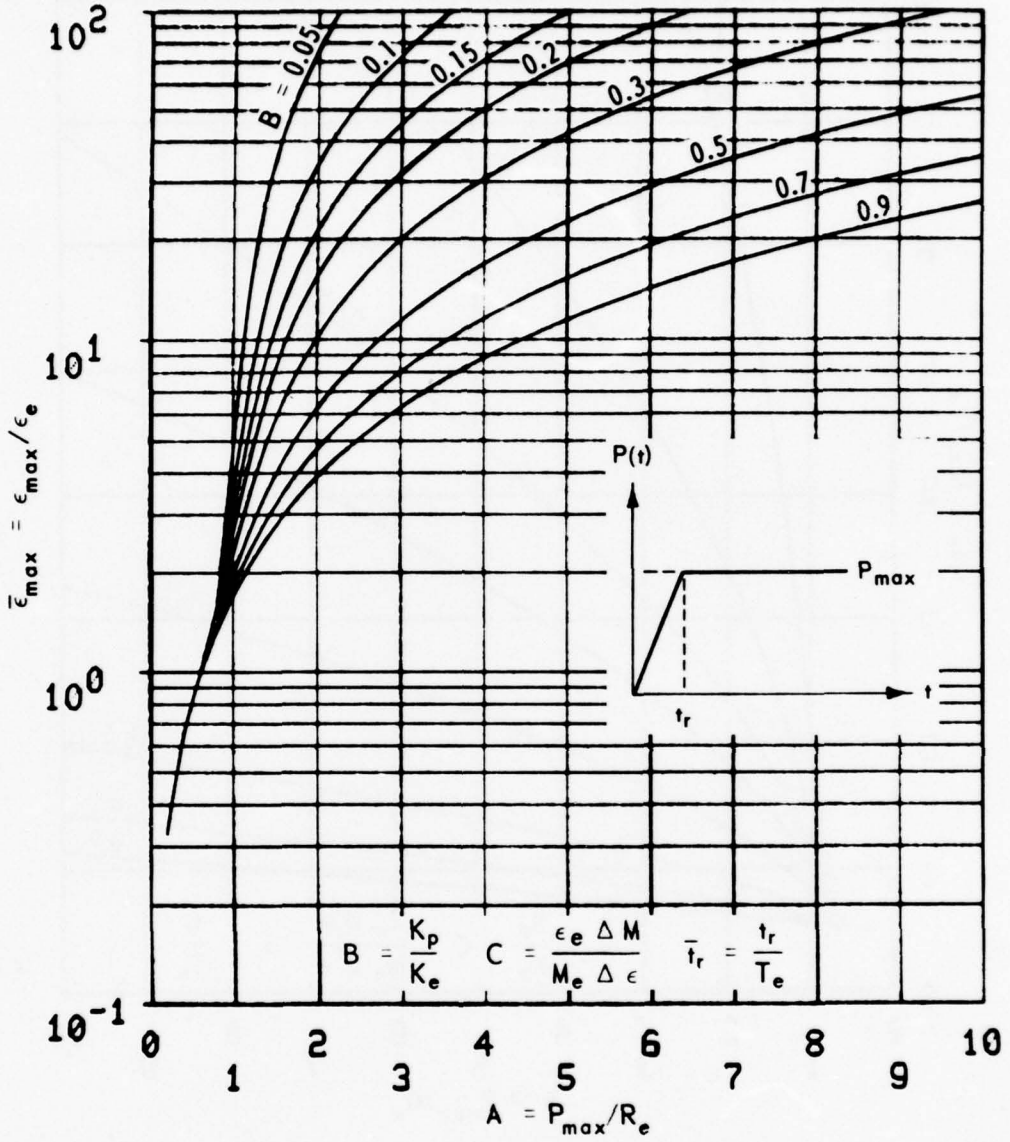

Figure A.19. $\bar{\epsilon}_{max}$ curves for tunnel-liner systems with $C = 0.3$ and $\bar{t}_r = 0.5$.

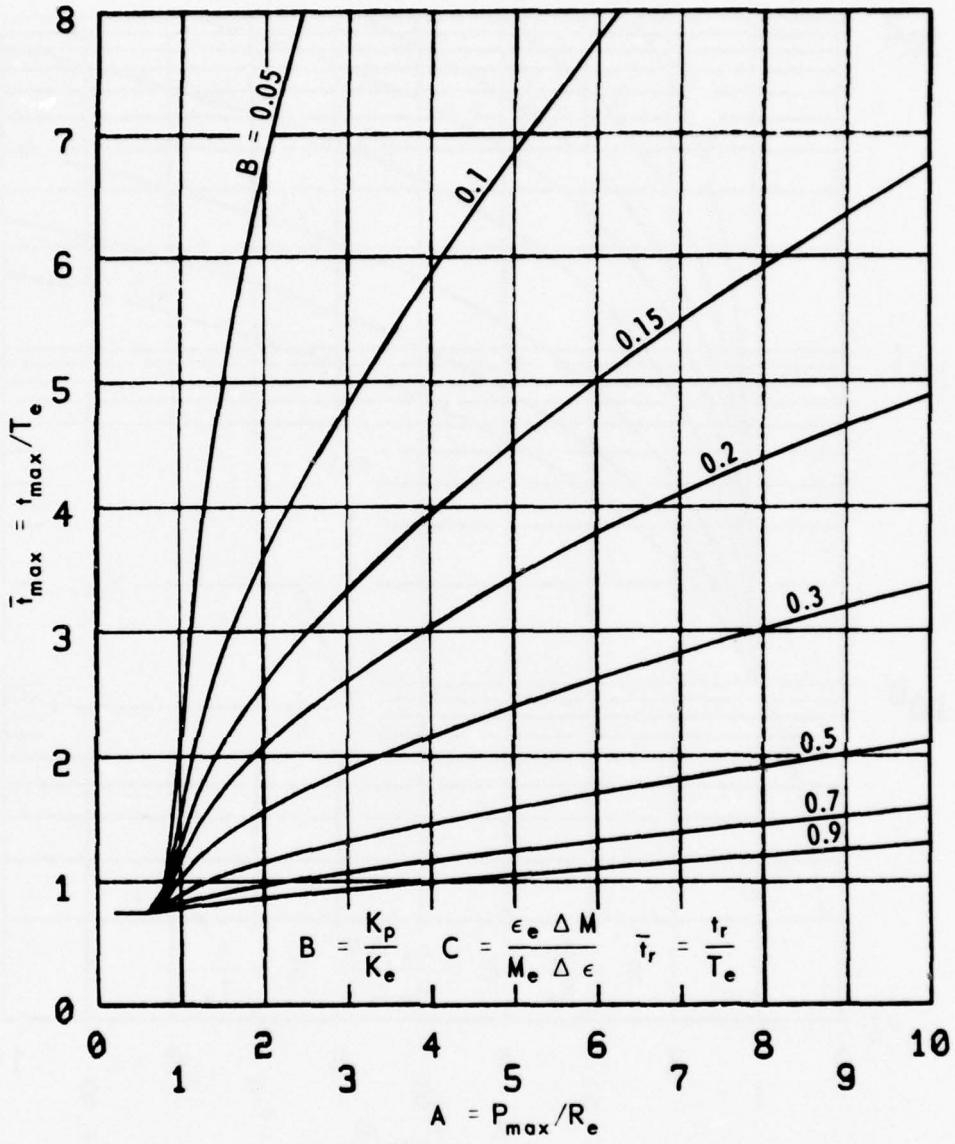

Figure A.20. $\bar{t}_{max}$ curves for tunnel-liner systems with $C = 0.3$ and $\bar{t}_r = 0.5$.

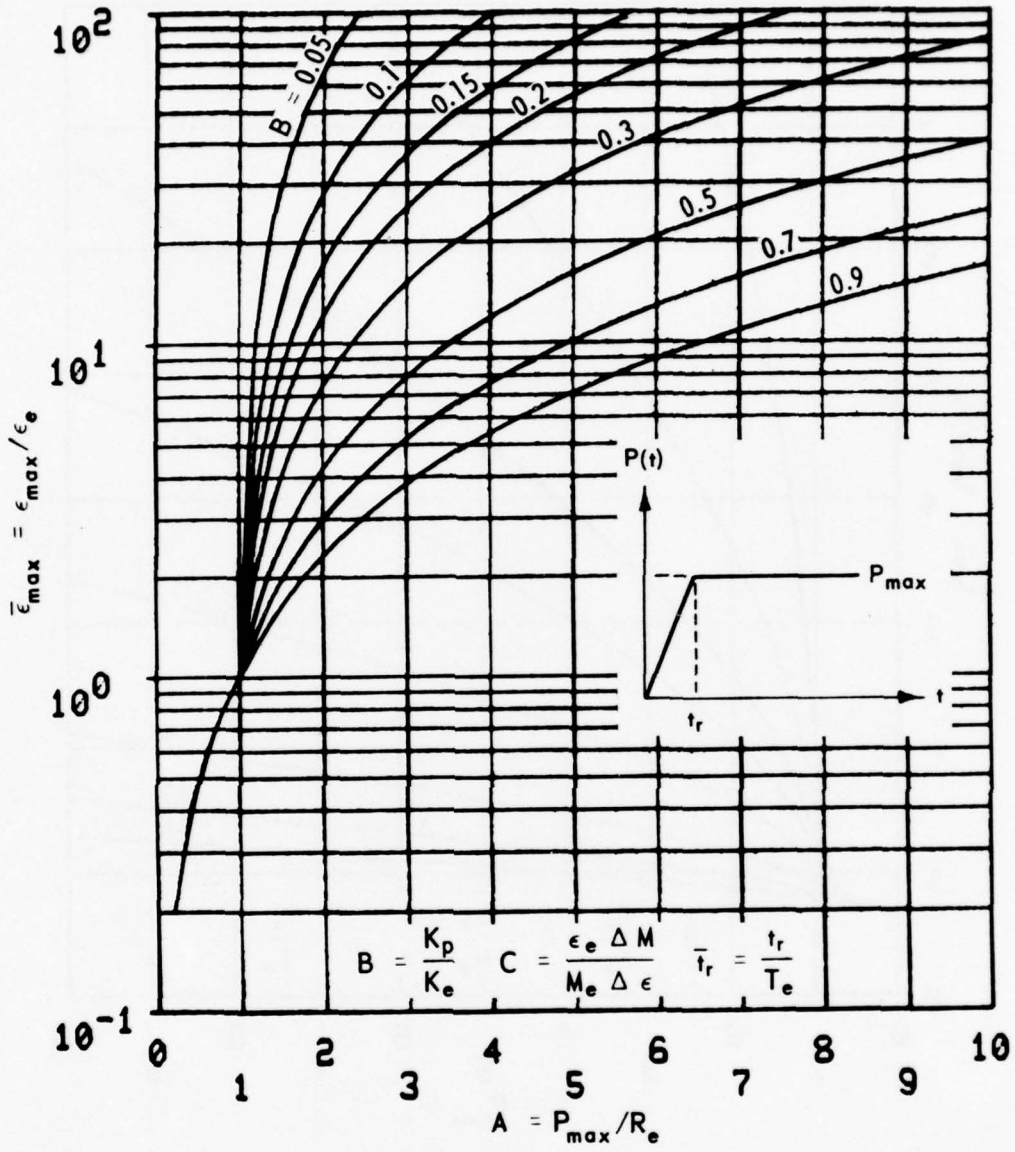

Figure A.21. $\bar{\epsilon}_{max}$ curves for tunnel-liner systems with C = 0.3 and $\bar{t}_r = 1$.

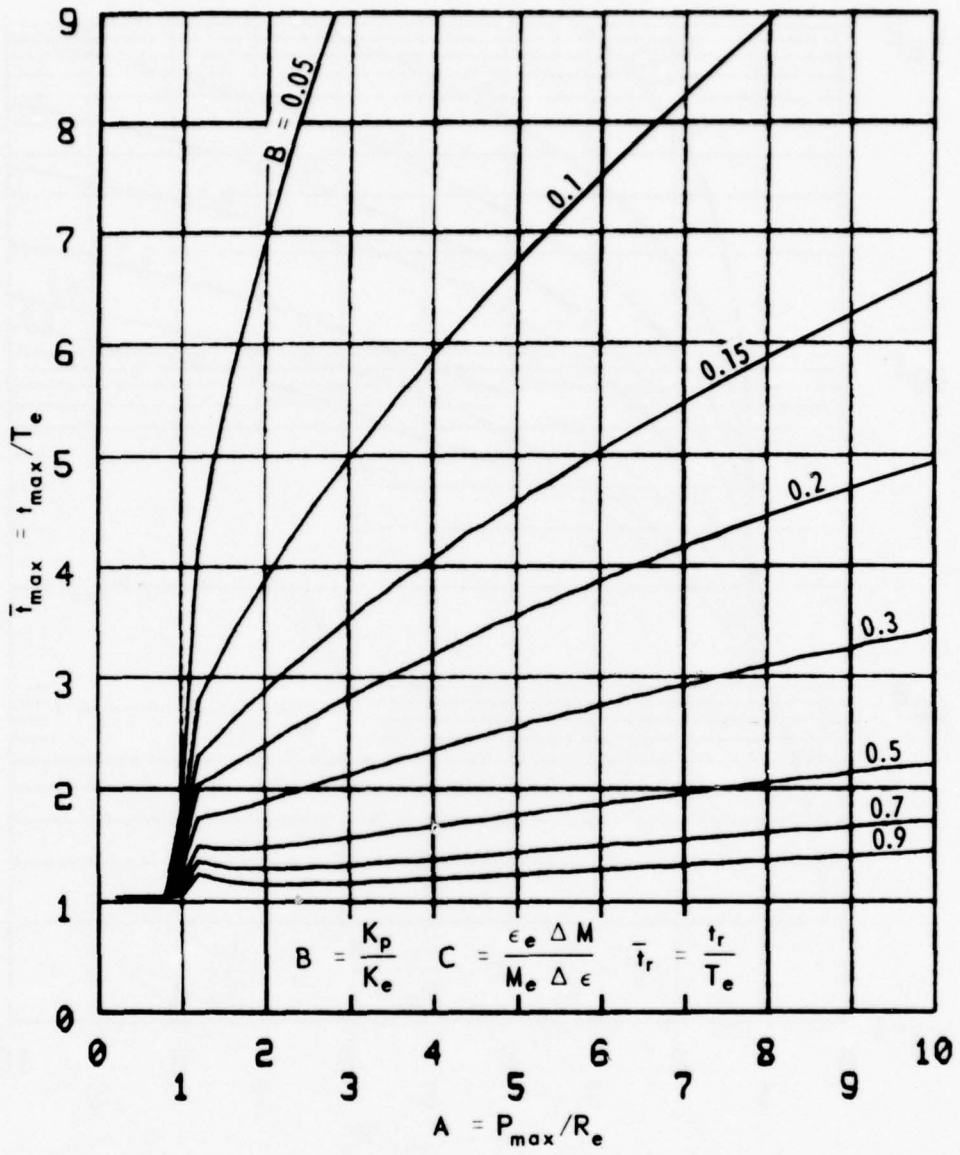

Figure A.22. $\bar{t}_{max}$ curves for tunnel-liner systems with $C = 0.3$ and $\bar{t}_r = 1$.

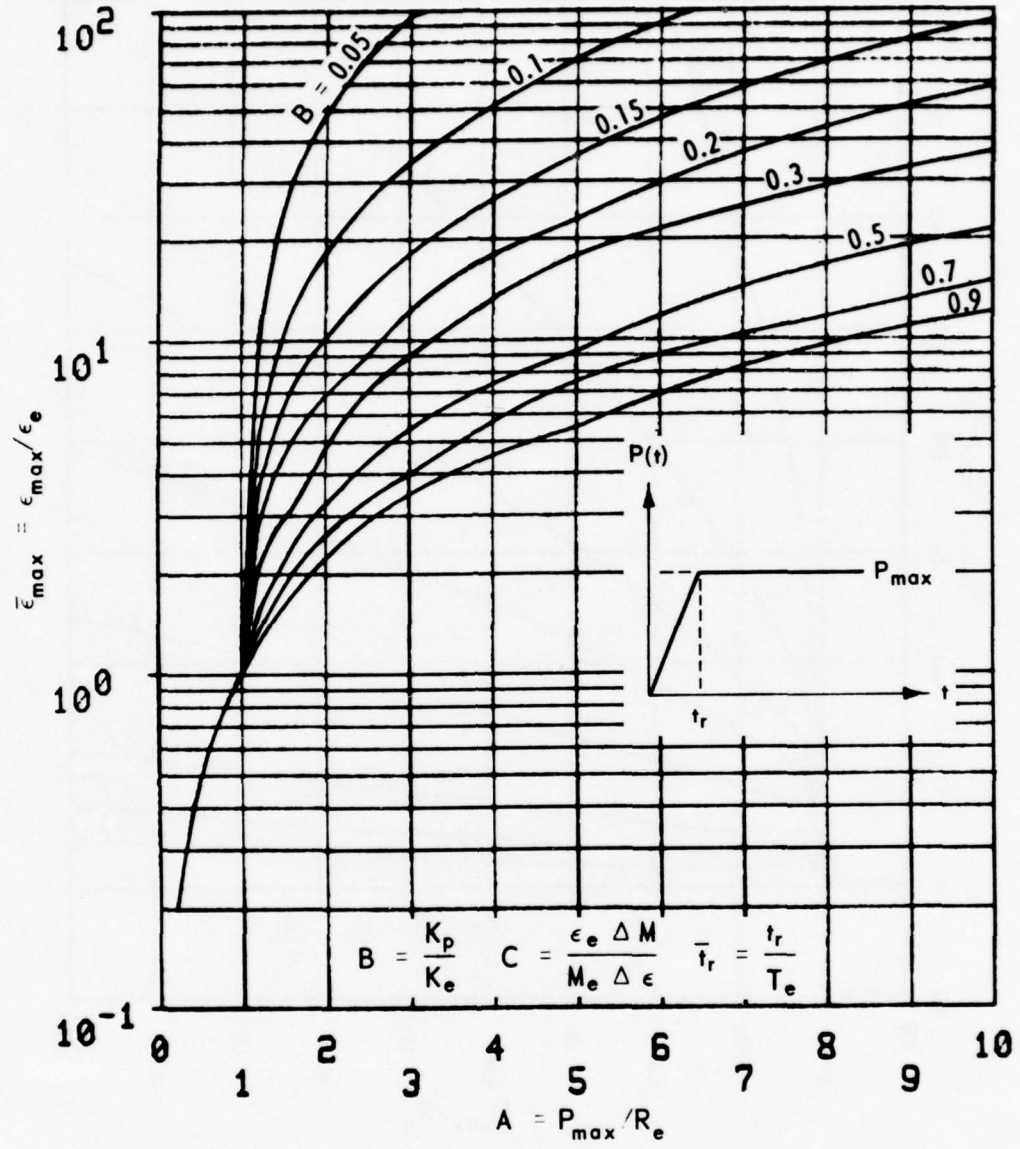

Figure A.23. $\bar{\epsilon}_{max}$ curves for tunnel-liner systems with C = 0.3 and $\bar{t}_r = 5$.

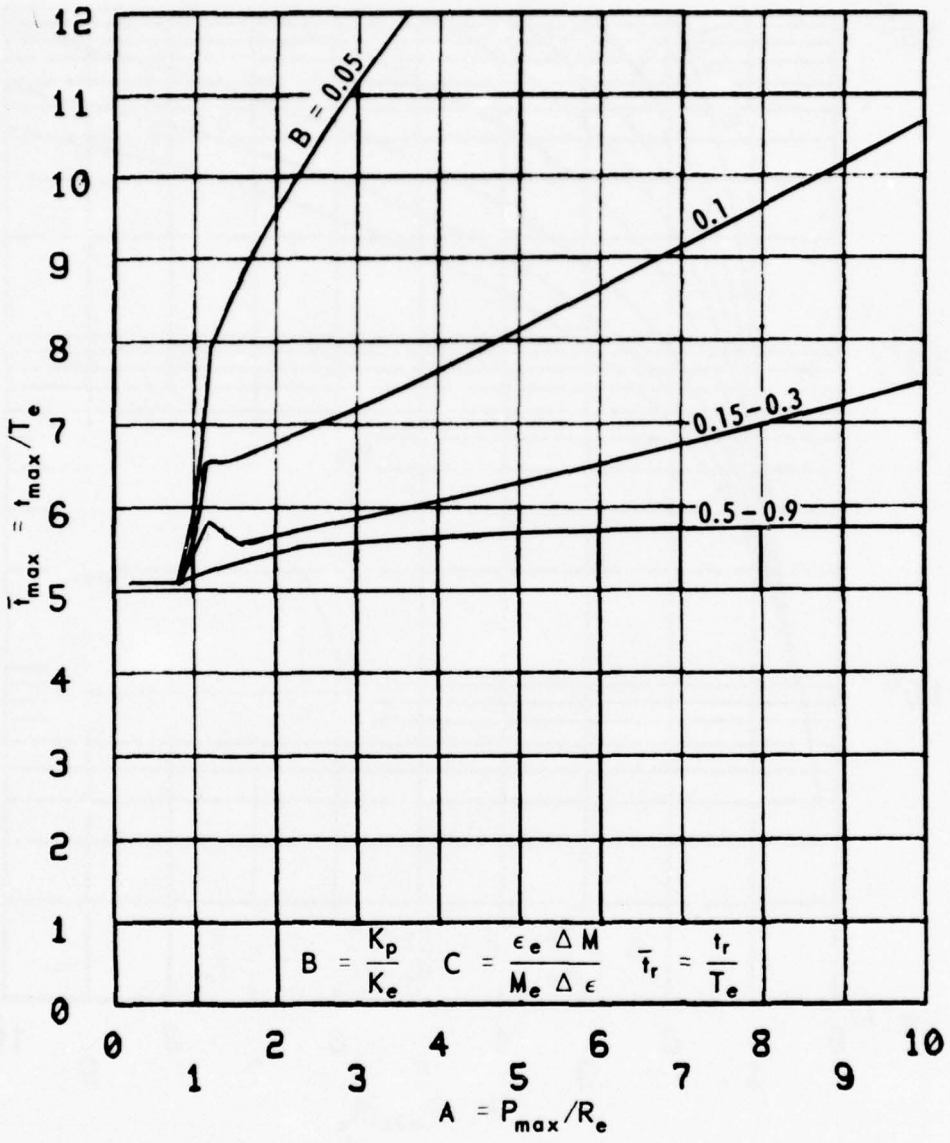

Figure A.24. $\bar{t}_{max}$ curves for tunnel-liner systems with C = 0.3 and $\bar{t}_r = 5$.

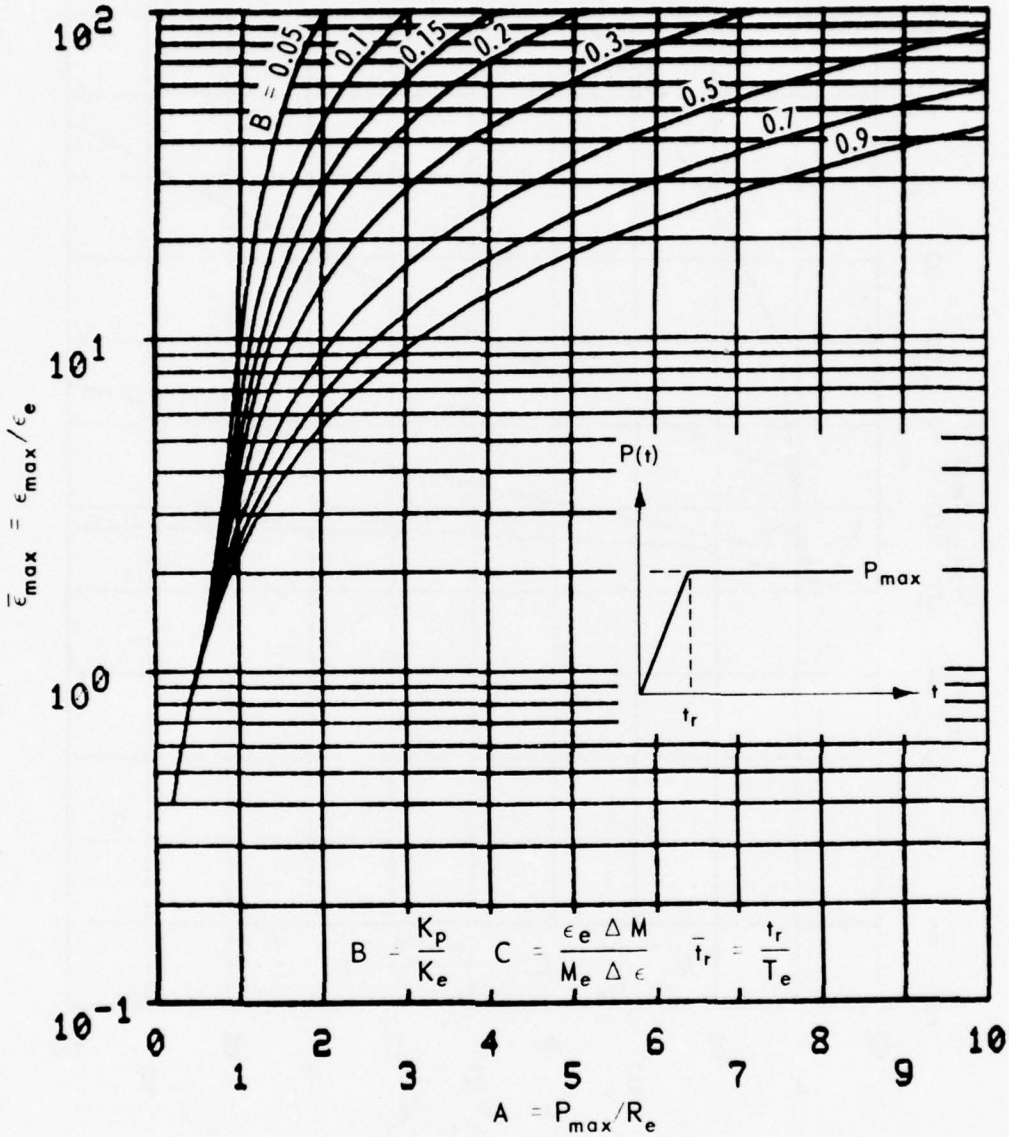

Figure A.25. $\bar{\epsilon}_{max}$ curves for tunnel-liner systems with C = 0.5 and $\bar{t}_r = 0$.

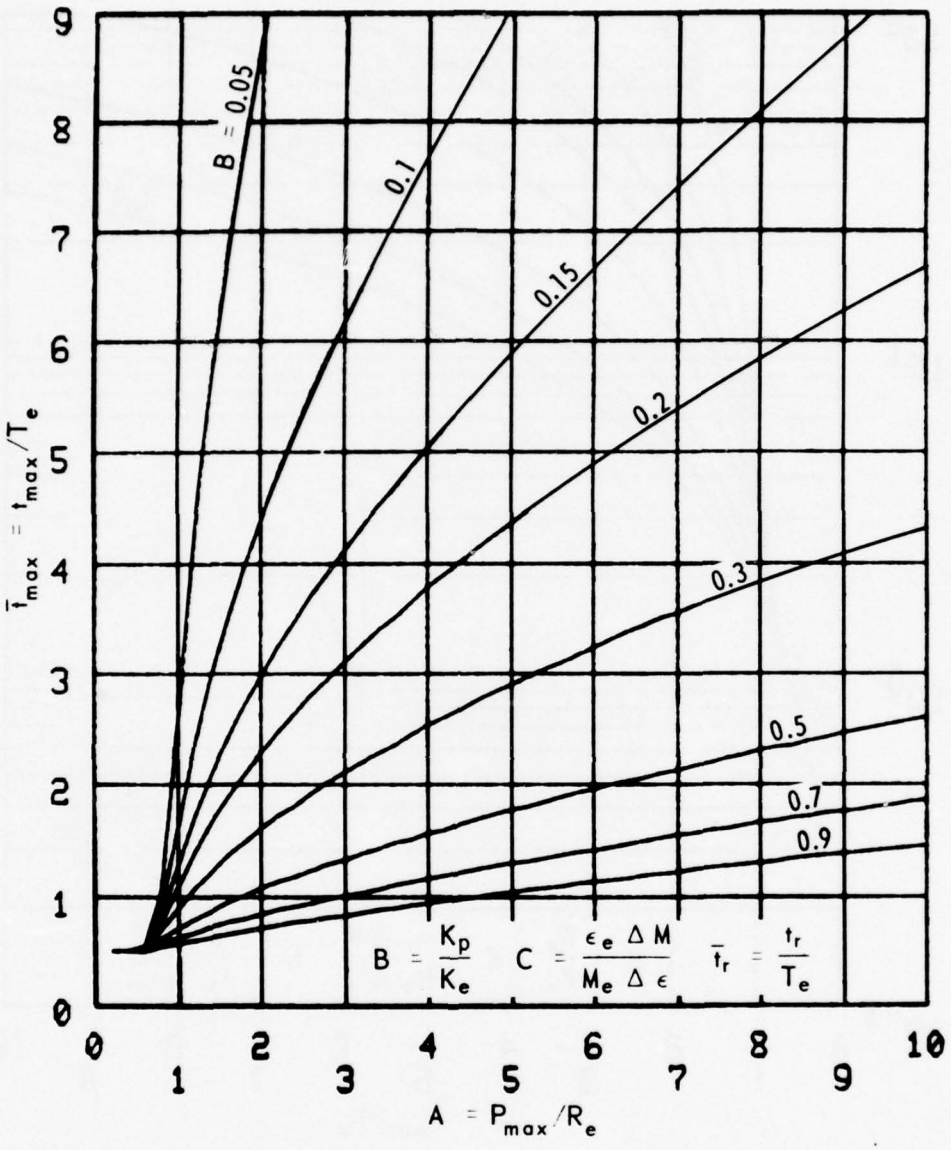

Figure A.26. $\bar{t}_{max}$ curves for tunnel-liner systems with $C = 0.5$ and $\bar{t}_r = 0$.

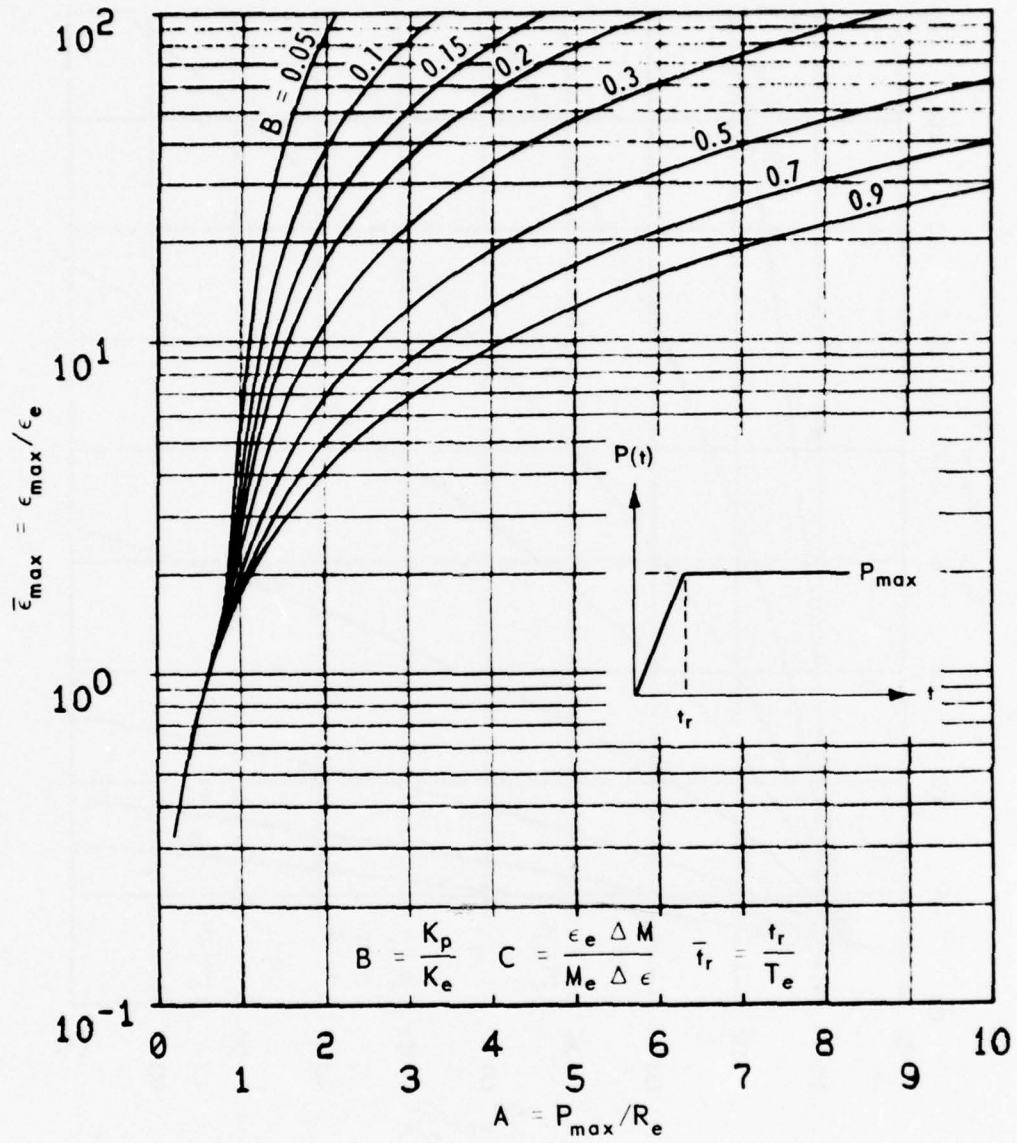

Figure A.27. $\bar{\epsilon}_{max}$ curves for tunnel-liner systems with C = 0.5 and $\bar{t}_r = 0.5$.

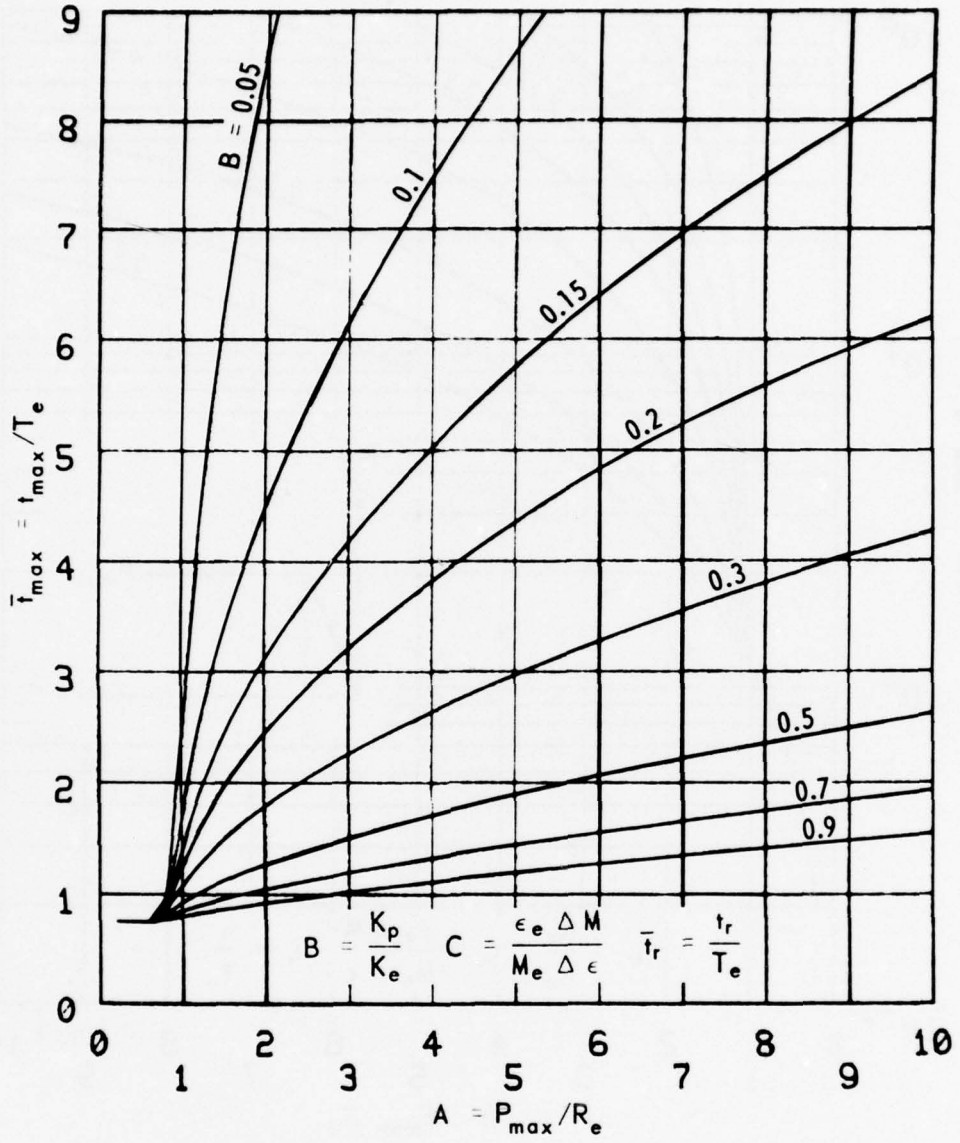

Figure A.28. $\bar{t}_{max}$ curves for tunnel-liner systems with C = 0.5 and $\bar{t}_r = 0.5$.

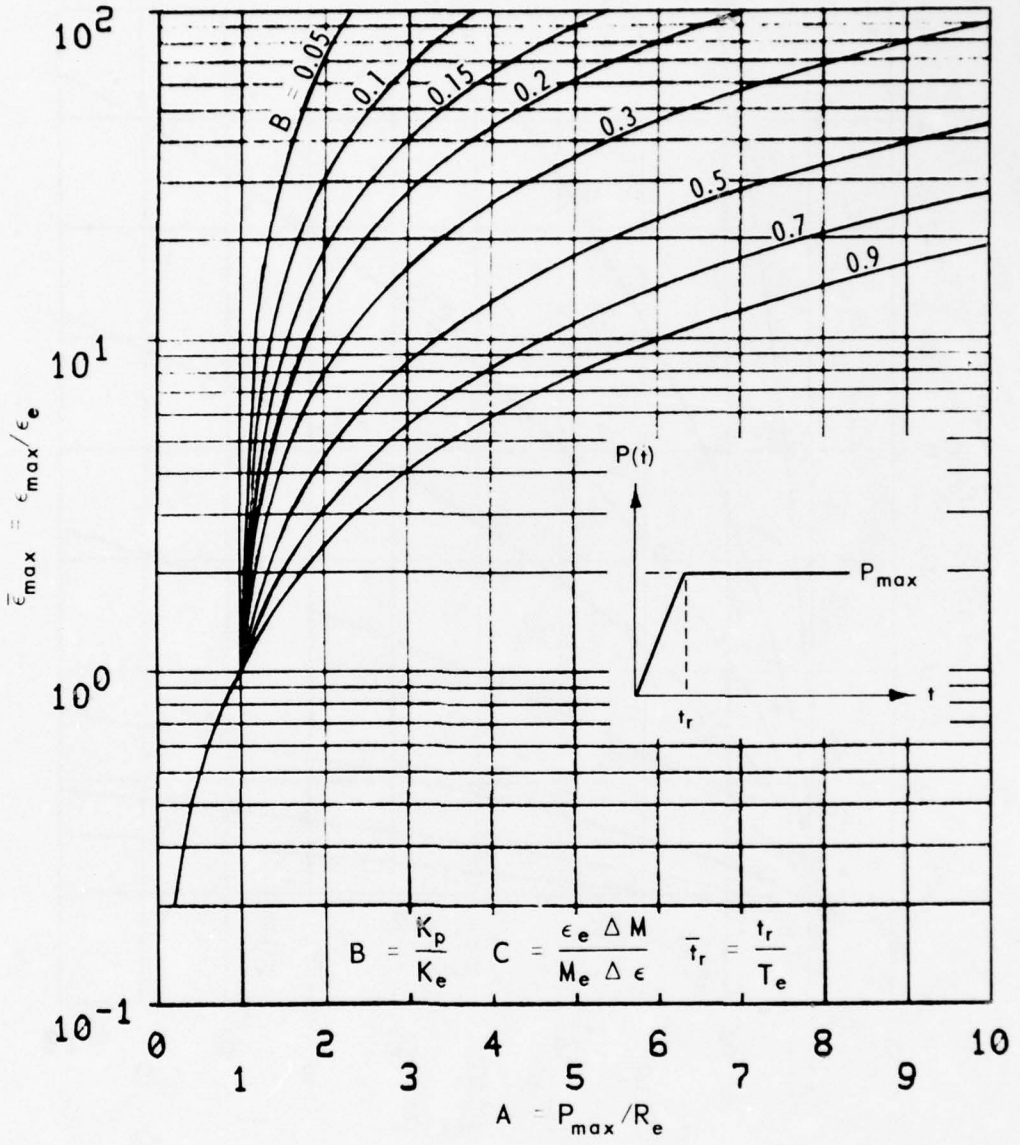

Figure A.29. $\bar{\epsilon}_{max}$ curves for tunnel-liner systems with $C = 0.5$ and $\bar{t}_r = 1$.

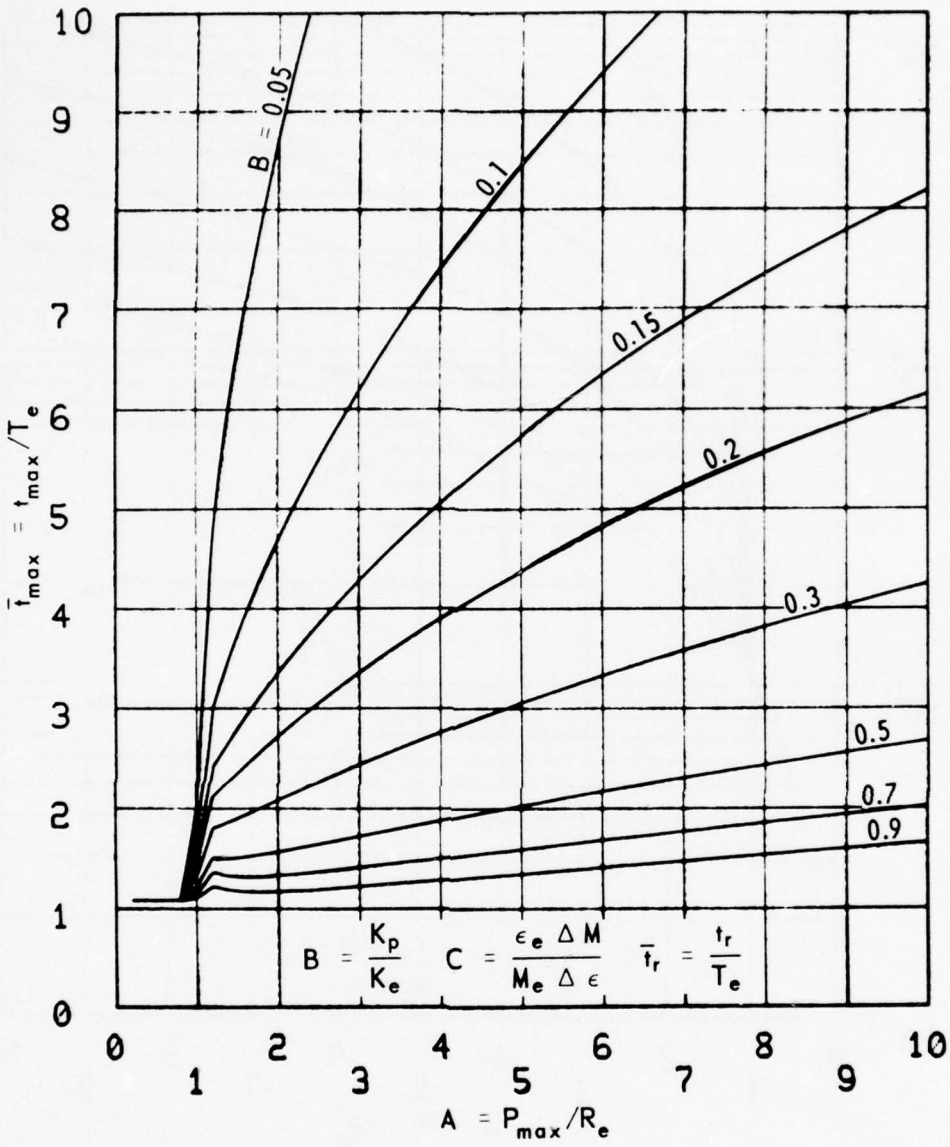

Figure A.30. $\bar{t}_{max}$ curves for tunnel-liner systems with $C = 0.5$ and $\bar{t}_r = 1$.

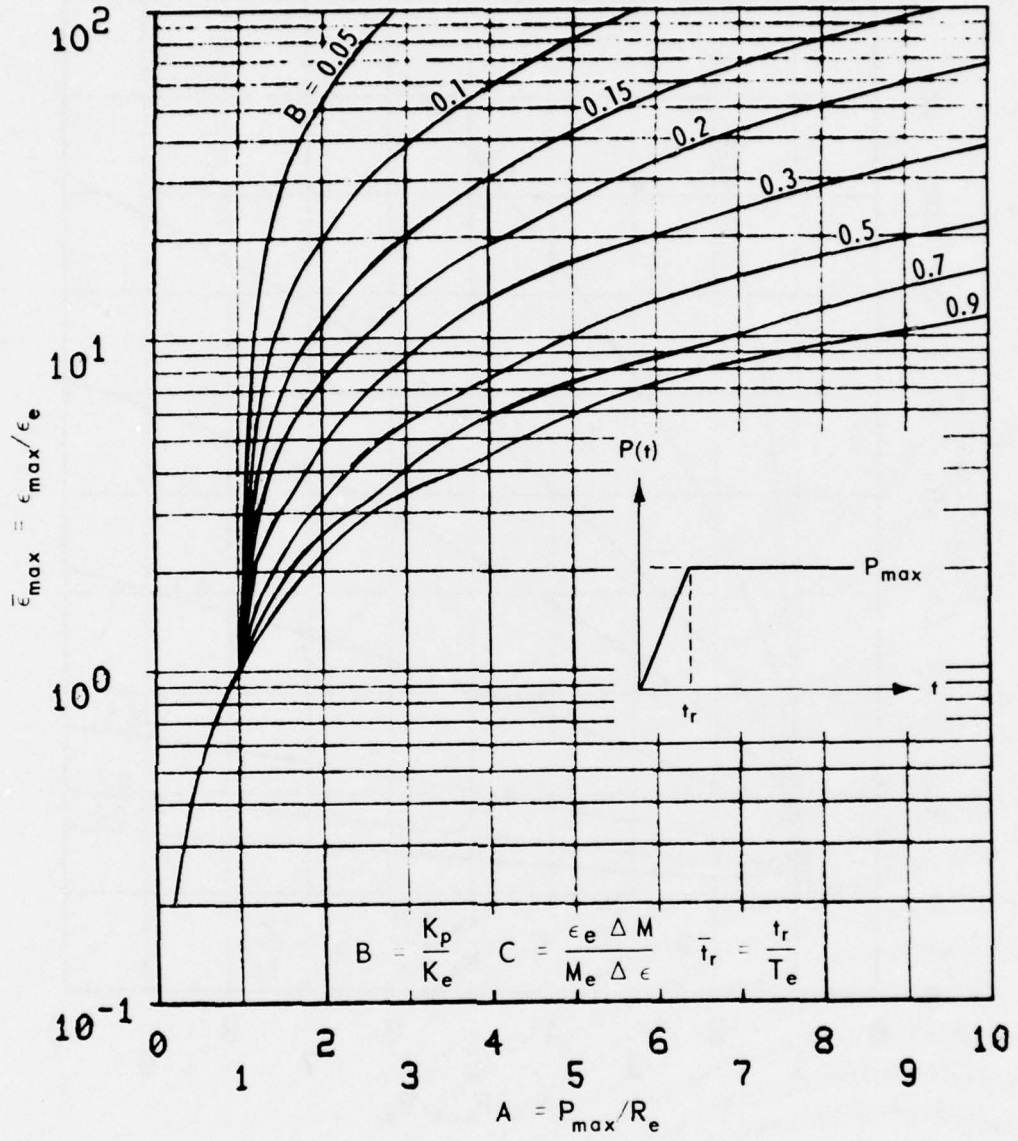

Figure A.31. $\bar{\epsilon}_{max}$ curves for tunnel-liner systems with $C = 0.5$ and $\bar{t}_r = 5$.

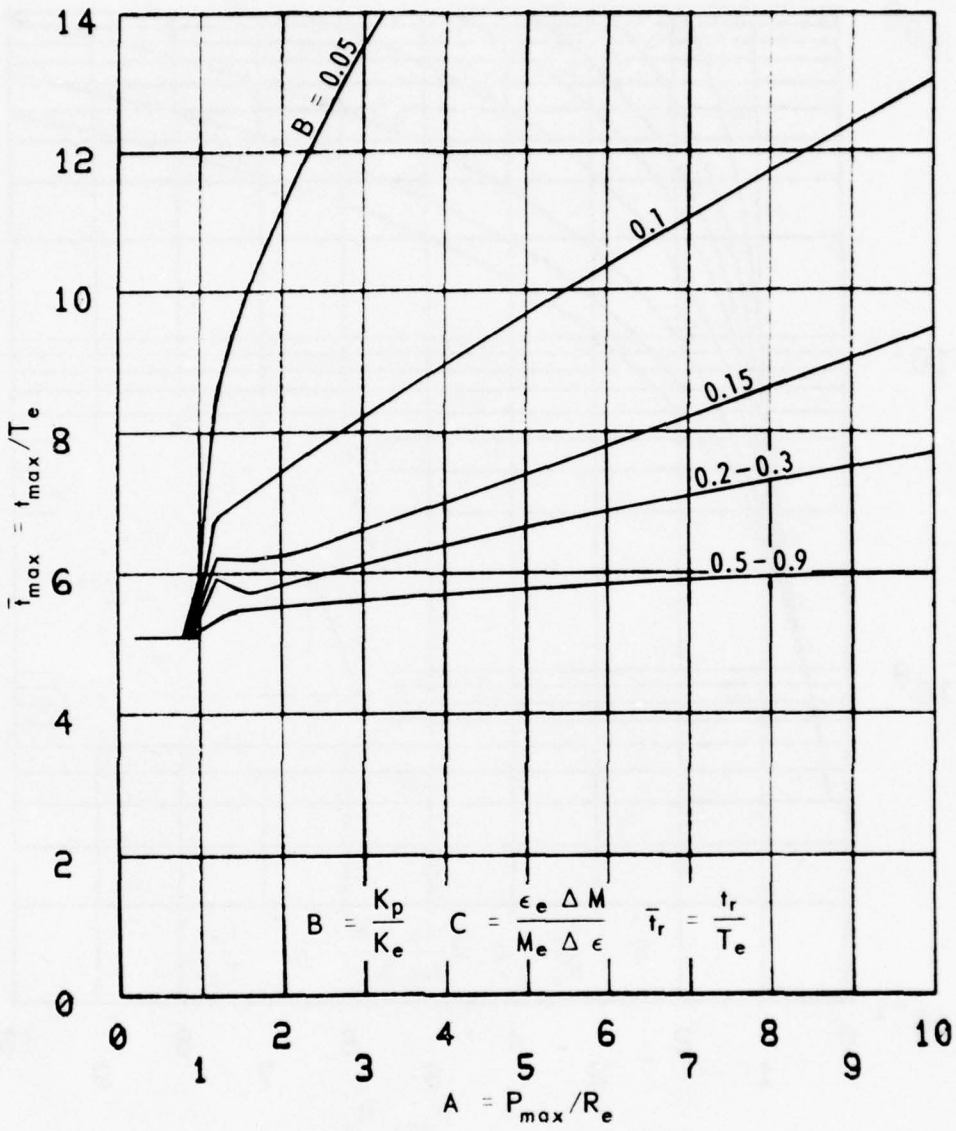

Figure A.32. $\bar{t}_{max}$ curves for tunnel-liner systems with $C = 0.5$ and $\bar{t}_r = 5$.

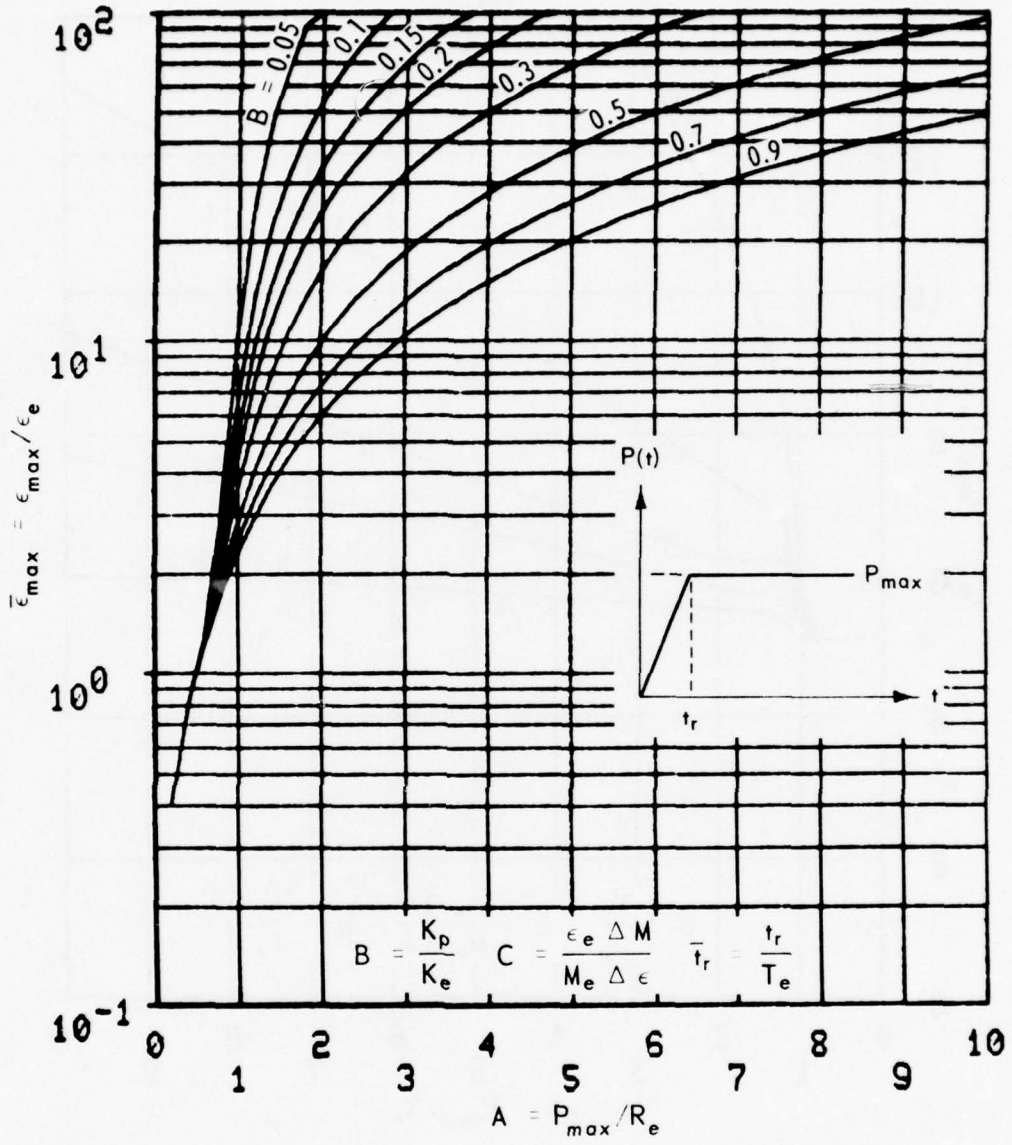

Figure A.33. $\bar{\epsilon}_{max}$ curves for tunnel-liner systems with C = 0.7 and $\bar{t}_r = 0$.

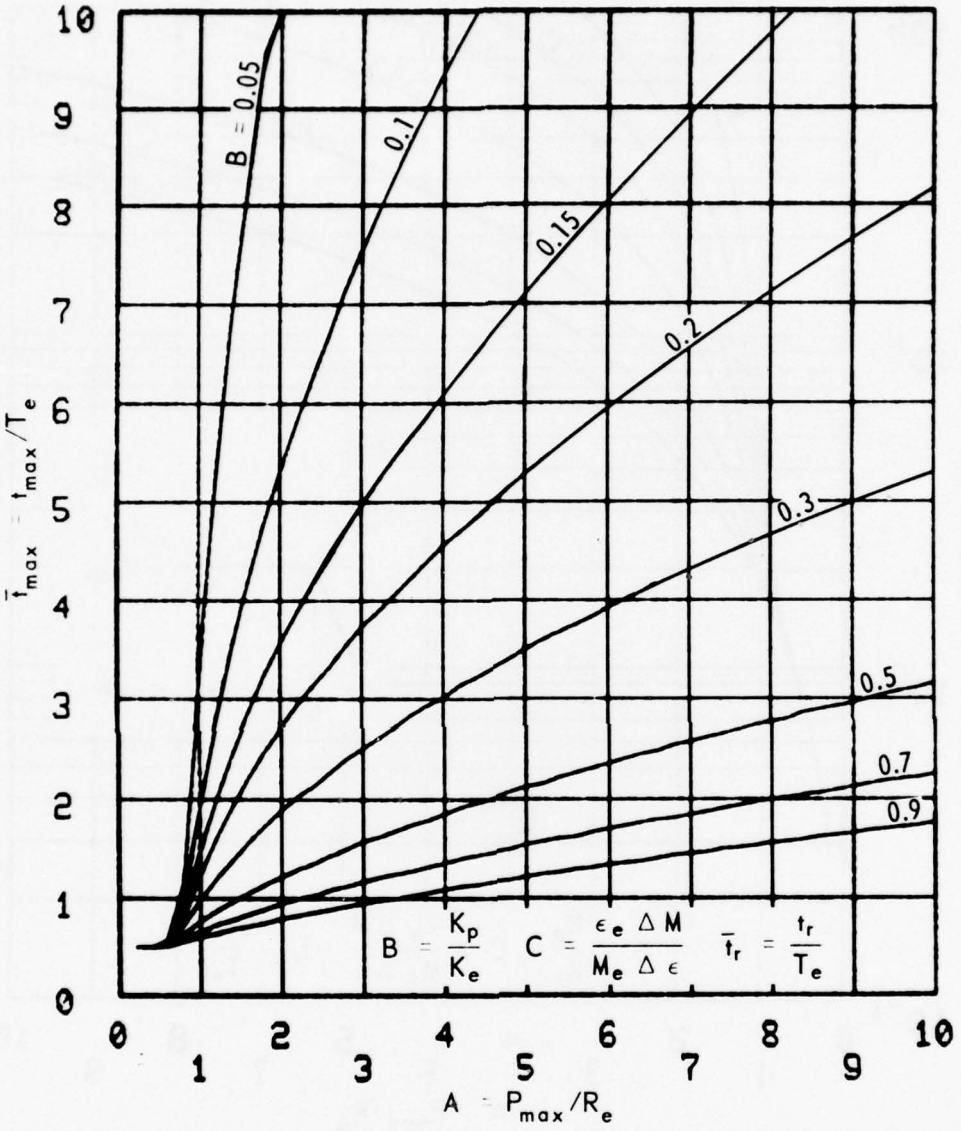

Figure A.34. $\bar{t}_{max}$ curves for tunnel-liner systems with C = 0.7 and $\bar{t}_r = 0$.

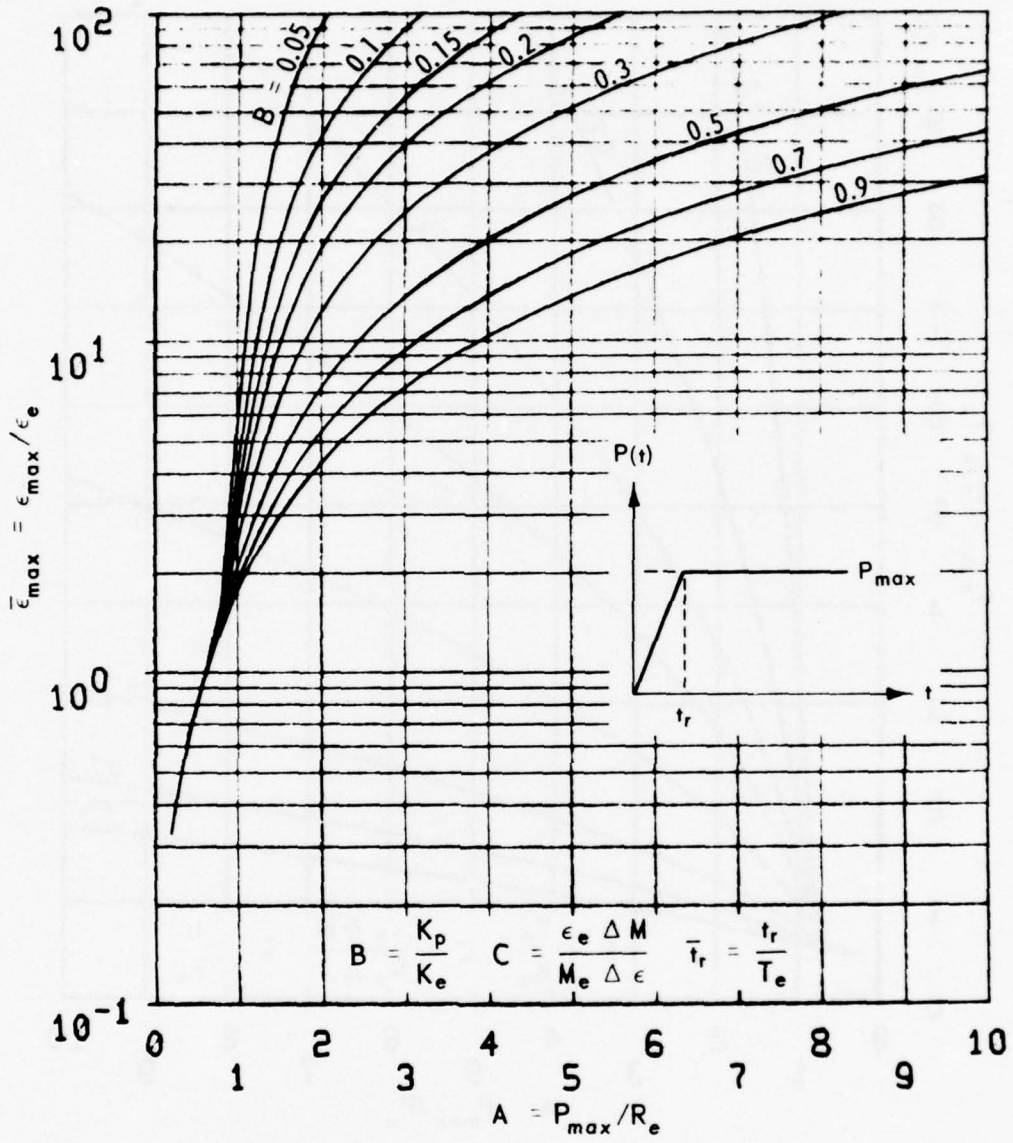

Figure A.35. $\bar{\epsilon}_{max}$ curves for tunnel-liner systems with $C = 0.7$ and $\bar{t}_r = 0.5$.

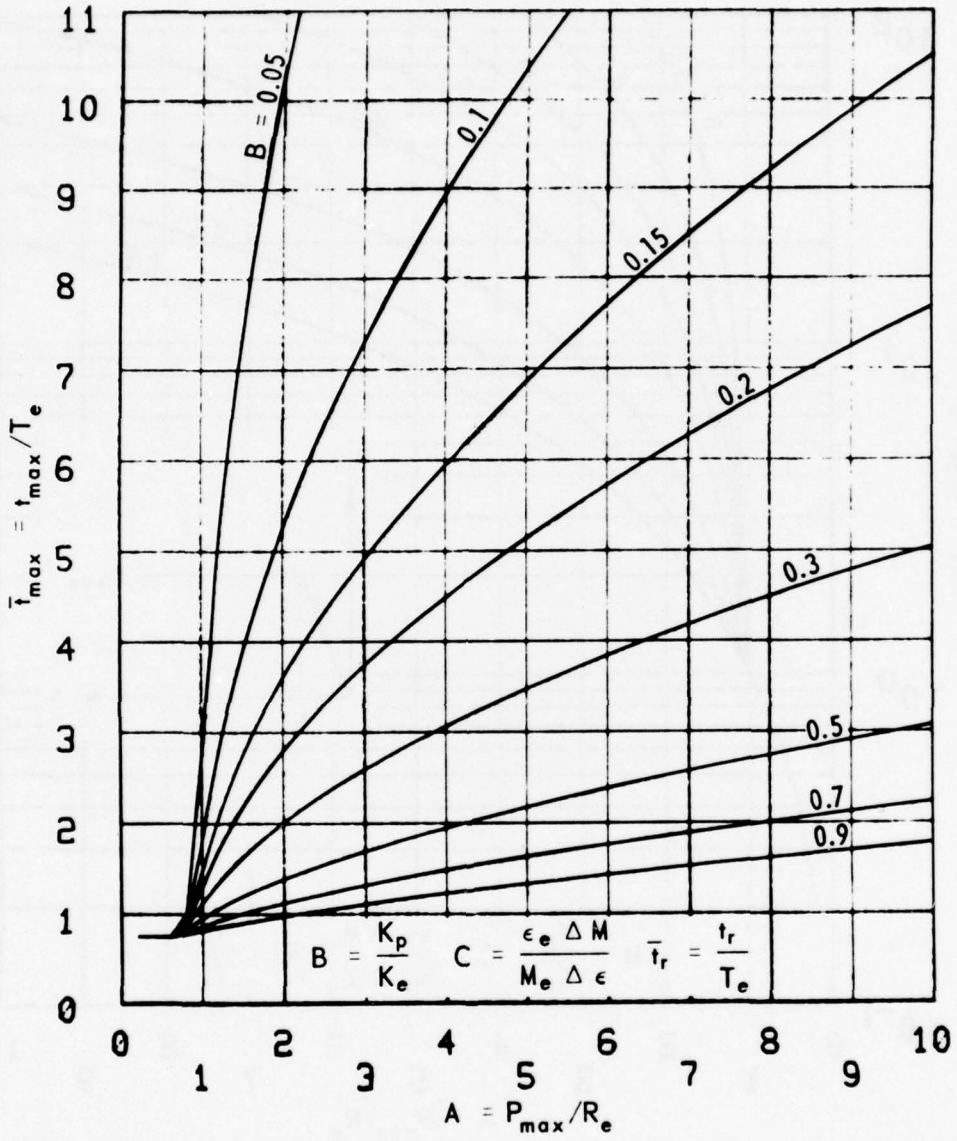

Figure A.36. $\bar{t}_{max}$ curves for tunnel-liner systems with C = 0.7 and $\bar{t}_r = 0.5$.

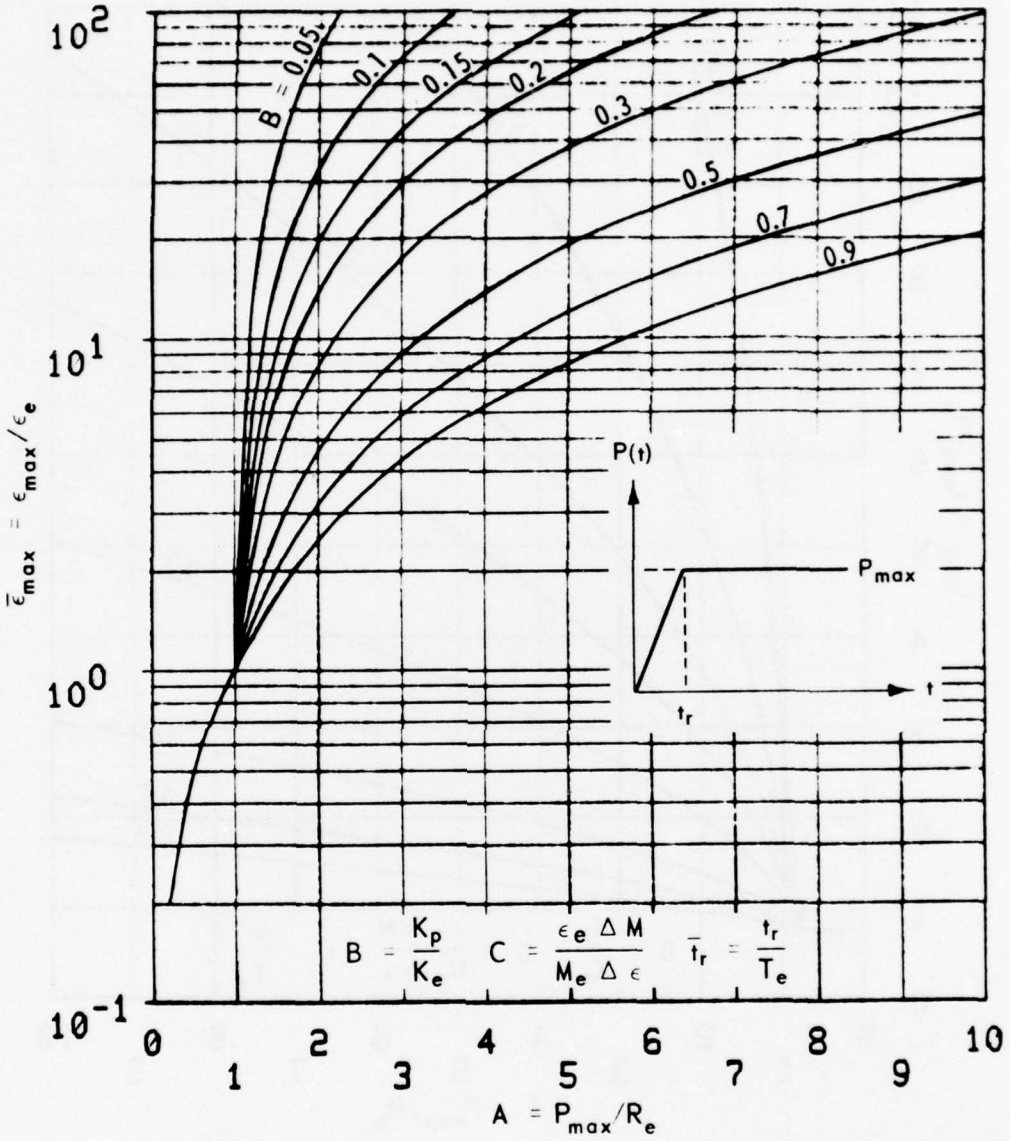

Figure A.37. $\bar{\epsilon}_{max}$ curves for tunnel-liner systems with C = 0.7 and $\bar{t}_r = 1$.

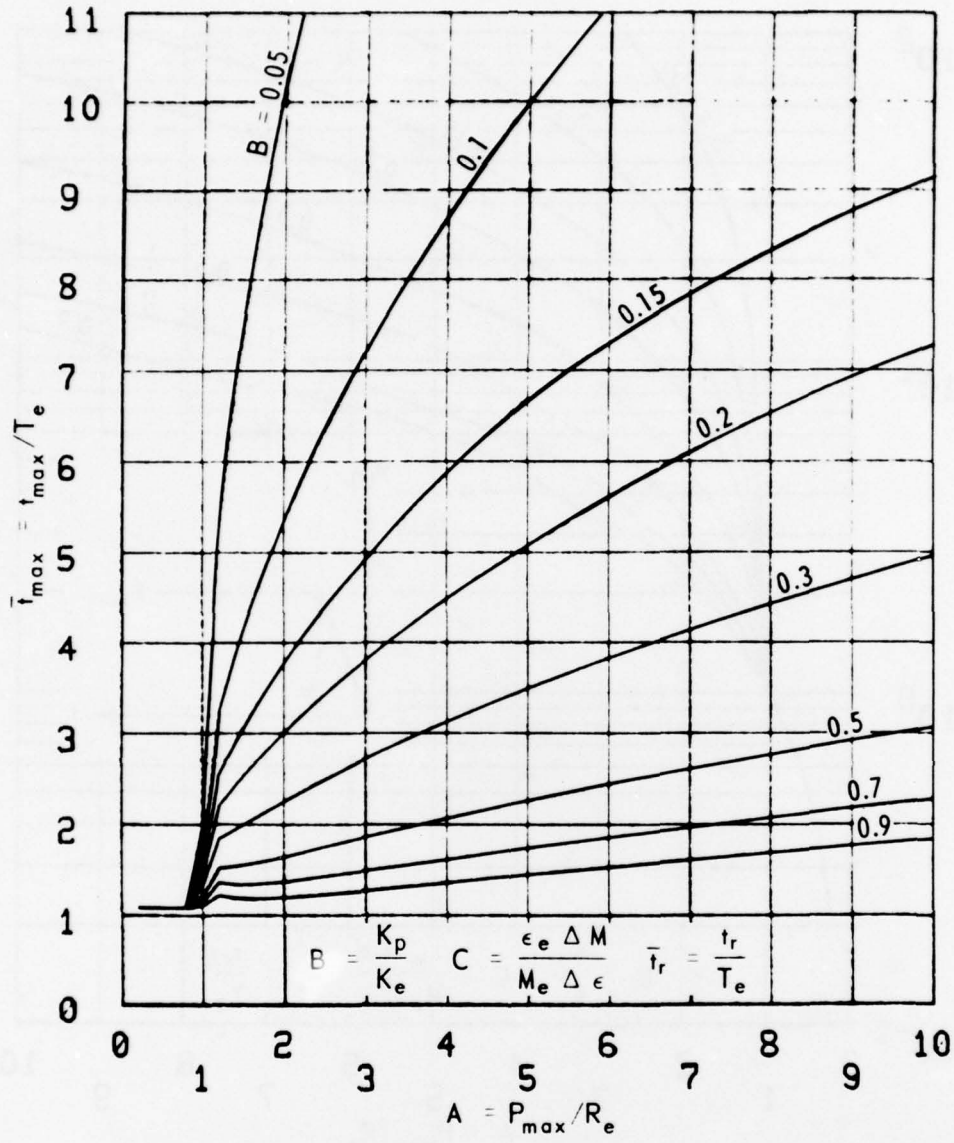

Figure A.38. $\bar{t}_{max}$ curves for tunnel-liner systems with $C = 0.7$ and $\bar{t}_r = 1$.

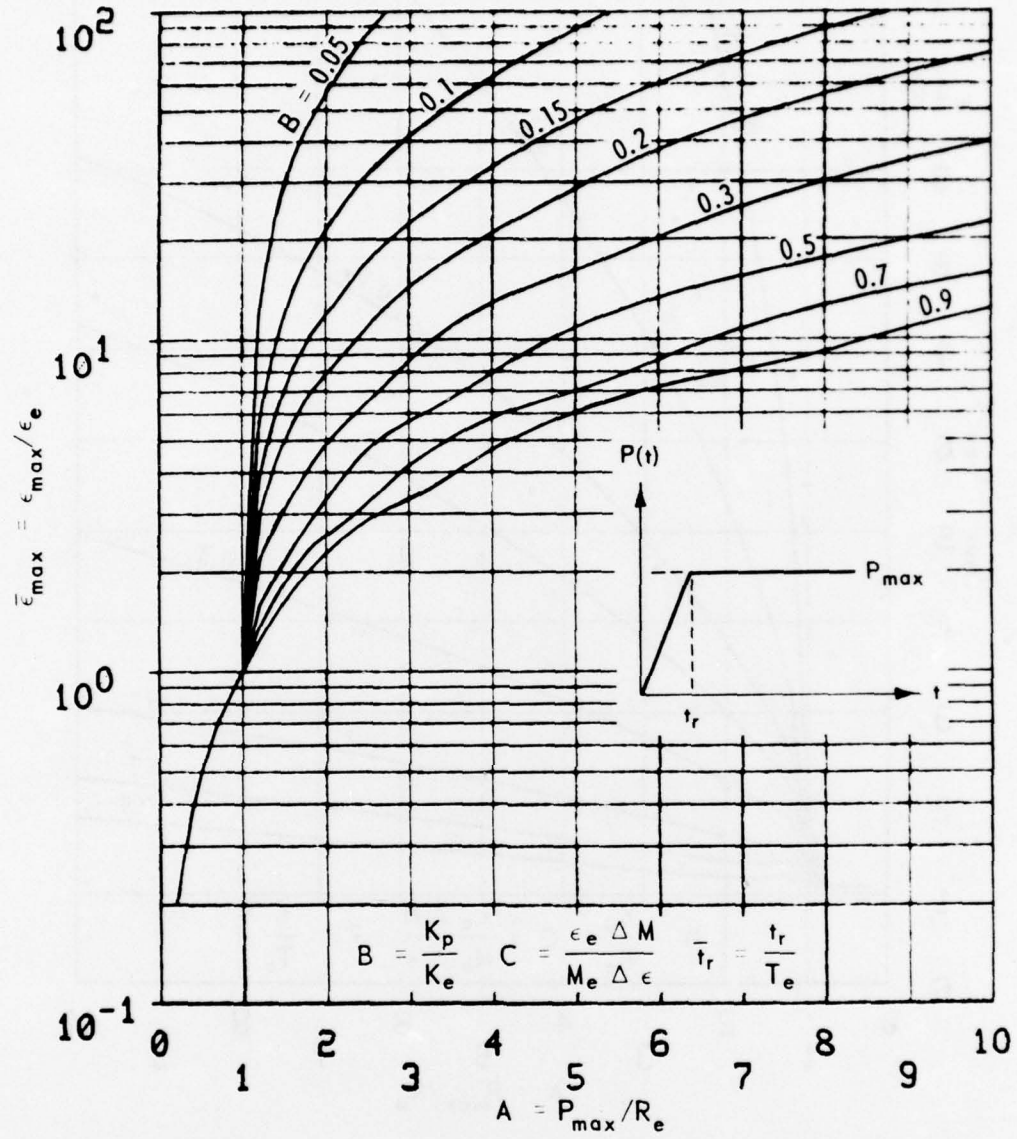

Figure A.39. $\bar{\epsilon}_{max}$ curves for tunnel-liner systems with $C = 0.7$ and $\bar{t}_r = 5$.

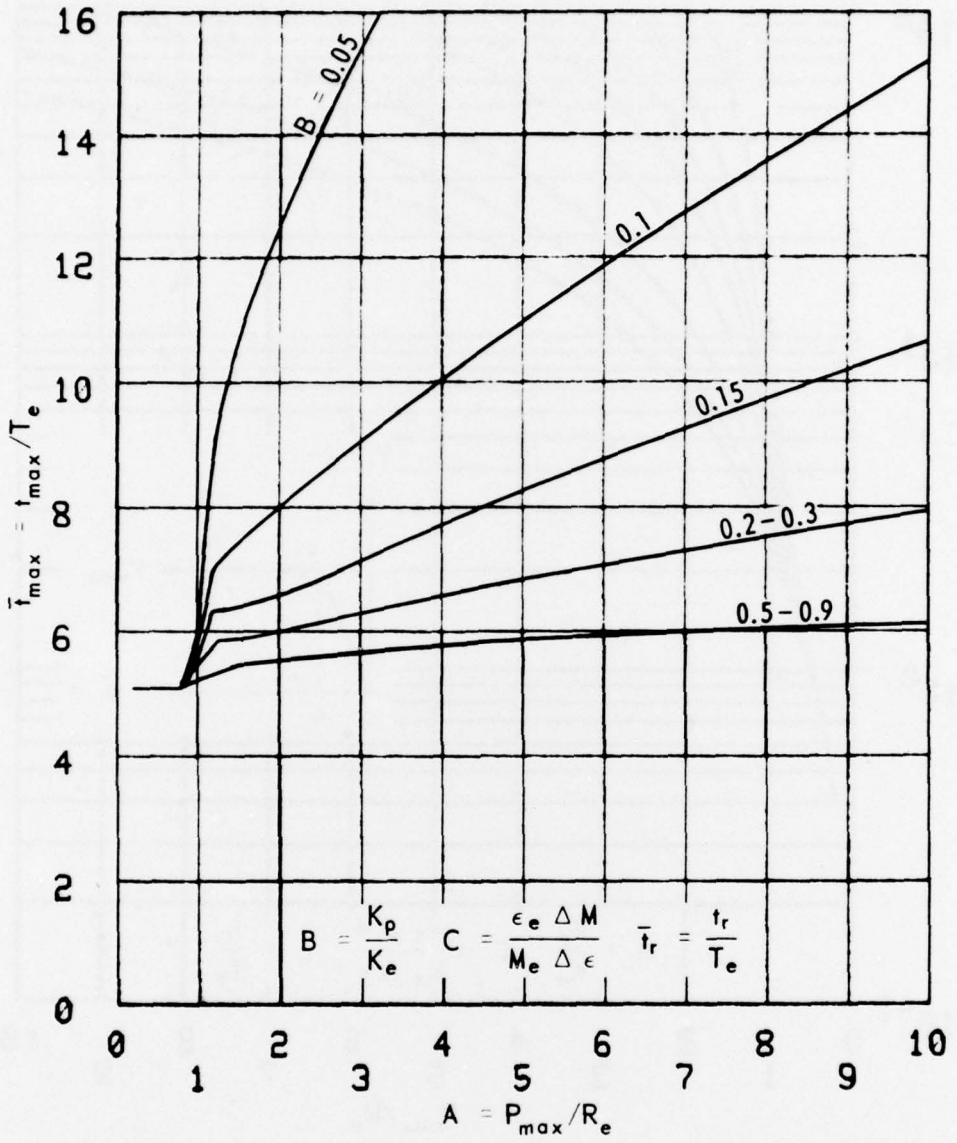

Figure A.40. $\bar{t}_{max}$ curves for tunnel-liner systems with $C = 0.7$ and $\bar{t}_r = 5$.

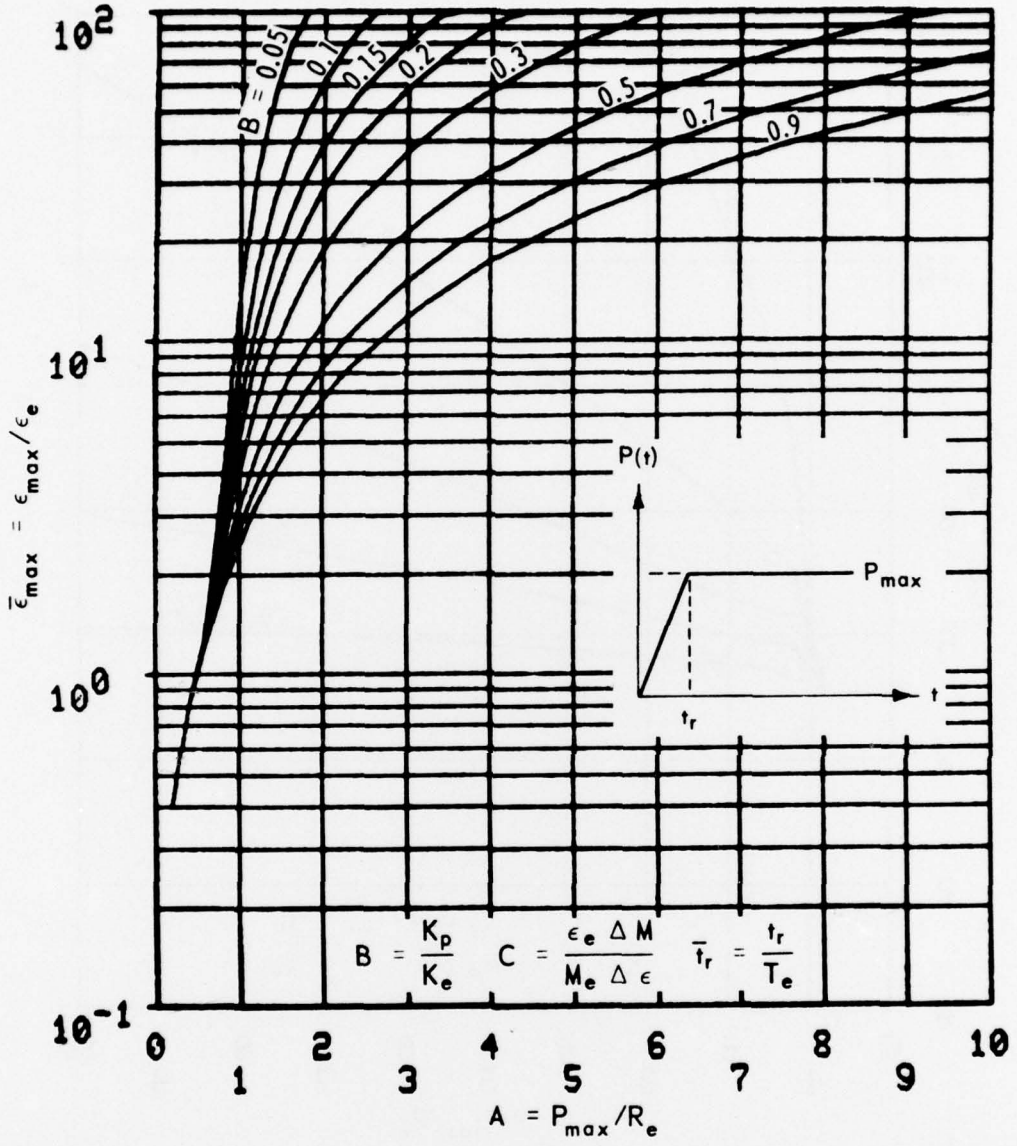

Figure A.41. $\bar{\epsilon}_{max}$ curves for tunnel-liner systems with $C = 1$ and $\bar{t}_r = 0$.

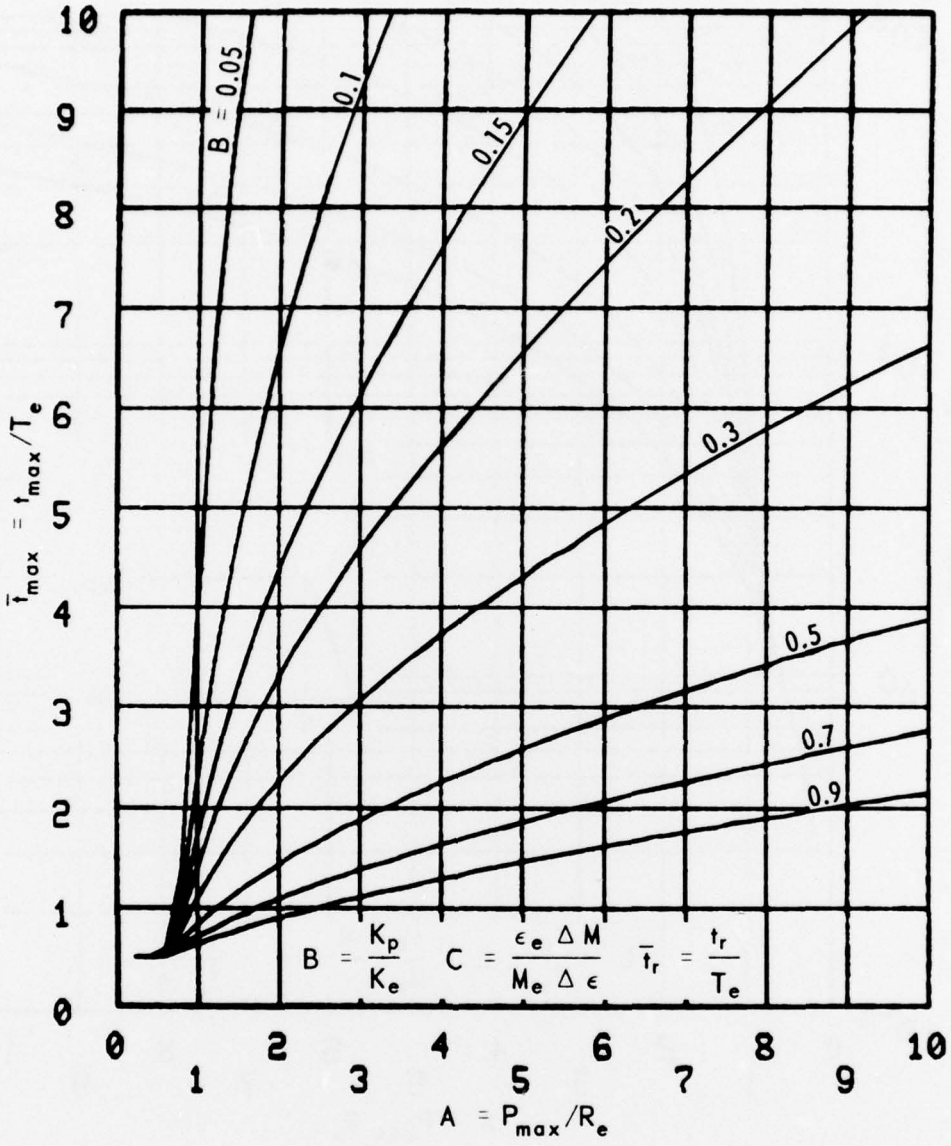

Figure A.42. $\bar{t}_{max}$ curves for tunnel-liner systems with $C = 1$ and $\bar{t}_r = 0$.

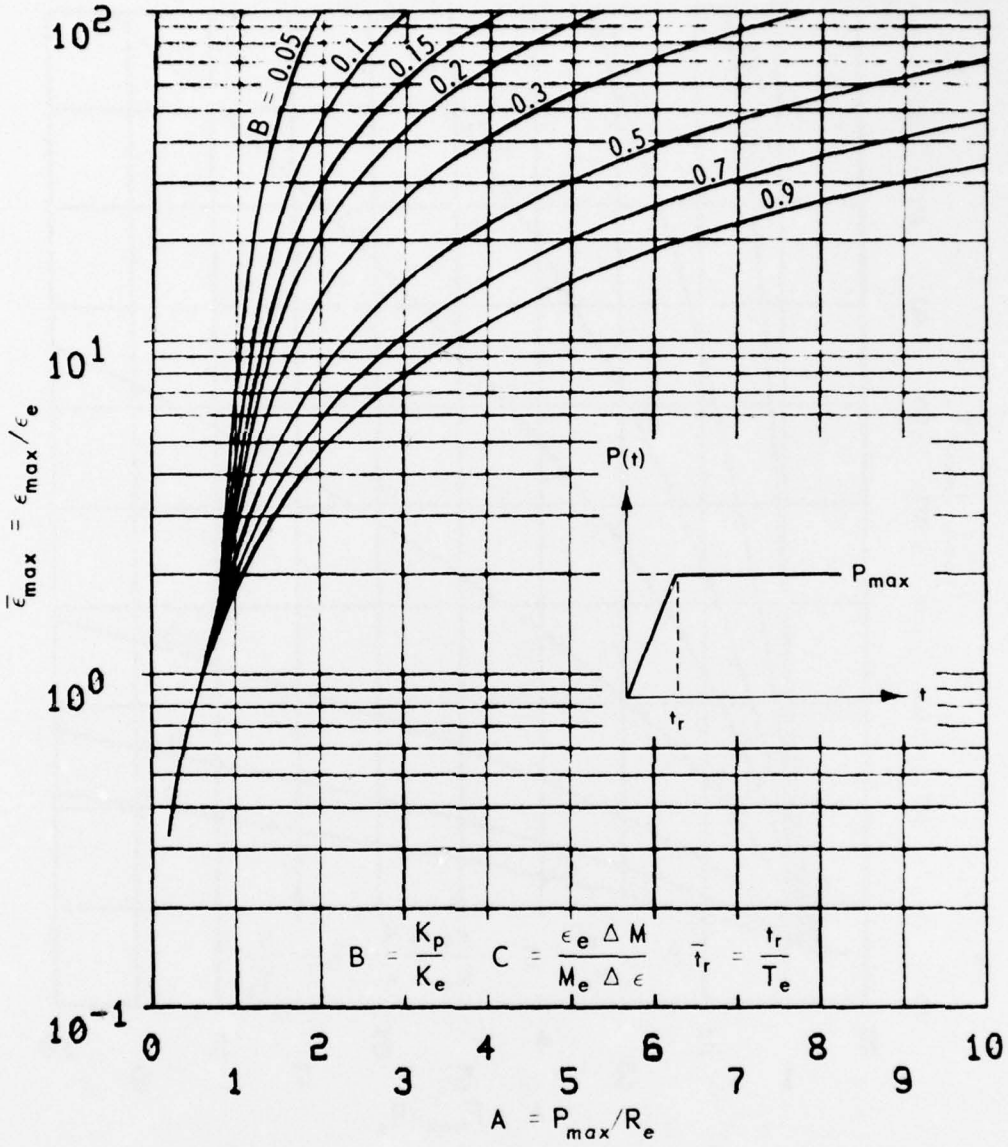

Figure A.43. $\bar{\epsilon}_{max}$ curves for tunnel-liner systems with C = 1 and $\bar{t}_r = 0.5$.

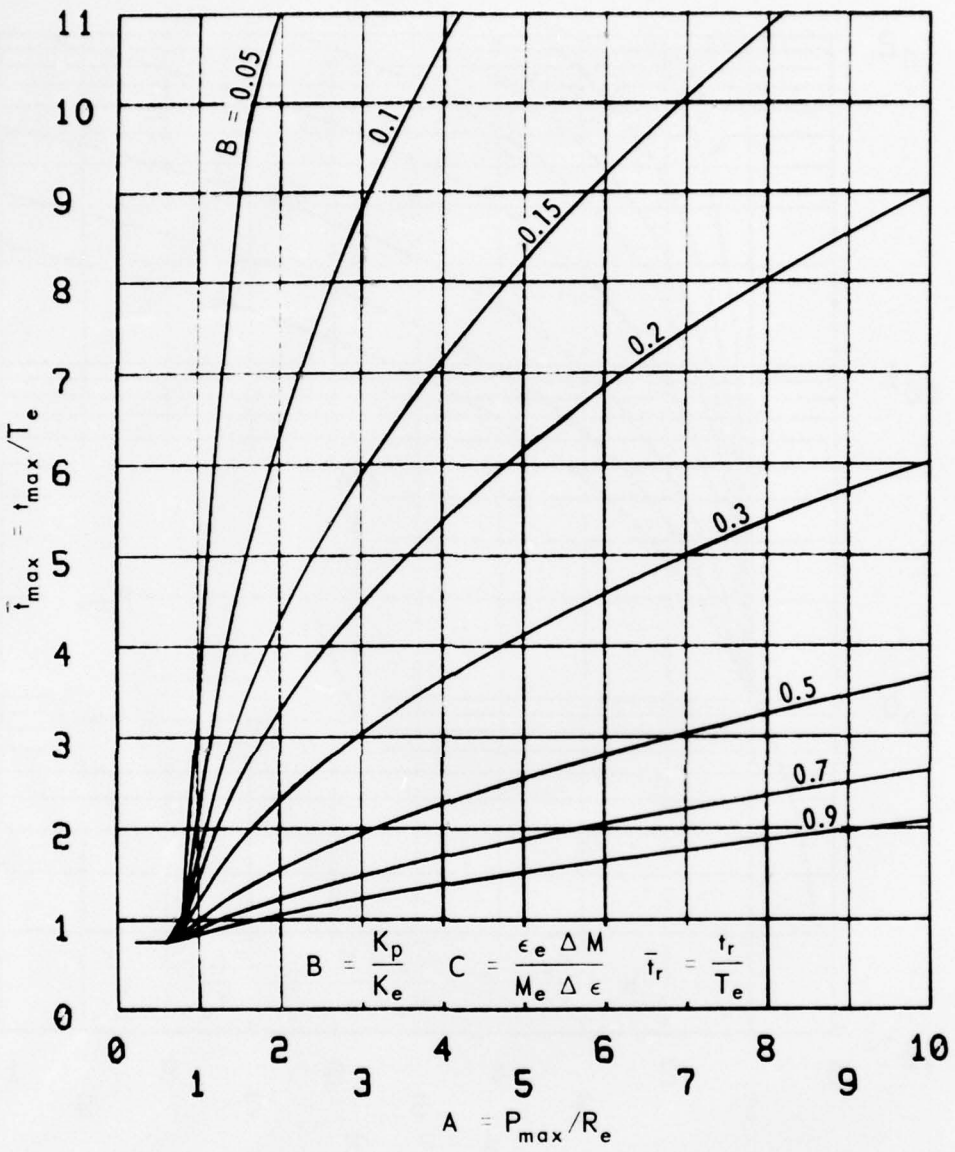

Figure A.44. $\bar{t}_{max}$ curves for tunnel-liner systems with $C = 1$ and $\bar{t}_r = 0.5$.

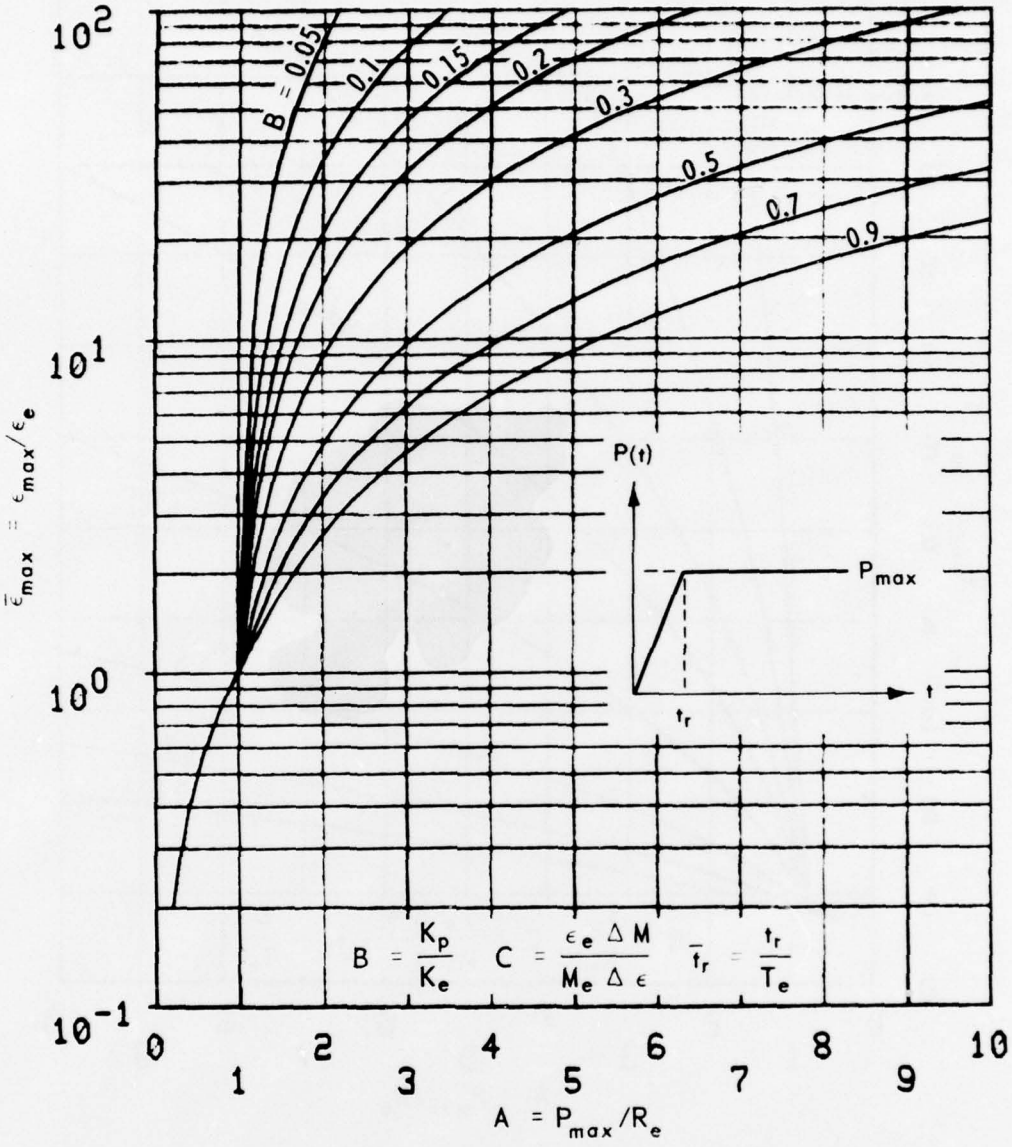

Figure A.45. $\bar{\epsilon}_{max}$ curves for tunnel-liner systems with $C = 1$ and $\bar{t}_r = 1$.

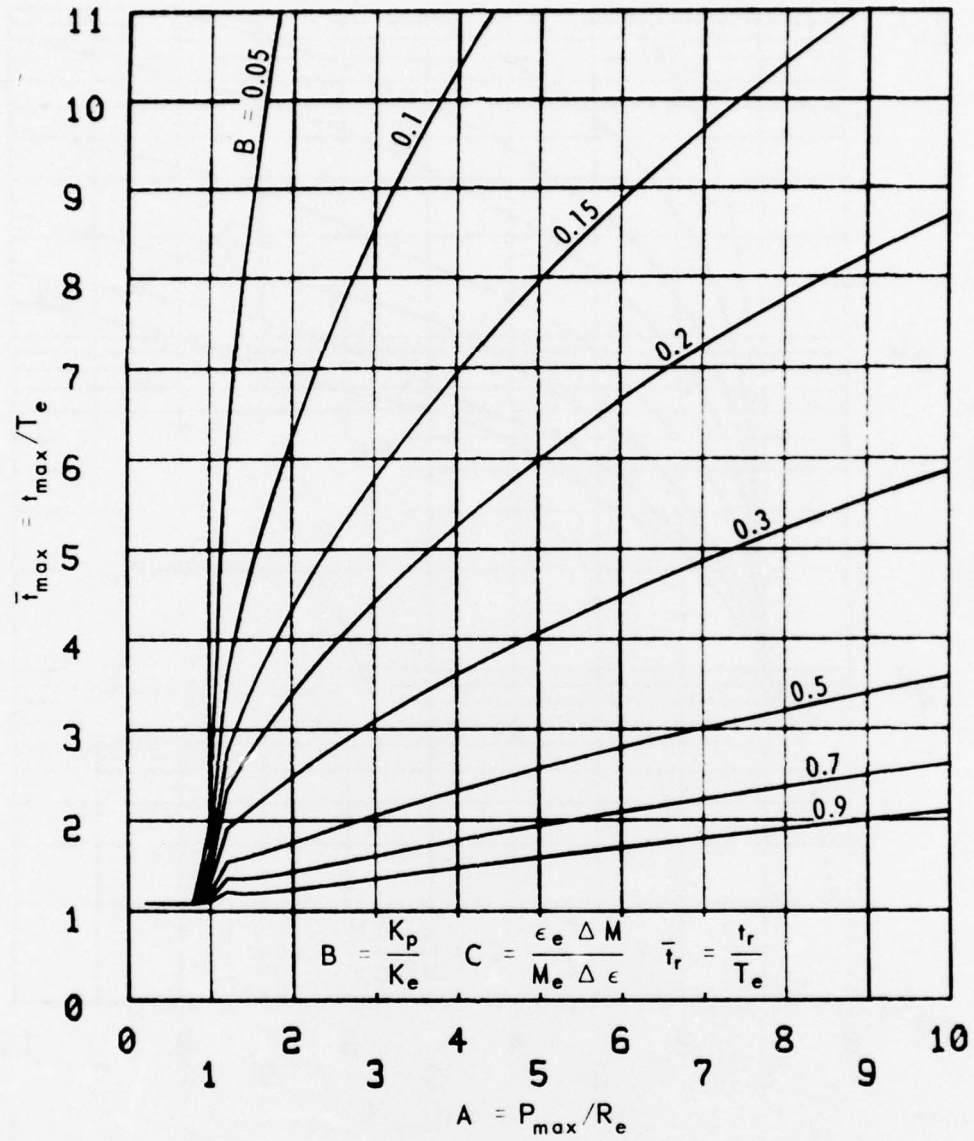

Figure A.46. $\bar{t}_{max}$ curves for tunnel-liner systems with $C = 1$ and $\bar{t}_r = 1$.

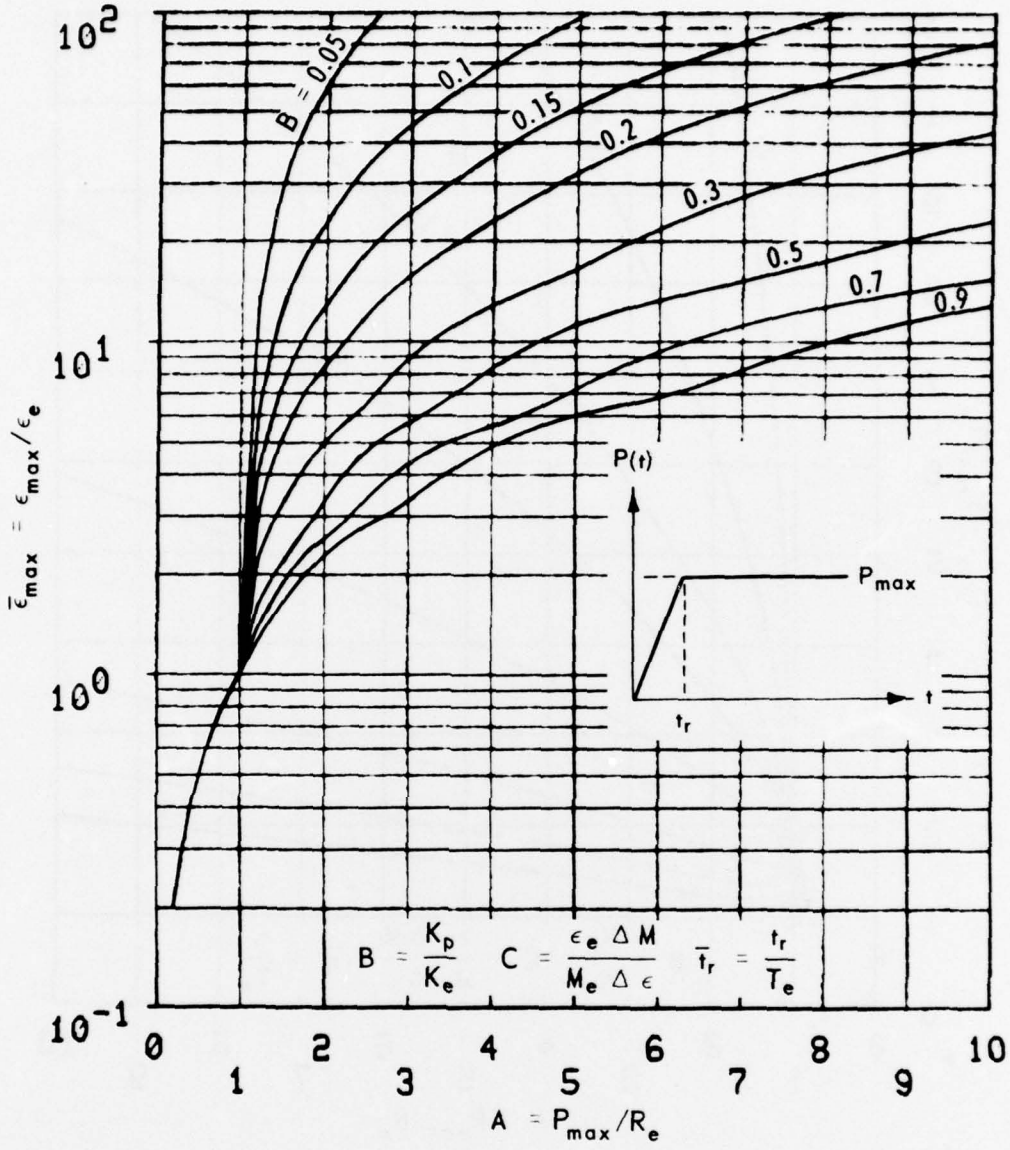

Figure A.47. $\bar{\epsilon}_{max}$ curves for tunnel-liner systems with $C = 1$ and $\bar{t}_r = 5$.

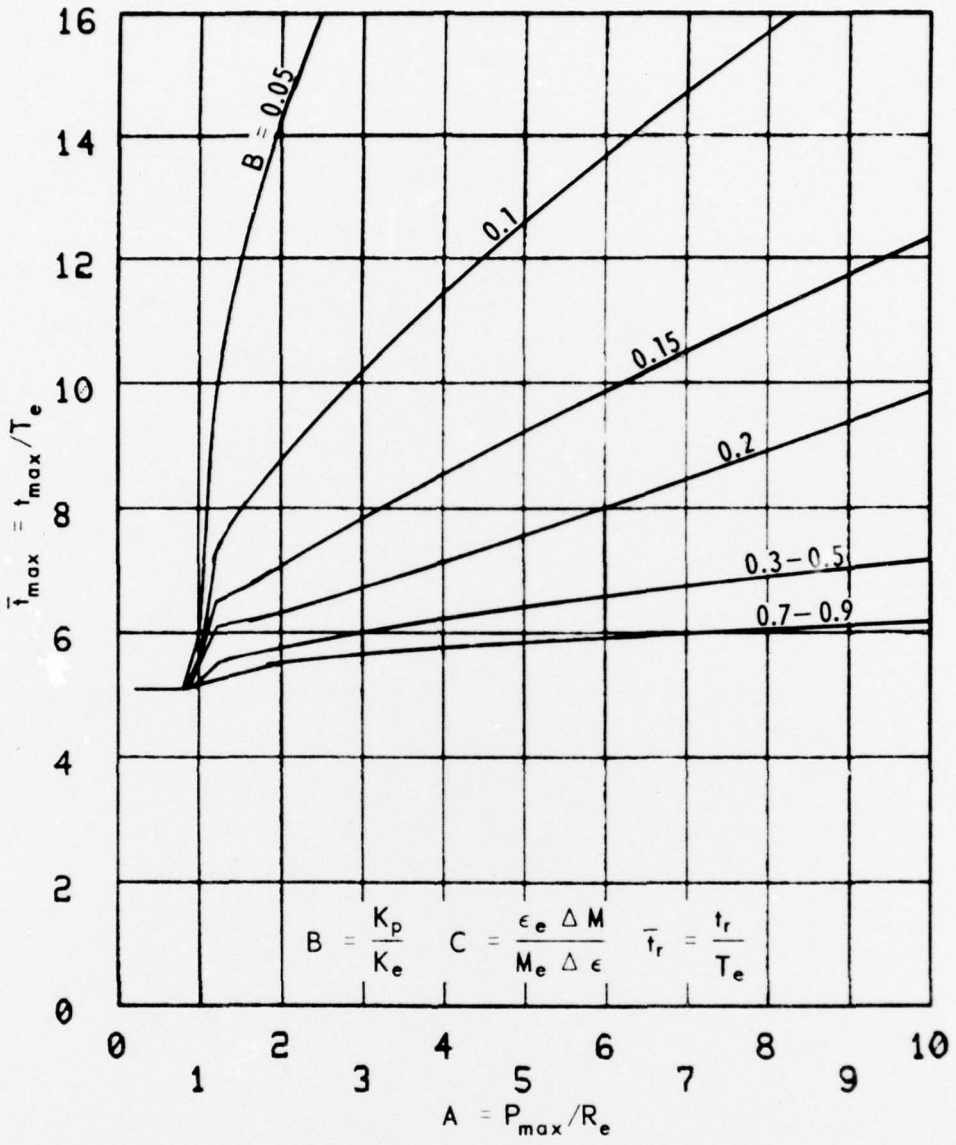

Figure A.48. $\bar{t}_{max}$ curves for tunnel-liner systems with $C = 1$ and $\bar{t}_r = 5$.

APPENDIX B

NOTATION

$A = P_{max}/R_e$	Dimensionless peak free-field stress
$B = K_p/K_e$	Dimensionless plastic stiffness
$C = (\varepsilon_e/M_e)(\Delta M/\Delta\varepsilon)$	Dimensionless rate of change of $\overline{M}(\overline{\varepsilon})$ in plastic deformation
E	Young's modulus
G_i	Shear modulus
i	Subscript referring to a component material layer
K_e	Effective elastic stiffness
K_i	Effective elastic stiffness of layer i
$K_p = \Delta R/\Delta\varepsilon$	Effective plastic stiffness
m	Number of material layers in liner-rock system
M	Effective mass (mass/length)
M_e	Effective mass (mass/length) in elastic deformation
$\overline{M}(\overline{\varepsilon}) = M/M_e$	Dimensionless effective mass (mass/length)
n_i	$2 \sin \phi_i/(1 - \sin \phi_i)$
P_{max}	Peak value of $P(t)$
$P(t)$	External load (or free-field stress)
q_i	Cohesion
r_i	Radius to inside of material layer i
r_{pi}	Radius to the outer boundary of the plastic region of material layer i
$R_e = K_e\varepsilon_e$	Maximum elastic resistance
$R(\varepsilon)$	Internal load-resistance
$\overline{R}(\overline{\varepsilon}) = R(\varepsilon)/R_e$	Dimensionless resistance
t	Time
$\overline{t} = t/T_e$	Dimensionless time
t_{max}	Time at which ε_{max} occurs
$\overline{t}_{max} = t_{max}/T_e$	Dimensionless time at maximum strain
t_r	Rise time of external load
$\overline{t}_r = t_r/T_e$	Normalized rise time of $P(t)$
$T_e = 2\pi\sqrt{M_e/K_e}$	Effective elastic period

Y_i	Effective plastic resistance of layer i
ε	Diametrical strain, positive inward
$\bar{\varepsilon} = \varepsilon/\varepsilon_e$	Normalized diametrical strain
ε_e	Elastic limit, maximum elastic strain
ε_{max}	Maximum value of diametrical strain $\varepsilon(t)$
$\bar{\varepsilon}_{max} = \varepsilon_{max}/\varepsilon_e$	Normalized maximum strain
ε^c_{max}	ε_{max} corrected for compressibility
$\bar{\varepsilon}^c_{max}$	$\bar{\varepsilon}_{max}$ corrected for compressibility
ν_i	Poisson's ratio
ρ_i	Density of material layer numbered i
σ_u	Unconfined compressive strength
ϕ_i	Angle of internal friction

In accordance with ER 70-2-3, paragraph 6c(1)(b), dated 15 February 1973, a facsimile catalog card in Library of Congress format is reproduced below.

Britt, James R

Charts for preliminary design of deep underground structures subjected to dynamic loads, by J. R. Britt. Vicksburg, U. S. Army Engineer Waterways Experiment Station, 1977.

74 p. illus. 27 cm. (U. S. Waterways Experiment Station. Miscellaneous paper N-77-3)

Prepared for Defense Nuclear Agency, Washington, D. C., and Office, Chief of Engineers, U. S. Army, Washington, D. C., under DNA Subtask J34CAXSX311 and OCE Subtask 4A762719AT40/A1/017.

1. Charts. 2. Dynamic loads. 3. Ground shock. 4. Nuclear explosion effects. 5. Underground structures. I. Defense Nuclear Agency. II. U. S. Army. Corps of Engineers. (Series: U. S. Waterways Experiment Station, Vicksburg, Miss. Miscellaneous paper N-77-3)
TA7.W34m no.N-77-3